Collection of Freeze-Thaw Performance Data on Vail Avenue

Final Report
August 2017



IOWA STATE UNIVERSITY
Institute for Transportation

Sponsored by
Iowa Department of Transportation
(Iowa DOT Project HR-3013)
(InTrans Project 16-601)

About the Institute for Transportation

The mission of the Institute for Transportation (InTrans) at Iowa State University is to develop and implement innovative methods, materials, and technologies for improving transportation efficiency, safety, reliability, and sustainability while improving the learning environment of students, faculty, and staff in transportation-related fields.

Disclaimer Notice

The contents of this report reflect the views of the authors, who are responsible for the facts and the accuracy of the information presented herein. The opinions, findings and conclusions expressed in this publication are those of the authors and not necessarily those of the sponsors.

The sponsors assume no liability for the contents or use of the information contained in this document. This report does not constitute a standard, specification, or regulation.

The sponsors do not endorse products or manufacturers. Trademarks or manufacturers' names appear in this report only because they are considered essential to the objective of the document.

Non-Discrimination Statement

Iowa State University does not discriminate on the basis of race, color, age, ethnicity, religion, national origin, pregnancy, sexual orientation, gender identity, genetic information, sex, marital status, disability, or status as a U.S. veteran. Inquiries regarding non-discrimination policies may be directed to Office of Equal Opportunity, 3410 Beardshear Hall, 515 Morrill Road, Ames, Iowa 50011, Tel. 515-294-7612, Hotline: 515-294-1222, email eooffice@iastate.edu.

Iowa Department of Transportation Statements

Federal and state laws prohibit employment and/or public accommodation discrimination on the basis of age, color, creed, disability, gender identity, national origin, pregnancy, race, religion, sex, sexual orientation or veteran's status. If you believe you have been discriminated against, please contact the Iowa Civil Rights Commission at 800-457-4416 or the Iowa Department of Transportation affirmative action officer. If you need accommodations because of a disability to access the Iowa Department of Transportation's services, contact the agency's affirmative action officer at 800-262-0003.

The preparation of this report was financed in part through funds provided by the Iowa Department of Transportation through its "Second Revised Agreement for the Management of Research Conducted by Iowa State University for the Iowa Department of Transportation" and its amendments.

The opinions, findings, and conclusions expressed in this publication are those of the authors and not necessarily those of the Iowa Department of Transportation.

Technical Report Documentation Page

1. Report No. Iowa DOT Project HR-3013	**2. Government Accession No.**	**3. Recipient's Catalog No.**	
4. Title and Subtitle Collection of Freeze-Thaw Performance Data on Vail Avenue		**5. Report Date** August 2017	
		6. Performing Organization Code	
7. Author(s) Cheng Li (orcid.org/0000-0003-0577-2117) and Jeramy Ashlock (orcid.org/0000-0003-0677-9900)		**8. Performing Organization Report No.** InTrans Project 16-601	
9. Performing Organization Name and Address Institute for Transportation Iowa State University 2711 South Loop Drive, Suite 4700 Ames, IA 50010-8664		**10. Work Unit No. (TRAIS)**	
		11. Contract or Grant No.	
12. Sponsoring Organization Name and Address Iowa Department of Transportation 800 Lincoln Way Ames, IA 50010		**13. Type of Report and Period Covered** Final Report	
		14. Sponsoring Agency Code	

15. Supplementary Notes

Visit www.intrans.iastate.edu for color pdfs of this and other research reports.

16. Abstract

Granular-surfaced roads in seasonally cold regions are frequently subjected to freeze-thaw cycles, leading to severe damage during thawing periods. To identify cost-effective technologies and geomaterials for improving the performance of and mitigating freeze-thaw damage on granular-surfaced roads, the recently completed Iowa Highway Research Board project TR-664, Low-Cost Rural Surface Alternatives: Demonstration Project, studied 17 stabilized demonstration sections over a two-mile stretch of Vail Avenue in Hamilton County, Iowa, which is a heavily used granular-surfaced road.

In the TR-664 project, field tests and visual surveys were performed over the 2013–2014 and 2014–2015 seasonal freeze-thaw cycles. The construction procedures, costs, and performance of the test sections were documented in the TR-664 final report.

The present project was conducted to continue monitoring the performance and documenting the maintenance costs of the test sections through the 2016–2017 seasonal freeze-thaw cycles, and to maintain continuity of the field performance data in subsequent phases of this research. In the present project, performance-based field tests were conducted on all of the test sections. Additionally, the weather data, ground temperature profile, surface performance, and maintenance costs of the various sections were recorded.

Based on the newly collected field test and maintenance data, it was concluded that the sections with macadam stone base layers continued to perform better than all other sections, while the stiffnesses of the chemically stabilized sections decreased significantly after two years of service. The updated break-even periods of the various stabilization methods were found to be approximately the same as those determined in the TR-664 project.

17. Key Words field test—freeze-thaw—frost boil—granular-surfaced road—gravel road—ground temperature—stabilization		**18. Distribution Statement** No restrictions.	
19. Security Classification (of this report) Unclassified.	**20. Security Classification (of this page)** Unclassified.	**21. No. of Pages** 87	**22. Price** NA

Form DOT F 1700.7 (8-72) **Reproduction of completed page authorized**

COLLECTION OF FREEZE-THAW PERFORMANCE DATA ON VAIL AVENUE

Final Report
August 2017

Principal Investigator
Jeramy C. Ashlock, Associate Professor
Institute for Transportation, Iowa State University

Research Assistant
Cheng Li

Authors
Cheng Li and Jeramy C. Ashlock

Sponsored by
Iowa Department of Transportation
(Iowa DOT Project HR-3013)

Preparation of this report was financed in part
through funds provided by the Iowa Department of Transportation
through its Research Management Agreement with the
Institute for Transportation
(InTrans Project 16-601)

A report from
Institute for Transportation
Iowa State University
2711 South Loop Drive, Suite 4700
Ames, IA 50010-8664
Phone: 515-294-8103 / Fax: 515-294-0467
www.intrans.iastate.edu

TABLE OF CONTENTS

LIST OF FIGURES

LIST OF TABLES

ACKNOWLEDGMENTS

The research project was sponsored by the Iowa Department of Transportation (DOT). The authors would like to acknowledge the assistance of the Hamilton County Secondary Roads Department in documenting the maintenance activities for the test sections, and the Iowa DOT Office of Construction and Materials for conducting the falling weight deflectometer (FWD) tests. The assistance of graduate and undergraduate students Sajjad Satvati, Yijun Wu, HaSung Kim, Ziqaing Xue, Tom Berry, Aleksei Hnastchenko, and Derya Genc in field and laboratory testing is greatly appreciated.

EXECUTIVE SUMMARY

In the recently completed Iowa Highway Research Board (IHRB) project TR-664, Low-Cost Rural Surface Alternatives: Demonstration Project, several stabilization methods for improving the performance of and minimizing freeze-thaw damage on granular-surfaced roads were studied over a two-mile stretch of Vail Avenue in Hamilton County, Iowa. The performance of the stabilized and control sections over the 2013–2014 and 2014–2015 seasonal freeze-thaw periods were assessed using laboratory tests, field tests, visual surveys, subsurface temperature sensors, and a weather station.

The present project was conducted to continue to monitor the performance and document the maintenance costs of the test sections through the 2016–2017 seasonal freeze-thaw period. Performance-based field tests, including dynamic cone penetrometer (DCP), falling weight deflectometer (FWD), and multichannel analysis of surface waves (MASW) tests, were conducted on the sections before freezing in November 2016 and after thawing in April 2017. The surface performance and maintenance costs of the test sections as well as the ground temperatures of the test site were also monitored.

Compared to the winters of 2013–2014 and 2014–2015, that of 2016–2017 was much warmer, with shorter freezing and thawing periods (74 freezing and 8 thawing days), resulting in a much shallower frost penetration depth of 2 ft compared to 4 and 5 ft in the previous winters.

Before freezing, all stabilized surface layers exhibited high California Bearing Ratio (CBR) values above 60%, but the CBR of the fly ash-stabilized surface layer decreased significantly after two years of service. Due to the relatively warmer and shorter winter of 2016–2017, the CBR values of most sections did not decrease significantly after thawing. As observed in the TR-664 study, the CBR values of the subgrades beneath the macadam-based sections continued to be approximately twice those of the non-macadam sections in both pre-freezing and post-thawing tests.

In general, the 2016–2017 pre-freezing and post-thawing FWD tests showed that the stiffnesses of most sections decreased after thawing, except for the clean macadam sections (Section 5 and 6), whose stiffnesses remained nearly constant. Compared to the 2013–2014 and 2014–2015 test results, the stiffness reductions from fall 2016 to spring 2017 were smaller due to the relatively shorter freezing and thawing periods, shallower frost penetration depth, and lower levels of precipitation. Similar to the CBR results, the FWD tests on the macadam sections yielded composite stiffnesses that were still approximately twice those of the non-macadam sections, with the recycled portland cement concrete (RPCC) macadam sections yielding the highest average surface course modulus due to continued hydration of the portland cement in the recycled materials. In contrast, the fly ash- and cement-treated sections suffered significant reductions in stiffness two years after construction.

The results of the MASW tests exhibited trends that were in close agreement with those of the FWD tests and therefore support the conclusions drawn from the FWD tests.

Maintenance activities were recorded by the Hamilton County Secondary Roads Department. The sections were bladed by motor grader only two to three times each year, except for one instance in which a total of 640 tons of fresh rock was dumped to resurface the entire two-mile stretch of test sections. Based on the newly collected maintenance data, the recalculated break-even periods for the various stabilization methods were approximately the same as those determined in the TR-664 report.

Survey photos taken during the 2016–2017 freeze-thaw periods showed that all of the stabilized sections yielded much less rutting than the control sections during the thawing period. However, many potholes appeared on the stabilized sections with stronger base layers (i.e., the macadam and chemically stabilized sections). This behavior was not observed in the 2014 and 2015 thawing periods. The formation of potholes in these sections may be attributable to the gradation and quality of the new surfacing materials and non-uniform support conditions in the stiffer base layers. Further study is needed to better understand the mechanism of the observed increase in potholes in these sections.

CHAPTER 1. INTRODUCTION

The Iowa Highway Research Board (IHRB) Phase I project TR-632, Low-Cost Rural Surface Alternatives: Literature Review and Recommendations, produced a comprehensive literature review to assess cost-effective technologies and geomaterials for improving the performance of and mitigating freeze-thaw damage on low-volume roads (White and Vennapusa 2013). Based on the recommendations of the TR-632 project, the recently completed IHRB project TR-664, Low-Cost Rural Surface Alternatives: Demonstration Project, featured the design, construction, and monitoring of 17 stabilized demonstration sections over a two-mile stretch of the heavily used granular-surfaced Vail Avenue in Hamilton County, Iowa. A total of nine different geomaterials, three chemical stabilizers, and four types of geosynthetics were used to mechanically or chemically stabilize the various sections. The construction procedures, costs, and performance of the test sections were documented in the TR-664 project report (Li et al. 2015). Statistical analyses were also conducted on the field test data to evaluate the relative effectiveness of the different stabilization methods (Li et al. 2017b).

To continue to evaluate the performance and durability and document the maintenance costs of the test sections, field tests were conducted before freezing in November 2016 and after thawing in April 2017. Field tests, including multichannel analysis of surface waves (MASW), falling weight deflectometer (FWD), and dynamic cone penetrometer (DCP) tests, were conducted on all of the test sections. The surface performance and maintenance costs of the sections as well as the subgrade temperature profile of the test site were also monitored. Based on the newly collected field testing and maintenance cost data, the relative mechanistic performance and service lives of the different stabilization methods could be more accurately predicted.

1.1 Project Goals, Objectives, and Scope

The goals of this project were to continue to perform in situ tests and visual surveys and collect maintenance, weather, and subgrade temperature data over the 2016–2017 freeze-thaw cycle in order to further quantify the performance of the demonstration sections. These data were used to reassess the relative performance of the different stabilization methods, enabling more accurate long-term predictions of performance and maintenance costs and providing continuity with subsequent phases of this research.

The specific objectives of the project were as follows:

1. Perform additional field tests, including DCP, MASW, and FWD tests, to monitor the mechanical performance of the test sections.
2. Perform visual surveys to document any rutting, potholes, washboarding, frost heave, or other damage or distress.
3. Collect subgrade temperature data from the embedded thermocouples and weather data from the weather station installed at the site.
4. Document maintenance activities and costs.
5. Use the data to reassess the relative performance and projected life-cycle maintenance costs of the different stabilization methods.

1.2 Benefits of the Research

The long-term benefits of the multiple-phase demonstration project are to improve the quality, longevity, and state of good repair of Iowa roadways, which constitute a vital component of Iowa's infrastructure. The continuously collected field data can provide a better understanding of the longer-term performance, costs, and benefits of the various stabilization methods for granular-surfaced road systems. As a result, county engineers will have improved information that they can use to decide on stabilization methods to help prevent and minimize damage due to frost boils and moisture-related damage on unbound granular roads.

1.3 Organization of the Report

Chapter 2 contains the field testing and data analysis methods used in this study. Chapter 3 presents the weather and ground temperature data, maintenance costs, pre-freezing and post-thawing field test results, and surface performance of the test sections. Conclusions and recommendations are provided in Chapter 4, and raw field testing data and visual survey photos are summarized in the appendices.

CHAPTER 2. FIELD TESTING METHODS

Field tests used to determine the shear strength and stiffness of the various demonstration sections are detailed in the following sections.

2.1 Dynamic Cone Penetrometer Test

DCP tests were performed in accordance with ASTM D6951-09, Standard Test Method for Use of the Dynamic Cone Penetrometer in Shallow Pavement Applications, to estimate the shear strength of the surface course and subgrade materials. According to ASTM D 6951-09, DCP tests should not be used for testing granular materials containing a large percentage of aggregates greater than 2 in. in size. Therefore, the DCP tests for the macadam stone-based sections in the first mile were performed in boreholes drilled through the macadam base layers, as shown in Figure 1.

Figure 1. Dynamic cone penetrometer test: (a) drilling through macadam base layers and (b) performing the DCP test

The dynamic cone penetrometer index (DCPI), with units of inches per blow, was measured for the various demonstration sections and used in the empirical correlations of equations (1) through (3) to estimate the in situ California Bearing Ratio (CBR) values (referred to as DCP-CBR):

for all soils except CL soils with CBR < 10 and CH soils, $DCP\text{-}CBR = 292 / (DCPI \times 25.4)^{1.12}$ (1)

for CL soils with CBR < 10, $DCP\text{-}CBR = 1 / (0.432283 \times DCPI)^2$ (2)

for CH soils, $DCP\text{-}CBR = 1/(0.072923 \times DCPI)$ (3)

In this project, all of the demonstration sections were analyzed as two-layered systems consisting of a surface aggregate layer on top of a subgrade layer. Based on the DCP test results, the boundary between the two layers was identified by a sudden change in the slope of the depth profiles, as shown in Figure 2.

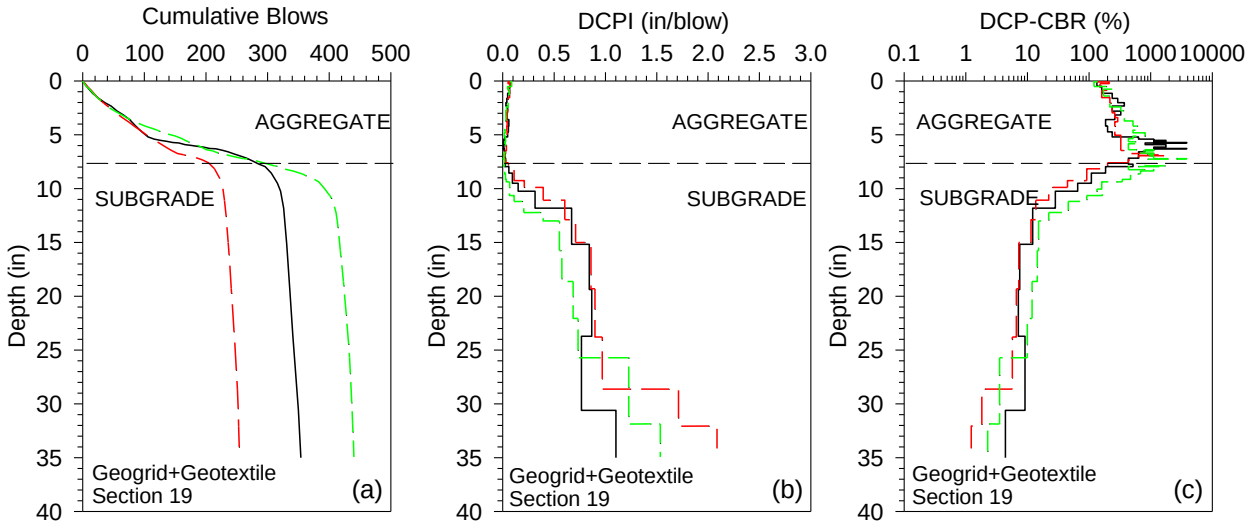

Figure 2. Example of DCP depth profiles: (a) cumulative blows, (b) DCPI, and (c) DCP-CBR

The weighted-average CBR of each material layer can also be calculated using equation (4). The notation $DCP\text{-}CBR_{AGG}$ is used to denote the weighted-average CBR of the surface aggregate layer, and $DCP\text{-}CBR_{SG}$ represents the weighted-average CBR of the subgrade over a depth of 18 in. below the interface of the surface aggregate and subgrade.

$$\text{Weighted-average } CBR = \frac{(CBR_i \times H_i) + (CBR_{i+1} \times H_{i+1}) \cdots (CBR_n \times H_n)}{\sum_i^n H} \quad (4)$$

2.2 Falling Weight Deflectometer Test

FWD tests were conducted to determine the stiffness of the test sections. A Kuab FWD device with an 11.81 in. segmented loading plate was used in project TR-664, but that device is no longer available. Therefore, the FWD tests in the present project were conducted by the Iowa DOT Office of Construction and Materials using a JILS-20 FWD with a 12 in. diameter rigid loading plate. The measurement ranges of the JILS FWD deflection sensors are much smaller than those of the Kuab sensors, so the maximum impact load for the post-thawing tests was limited to approximately 4,000 lbs for the second-mile sections to avoid overloading the sensors.

A single equivalent composite elastic modulus was calculated for each test location system using equation (5):

$$E_{FWD-Composite} = \frac{\left(1-\nu^2\right)\sigma_0 A}{d_0} \times f \quad (5)$$

where

$E_{FWD-Composite}$= composite elastic modulus (psi)
d_0 = measured deflection under the center of the loading plate (in.)
ν = Poisson's ratio (assumed to be 0.4)
σ_0 = normalized applied peak stress (psi)
A = radius of the plate (in.)
f = shape factor, assumed to be 8/3 because the rigid loading plate can result in a parabolic stress distribution on cohesionless materials (Vennapusa and White 2009)

The FWD test data were also used to calculate separate elastic moduli for the surface course and subgrade layers using the approach in the AASHTO Guide for the Design of Pavement Structures (AASHTO 1993). The AASHTO approach for calculating the moduli of a two-layered system is based on the equivalent layer theory and is detailed in Li et al. (2015).

2.3 Multi-channel Analysis of Surface Waves Test

MASW tests were used to evaluate the stiffness of a multi-layered representation of the test sections at lower strain levels than the FWD test. A 2 lbs ball-peen hammer with an attached accelerometer for triggering was used as a seismic source to impact a 6 in. square by 1 in. thick aluminum plate resting on the road surface to generate the surface waves. The vertical velocity of the surface was measured using an array of 24 4.5 Hz geophone receivers installed on a custom-built land streamer with 6 in. spacing. The testing procedure is detailed in Li et al. (2017a). The lower amount of energy (compared to the energy produced by a larger 10 lbs sledgehammer used in some tests) and close receiver spacing were used to focus the measurements on the surface gravel layer and top few inches of subgrade. The MASW test configuration is summarized in Table 1.

Table 1. Configuration used for the MASW test

Test setup parameter	Value
Source-to-first-receiver offset (x_1)	12 in.
Receiver spacing (d_x)	6 in.
Total number of receivers (N)	24
Total length of receiver spread (X_T)	11.5 ft

The MASW test measures the seismic Rayleigh wave velocity as a function of frequency, from which the shear wave velocity or, alternatively, the small-strain shear modulus (G_{max}) can be determined as a function of depth for the surface course and subgrade (Lin and Ashlock 2011). Data from the MASW tests were used to back-calculate the shear-wave velocity (V_s) profile through an inversion procedure that uses the measured dispersion characteristics of the surface (Rayleigh) wave velocity (V_R) as input. The phase velocity and intercept time scanning (PIS) method was used to generate experimental dispersion images from the MASW test data, and the hybrid genetic-simulated annealing (GSA) inversion procedure was used to back-calculate the layered shear wave velocity profiles. The PIS and GSA methods are detailed in Lin (2014).

The MASW back-calculation procedure typically involves specifying layer unit weights and Poisson's ratios, after which the optimization procedure automatically searches over ranges of layer thicknesses and shear wave velocities to find a best match between the measured and theoretical dispersion images. In this study, however, the thicknesses of the surface layers were set equal to the values determined from the DCP test data, so the back-calculation procedure searched only over a range of layer shear wave velocities. The standard Proctor maximum dry unit weights of the surface aggregate (140 pcf) and subgrade (98 pcf) determined in the previous phase of the project were used for all sections. The Poisson's ratios of the surface aggregate and subgrade material were assumed to be 0.3 and 0.4, respectively.

2.4 Ground Temperature Monitoring

To monitor the local weather conditions, ground temperature, and frost depth of a representative section of Vail Avenue, a weather station (Figure 3[a]) and six subgrade thermocouples (Figure 3[b]) were installed in November 2013. The Novalynx Model 110-WS-16 weather station was installed to record the average ambient air temperature, relative humidity, wind speed and direction, and precipitation at 15-minute intervals. Each of the Type T thermocouples was connected to a separate battery-powered data logger that recorded ground temperatures at 5-minute intervals with a precision of 0.5 °F. The depths of the thermocouples are shown in Figure 3(c). The top sensor is at the boundary between the surface gravel and subgrade, and the bottom sensor is 5 ft below the roadway surface.

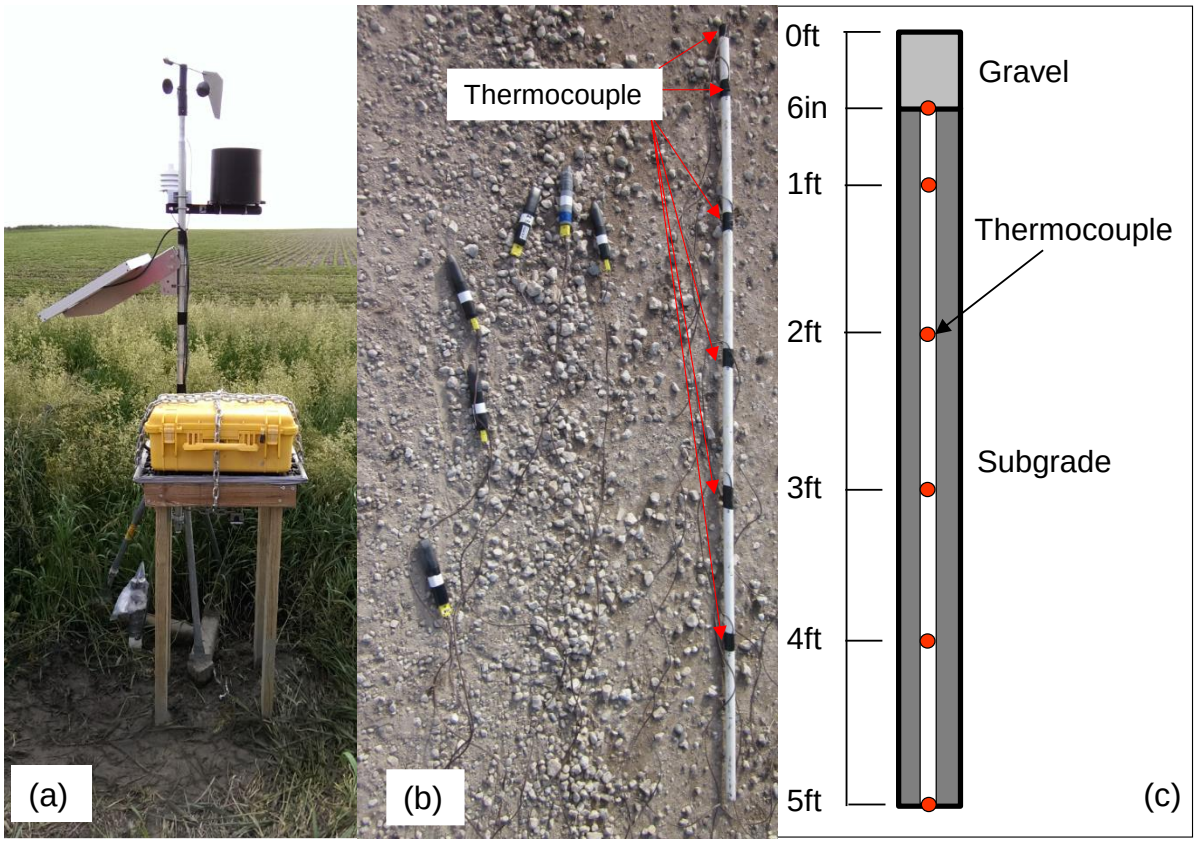

Li et al. 2015, Institute for Transportation

Figure 3. Weather and ground temperature monitoring equipment: (a) weather station, (b) subgrade thermocouples and data loggers, and (c) layout of thermocouples

CHAPTER 3. FIELD TEST RESULTS

The ground temperature, maintenance activities, and mechanical and surface performance of the Vail Avenue test sections were continuously monitored during the 2016–2017 seasonal freeze-thaw period. The nominal as-constructed cross-section profiles of the demonstration sections are shown in Figure 4.

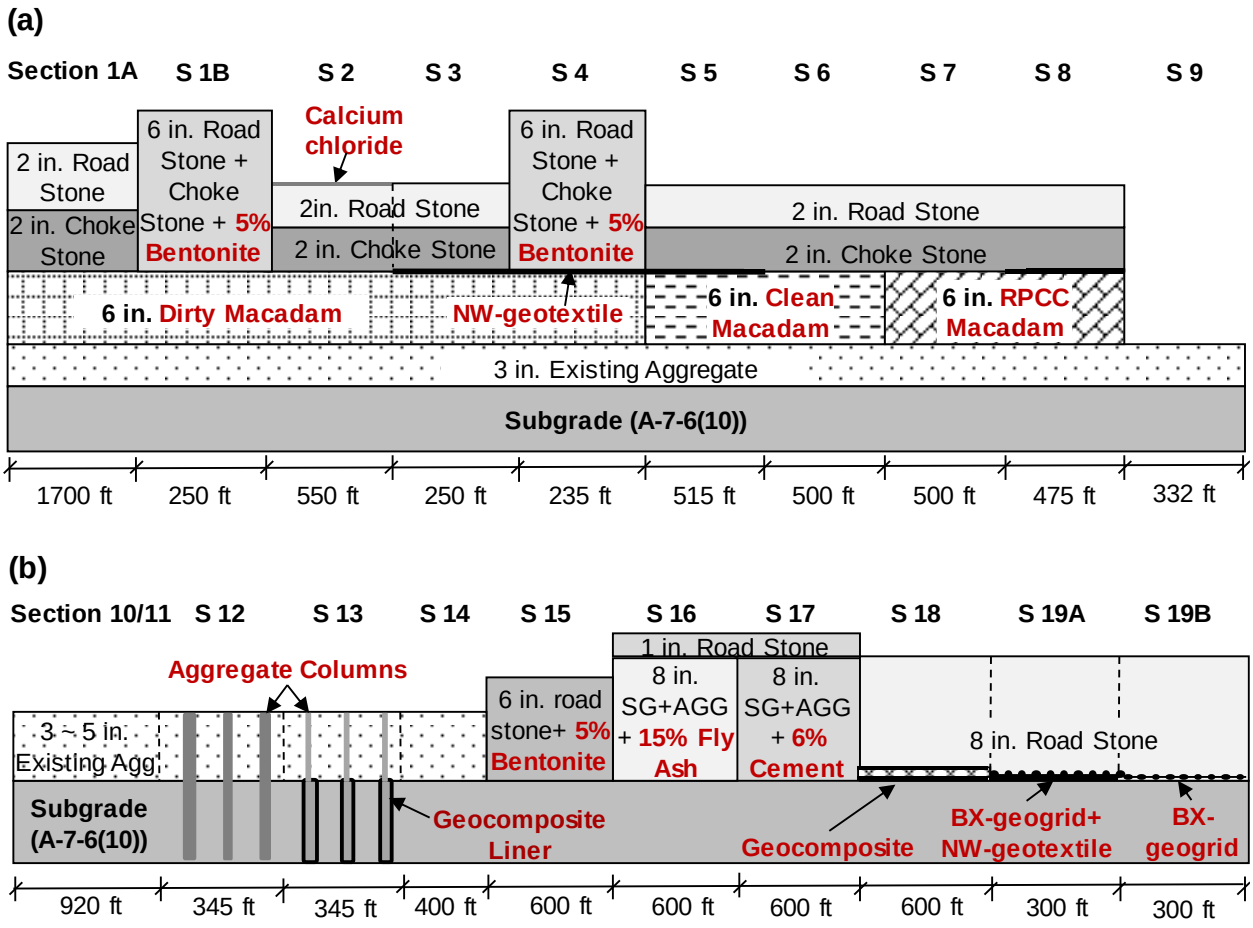

Figure 4. Nominal cross-section profiles of the test sections (not to scale): (a) 1st mile macadam-based stabilization sections and control section and (b) 2nd mile control, mechanically and chemically stabilized sections

The two control sections at the beginning of the second mile from the Phase II study were combined into a single control section in the present study. Additionally, the control section at the end of the second mile was not included in this study because its longitudinal grade is much steeper than that of the other sections.

3.1 Weather and Ground Temperature

Weather conditions and ground temperatures were monitored during the 2016–2017 seasonal free-thaw period, as shown in Figure 5.

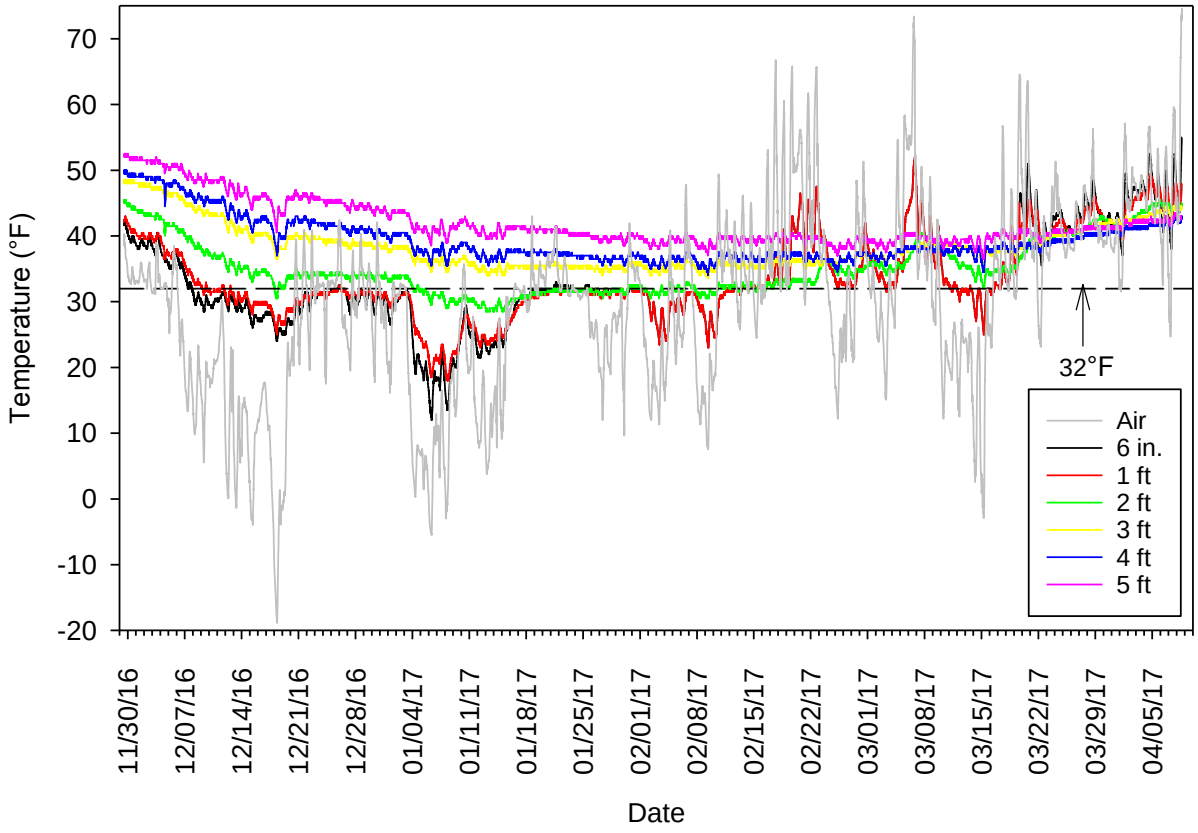

Figure 5. Air and ground temperature data during 2016–2017 seasonal freeze-thaw period

The air temperature first decreased below 32 °F on December 4, 2016, and the lowest air temperature of about -19 °F was reached on December 18, 2016. The air temperature increased and mostly remained above 32 °F after March 20, 2017. During the freezing period, four or five relatively long warm periods were observed.

Using the ground temperature data, the maximum frost penetration depth and the freezing and thawing periods were determined for the test site. The 2016–2017 32 °F isotherm line is compared to the data collected in the previous phase of the project in Figure 6.

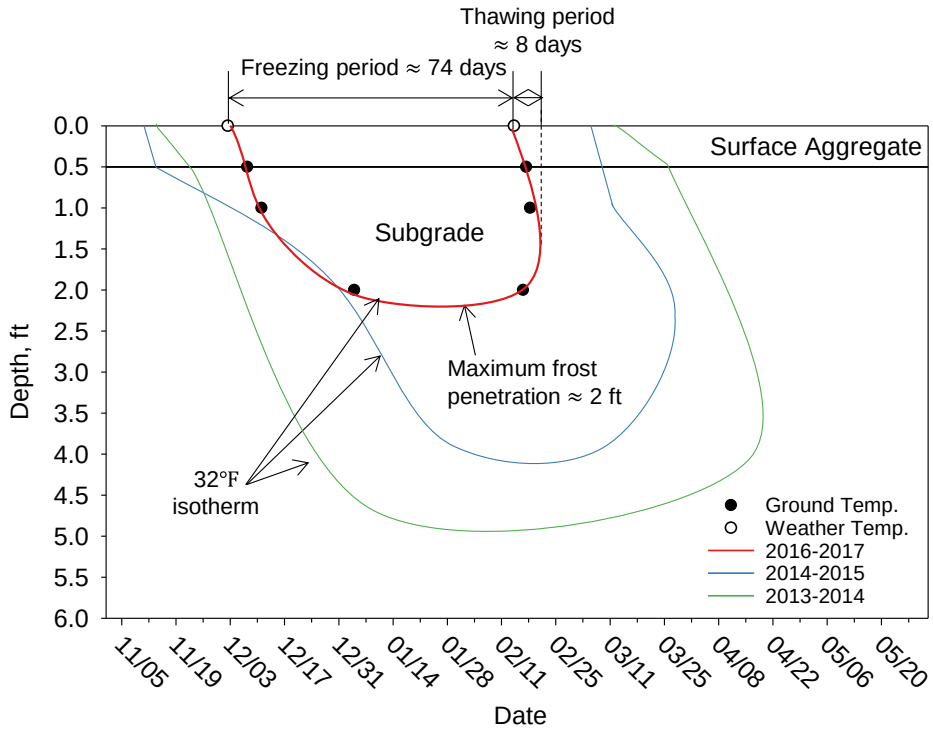

Figure 6. 2016–2017 ground freezing-thawing period of the project site compared with those of 2013–2014 and 2014–2015 winters

Relative to the winters of 2013–2014 and 2014–2015, the maximum frost penetration depth of the milder 2016–2017 winter was much shallower at only 2.25 ft, and the freezing and thawing periods were much shorter. The isotherms reveal that the freezing and thawing periods at the surface were approximately 74 and 8 days, respectively. The freezing period began around December 2, 2016 and progressed to a depth of about 2.25 ft by January 28, 2017. The ground started to thaw from the top down and the bottom up around the same date of February 14 and progressed until the last portion of frozen subgrade at a depth of approximately 1.5 ft thawed around February 21, 2017. The historical ground freezing-thawing data from the site are summarized in Table 2.

Table 2. Summary of measured ground freezing-thawing periods

Year	Max frost depth (ft)	Freezing period (days)	Thawing period (days)	Date of 1st freeze	Date of last thaw	Depth of last thaw (ft)
2013-2014	5+	119	40	Nov 13	Apr 21	3.75
2014-2015	4	116	23	Nov 15	Mar 30	2.5
2016-2017	2.25	74	8	Dec 8	Mar 17	1.5

Rainfall data were also recorded during the project. The cumulative precipitation at the site one month before the post-thawing field testing was 0.7 in., which is much lower than the cumulative precipitations of the same period in 2014 (12.88 in.) and 2015 (2.04 in.).

3.2 Maintenance Records

Maintenance activities for the test sections from the end of the Phase II project to May 15, 2017 were documented by the Hamilton County Secondary Roads Department. Based on the updated maintenance records, the break-even periods of the various stabilization methods relative to the costs of continuing the pre-2013 maintenance practice were recalculated and are shown in Figure 7.

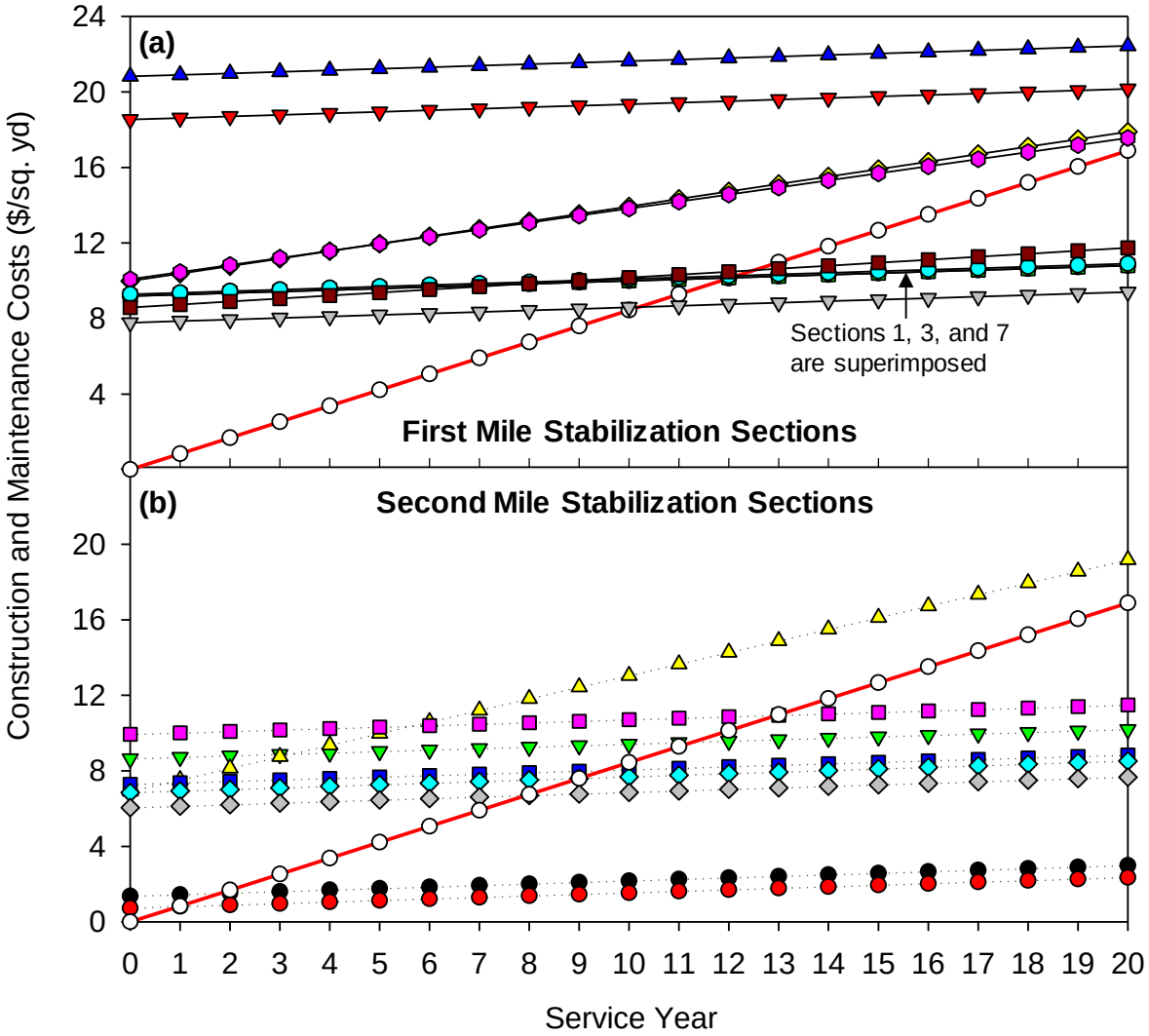

Section #	Break-Even Period
1A	12
1B	>20
2	12
3	>20
4	>20
5	>20
6	12
7	10
8	12
12	2
13	1
15	11
16	>20
17	9
18	12
19A	9
19B	8

Figure 7. Estimated break-even periods of the (a) 1st mile and (b) 2nd mile test sections

The cost shown at 0 years is the construction cost for each section. This cost is $0 for the continuation of pre-2013 maintenance practices (which is not adjusted for inflation because the construction costs were from 2013 and 2014). The slopes of the projected cumulative costs changed only slightly, such that the updated break-even periods are approximately the same as those calculated in the previous phase of the project (TR-664). The projected costs of the macadam sections containing bentonite or nonwoven geotextile changed somewhat, but their break-even periods remained consistent beyond 20 years. The only break-even periods below 20 years that changed based on the updated data were for the dirty macadam section (Section 1A), which increased from 11 to 12 years, and for RPCC macadam with nonwoven geotextile section (Section 8), which decreased from 13 to 12 years. Details and related costs associated with the maintenance activities are summarized in Table 3.

Table 3. Maintenance records and estimated costs of the test sections

Date	Section #	Material Cost	Equipment Cost	Labor Cost	Total Cost	Notes
5/19/2015	Control Sections	$0	$16	$8	$24	Bladed road from the weather station south to station 4975 for 15 minutes.
5/19/2015	Geotextile + Geogrid Section 19A	$300	$48	$23	$371	Hauled 1 load of rock between station 9707 and station 1007 and bladed for 15 minutes.
6/4/2015	All	$0	$64	$31	$95	Spent 1 hour blading the two miles of sections
11/19/2015	All	$0	$48	$23	$71	Bladed the two miles for 45 minutes.
4/1/2016	All	$8,873	$385	$186	$9,443	Hauled 640 T of 1 in. Road Stone to the two-mile research project. Total material cost was $8,872.60.
10/27/2016	All	$0	$85	$41	$126	Pulled in both sides of the whole two miles. Two rounds at 40 minutes per mile.
3/6/2017	All	$0	$64	$31	$95	Bladed the two miles of this road for 1 hour to get rid of some potholes.
4/14/2017	All	$0	$32	$16	$48	Spent 1.5 hours blading the two miles. One load of rock was added to the control Section 10.
5/12/2017	All	$0	$96	$47	$143	Spent 1.5 hours to fix potholes

In 2015, two routine motor grader bladings were performed on all of the test sections, and one truckload of rock was dumped to cover the exposed geosynthetic of the bi-axial geogrid with nonwoven geotextile section (Section 19A). In 2016, a total of 640 tons of 1 in. road stone was spread on all of the test sections due to material degradation of the wearing surface. Only one

blading was performed in October 2016 on all of the sections. During the 2017 thawing period, three bladings were performed to fix potholes in the test sections, which are shown and discussed in the survey photo section of this chapter. Based on the maintenance records, it can be concluded that all of the stabilized sections performed satisfactorily, but the wearing surface material degraded significantly after three years of service.

3.3 Changes in Thickness and Shear Strength of the Test Sections

The DCP tests were used to estimate the thicknesses of the surface aggregate layers as well as the CBR values of both the surface aggregate layers and subgrade. These pre-freezing and post-thawing DCP tests were conducted in November 2016 and April 2017, respectively. All of the DCP depth profiles are summarized in Appendix A and Appendix B. The average thicknesses of the surface aggregate layers and weighted-average CBR values of the surface and subgrade materials are compared in Table 4.

Table 4. 2016–2017 pre-freezing and post-thawing DCP test results

Section No.	Section Name	Surface Layer Thickness (in)			Weighted-average CBR_{AGG} (%)			Weighted-average CBR_{SG} (%)		
		Pre-freezing	Post-thawing	Change (Post-Pre)	Pre-freezing	Post-thawing	Change (Post-Pre)	Pre-freezing	Post-thawing	Change (Post-Pre)
1A	Dirty Macadam	16	17	1				15.6	13.8	-1.8
1B	Dirty Macadam + Bentonite	18	18	0				23.9	17.4	-6.5
2	Dirty Macadam + Calcium Chloride	16	18	2				19.9	13.4	-6.4
3	Dirty Macadam + Bentonite + Geotextile	14	13	0				24.9	15.6	-9.3
4	Dirty Macadam + NW geotextile	17	17	0		NA		28.3	16.8	-11.6
5	Clean Macadam + NW geotextile	16	15	-1				13.5	10.3	-3.2
6	Clean Macadam	14	14	0				29.7	13.0	-16.7
7	RPCC Macadam	15	16	1				17.9	14.9	-3.0
8	RPCC Macadam + NW geotextile	14	14	1				19.1	14.0	-5.0
9	Control	7	5	-2	63.4	116.0	52.5	11.6	9.2	-2.3
10 & 11	Control	6	8	1	148.9	117.2	-31.6	7.9	4.6	-3.3
12	Aggregate Columns + Geocomp. Linings	5	5	0	307.8	73.8	-234.0	12.1	3.6	-8.4
13	Aggregate Columns	4	4	0	81.1	49.9	-31.2	15.0	7.1	-8.0
14	Control	3	3	0	39.2	21.8	-17.5	9.4	4.7	-4.7
15	5% Bentonite	6	5	-1	62.7	54.0	-8.7	9.5	6.5	-3.0
16	15% Fly Ash	11	11	0	69.3	54.3	-15.0	8.9	13.4	4.5
17	6% Cement	12	11	-1	101.2	78.1	-23.1	8.0	15.6	7.5
18	Geocomposite Drainage Layer	6	6	0	80.1	103.7	23.6	8.3	17.3	9.1
19A	BX-Geogrid + NW-Geotextile	10	11	1	392.5	286.3	-106.2	14.0	9.1	-4.9
19B	BX-Geogrid	7	7	0	258.1	200.5	-57.6	10.9	6.8	-4.1

NA: CBR_{AGG} cannot be determined for the macadam base layers because their nominal aggregate sizes are larger than 2 in.

Outliers that exhibited significantly different values from other locations within the same test section were excluded for calculating the average values. The average surface layer thicknesses in the pre-freezing and post-thawing tests were very close. However, the DCP-measured thicknesses are 2 to 3 in. thicker than the nominal as-constructed cross-section profiles (Figure 4), possibly due to adding the fresh resurfacing aggregate. Additionally, the differences may be caused by the test itself, because the stiff top layer of the subgrade usually has similar shear strength to that of the aggregate material.

For the pre-freezing DCP tests, most sections had very high CBR_{AGG} values greater than 60%, except for the control section (Section 14). The average CBR_{AGG} of the fly ash-stabilized section was lower than those of the other sections, which indicates that the stabilization effect of the fly ash significantly degraded after two years of service. The aggregate columns with geocomposite section (Section 12) and bi-axial geogrid stabilized sections (Sections 19A and 19B) yielded pre-freezing CBR_{AGG} values that were more than twice those of the other sections.

After thawing, most sections did not show significantly lower CBR values due to the relatively warmer and shorter winter. One exception was the aggregate columns with geocomposite lining section (Section 12), for which the CBR_{AGG} decreased by 234%. This decrease may be a result of this section being installed next to the drainage tile crossing. Even after the 234% decrease, the post-thawing CBR_{AGG} of this section was still approximately 50% higher than that of the aggregate columns without geocomposite liners section (Section 13). For the subgrade, the CBR_{SG} of the macadam sections generally continued to be higher than those of all other sections for both the pre-freezing and post-thawing tests, as was found in the TR-664 study. In addition, the CBR_{SG} of the fly ash, cement, and geocomposite drainage layer sections increased slightly from the pre-freezing to the post-thawing tests, a trend that was not observed for any other sections.

3.4 Changes in Stiffness of the Test Sections

The FWD and MASW tests were conducted to determine the stiffness changes of the test sections.

3.4.1 Falling Weight Deflectometer Test Results

To determine the changes in stiffness of the test sections from the 2014 pre-freezing to the 2017 pre-freezing periods, the FWD test results are compared in Figure 8.

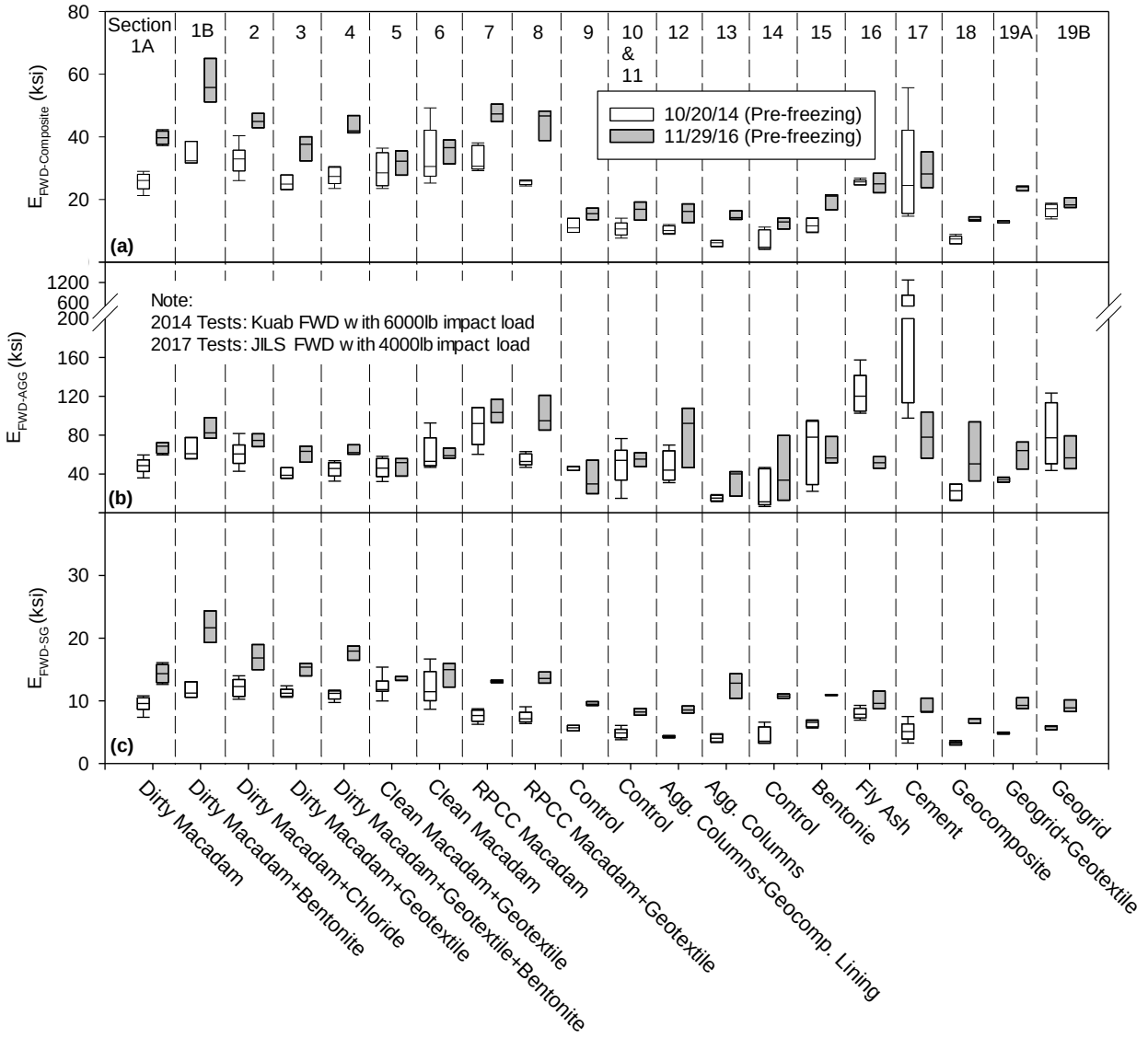

Figure 8. Comparison of 2014 and 2017 pre-freezing FWD test results

The results show that the 2017 composite modulus ($E_{FWD\text{-}Composite}$), surface aggregate modulus ($E_{FWD\text{-}AGG}$), and subgrade modulus ($E_{FWD\text{-}SG}$) values are higher than those from the 2014 test results for most of the test sections. The differences are expected due to the different weather, moisture, and temperature conditions. In addition, two different FWD devices were used, as described above, with the impact load applied by the new device reduced to 4,000 lbs from the lowest impact load (6,000 lbs) applied by the previous FWD device in order to avoid overloading the sensors of the new device, which had a smaller measurement range. This reduction in impact load can result in higher elastic modulus values due to the nonlinear dependence of modulus on strain level for geomaterials. However, the relative trends of the two groups of test results are similar from section to section.

The $E_{FWD\text{-}Composite}$ values of the macadam stone-based sections are approximately twice those of other sections, which is consistent with the findings of the TR-664 study. For the surface aggregate layer, the $E_{FWD\text{-}AGG}$ values generally increased between the 2014 and 2017 measurements for most of the sections. However, the fly ash- and cement-treated sections both exhibited significant modulus reductions in their aggregate layers over the three-year span. The RPCC macadam sections showed some of the greatest increases in $E_{FWD\text{-}AGG}$ values among all of the sections, likely due to continuous hydration of the portland cement, which may be a long-term benefit of using recycled PCC materials. The dirty macadam sections also showed significant increases in $E_{FWD\text{-}AGG}$ values.

The 2016–2017 pre-freezing and post-thawing FWD tests were conducted using the same JILS FWD device on November 29, 2016 and April 13, 2017, respectively. A heavy rainfall event occurred one day before the post-thawing FWD test, so the surface materials were very wet and in a weakened state. The test results are provided in Appendix C and compared using statistical box plots in Figure 9.

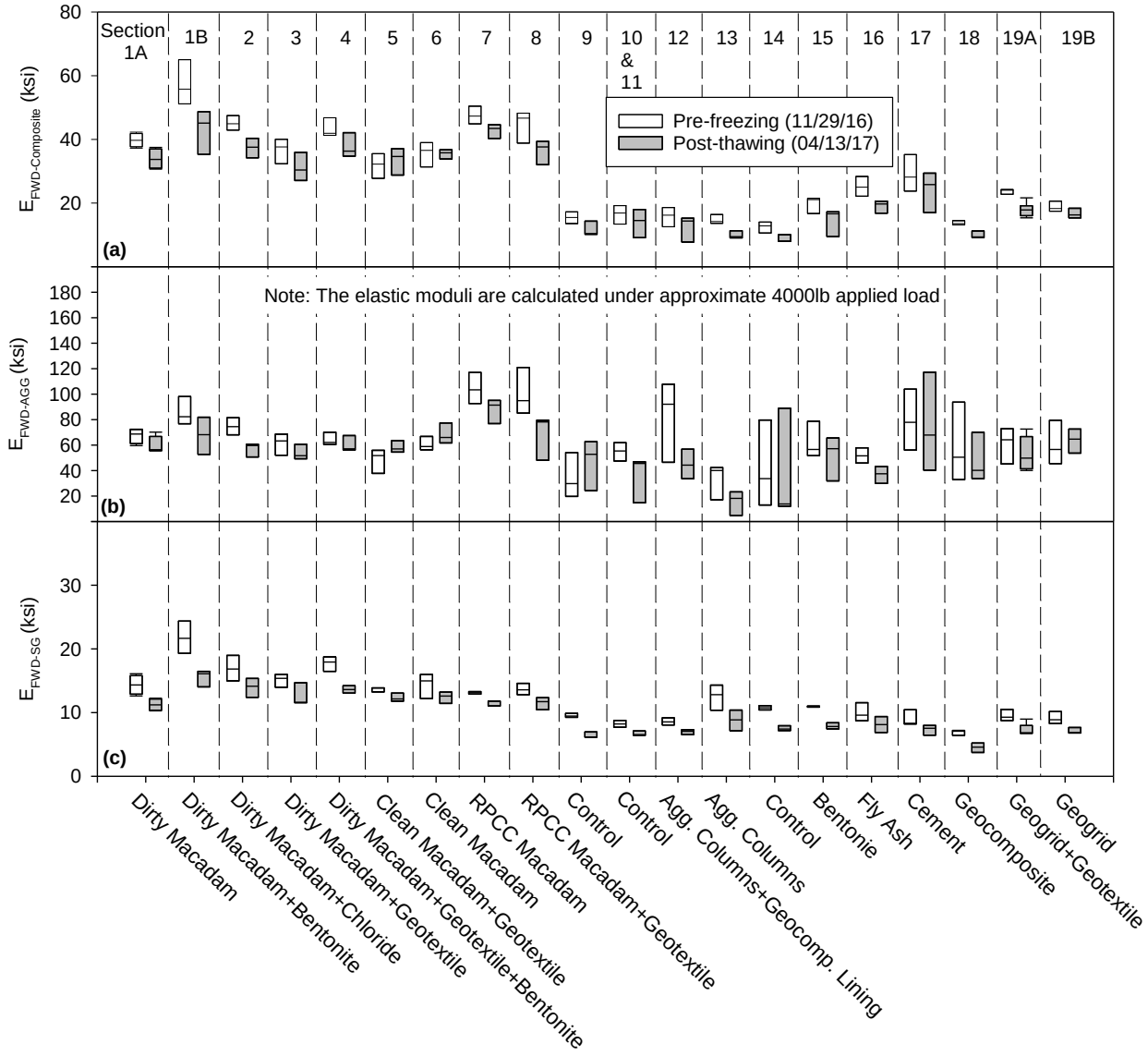

Figure 9. Comparison of 2016–2017 pre-freezing and post-thawing FWD test results

The FWD test results show very repeatable trends between the two test periods. The $E_{FWD\text{-}Composite}$ values decreased after thawing for most sections, except for the clean macadam sections (Sections 5 and 6), which remained almost unchanged. Both the surface aggregate layer $E_{FWD\text{-}AGG}$ and subgrade $E_{FWD\text{-}SG}$ values generally decreased after the 2016–2017 seasonal freeze-thaw period. However, compared to the test results of the 2013–2014 and 2014–2015 seasons, the reductions are smaller due to the relatively short freezing-thawing periods, shallower frost penetration depth, and lower levels of precipitation in 2016–2017.

3.4.2 Multichannel Analysis of Surface Waves Test Results

The MASW test is a nondestructive geophysical method for assessing the elastic modulus of multi-layered soil and pavement systems. In the Phase II project, the feasibility of using the

MASW test on granular-surfaced road systems was evaluated and compared to the feasibility of using the FWD test. The comparison revealed that the MASW test used with recently developed data analysis methods and a custom-built land streamer was capable of measuring multi-layered elastic moduli of granular-surfaced road systems (Li et al. 2017a). In the present study, MASW tests were again conducted for both the pre-freezing and post-thawing conditions. The dispersion images of the MASW tests are provided in Appendices D and E, and the corresponding pre-freezing and post-thawing moduli are compared in Figure 10. The surface and subgrade moduli of the macadam sections experienced much smaller reductions after thawing than the other sections, and the subgrade moduli of the macadam sections were also generally higher than those of most other sections.

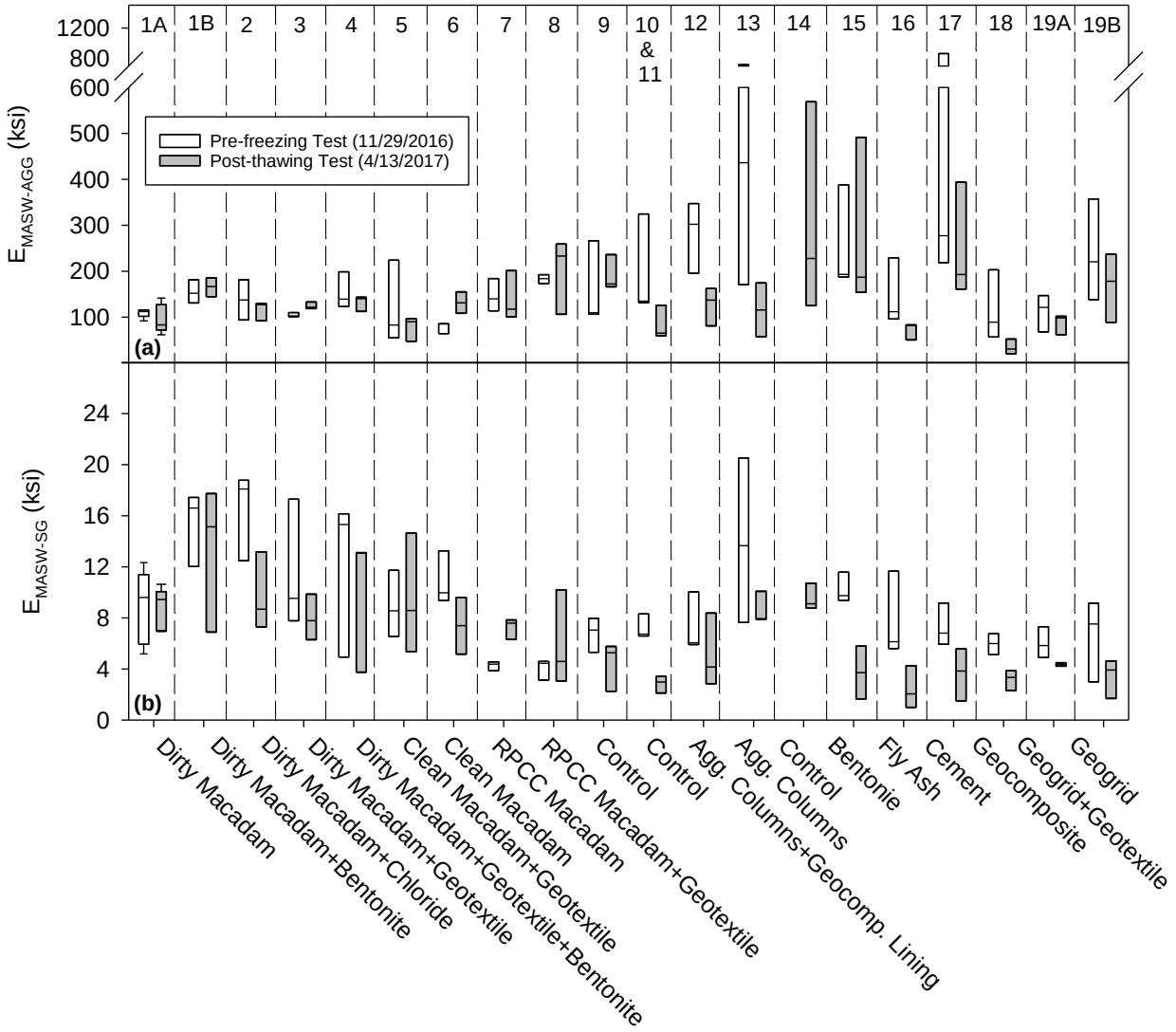

Figure 10. Comparison of 2016–2017 pre-freezing and post-thawing MASW test results

In the present study, MASW tests were conducted at the same times and locations as the FWD tests. The 2016–2017 MASW and FWD test results are compared in Figure 11 through Figure 14.

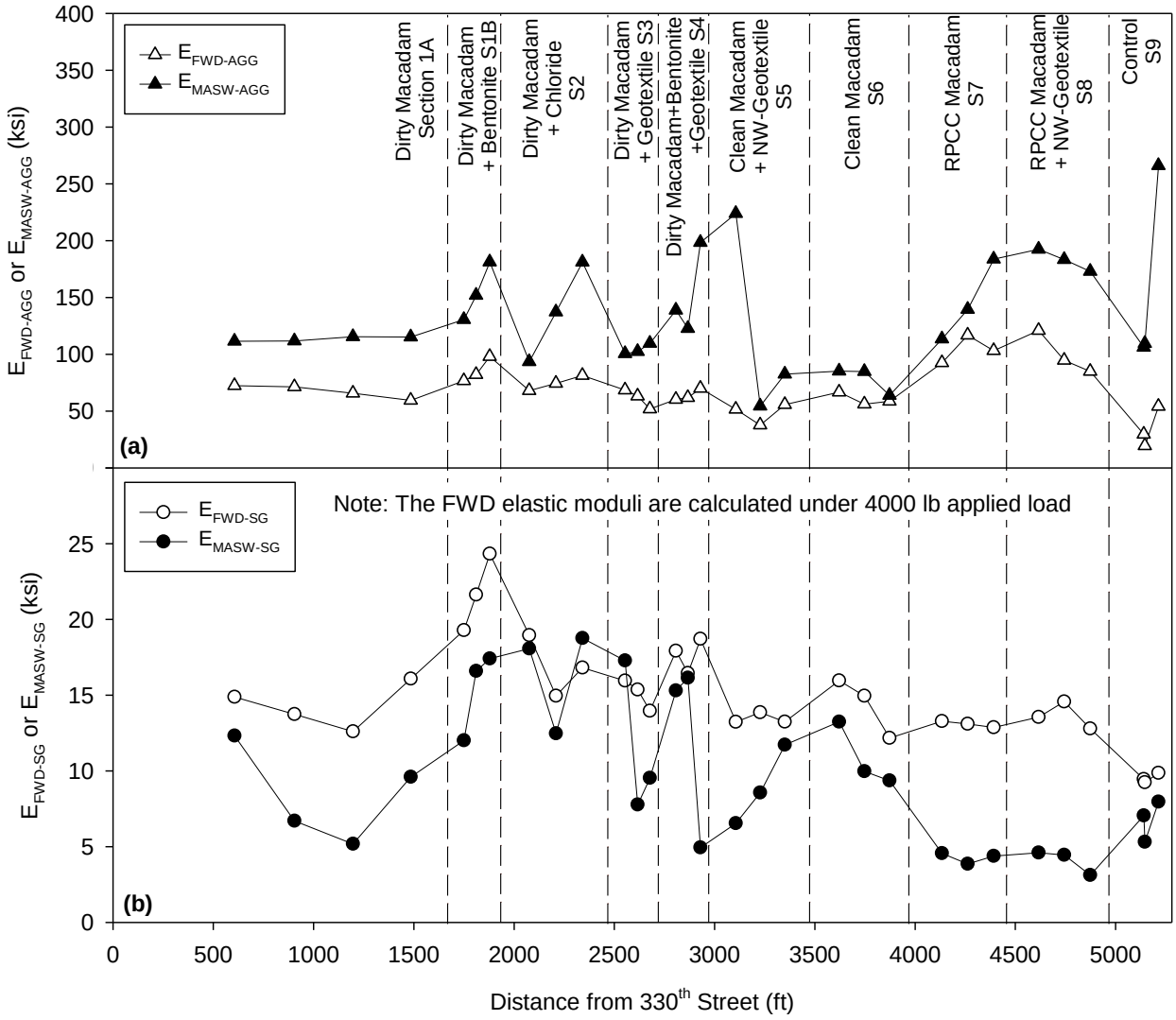

Figure 11. Comparison of 2016 pre-freezing MASW and FWD test results for the first mile sections

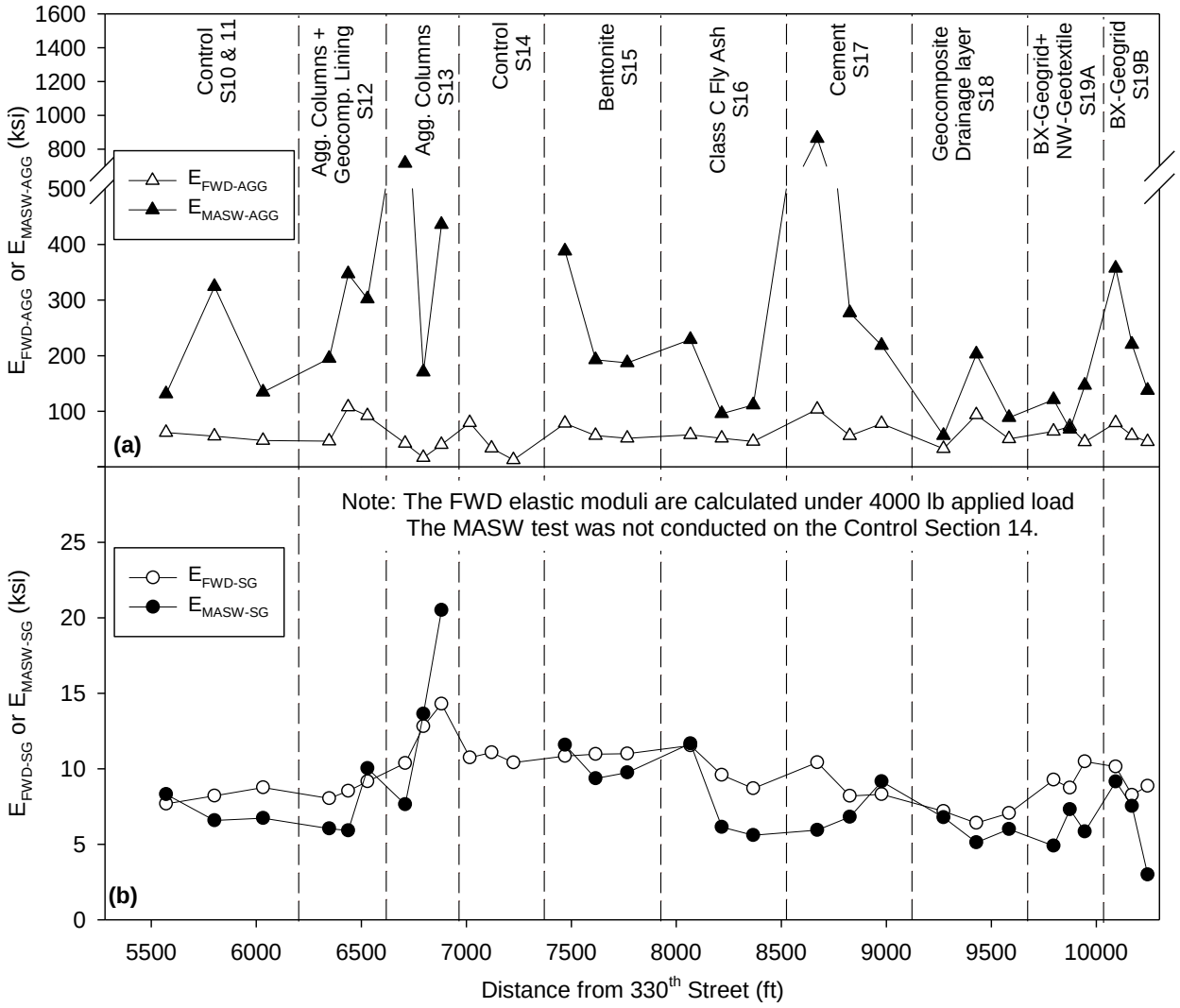

Figure 12. Comparison of 2016 pre-freezing MASW and FWD test results for the second mile sections

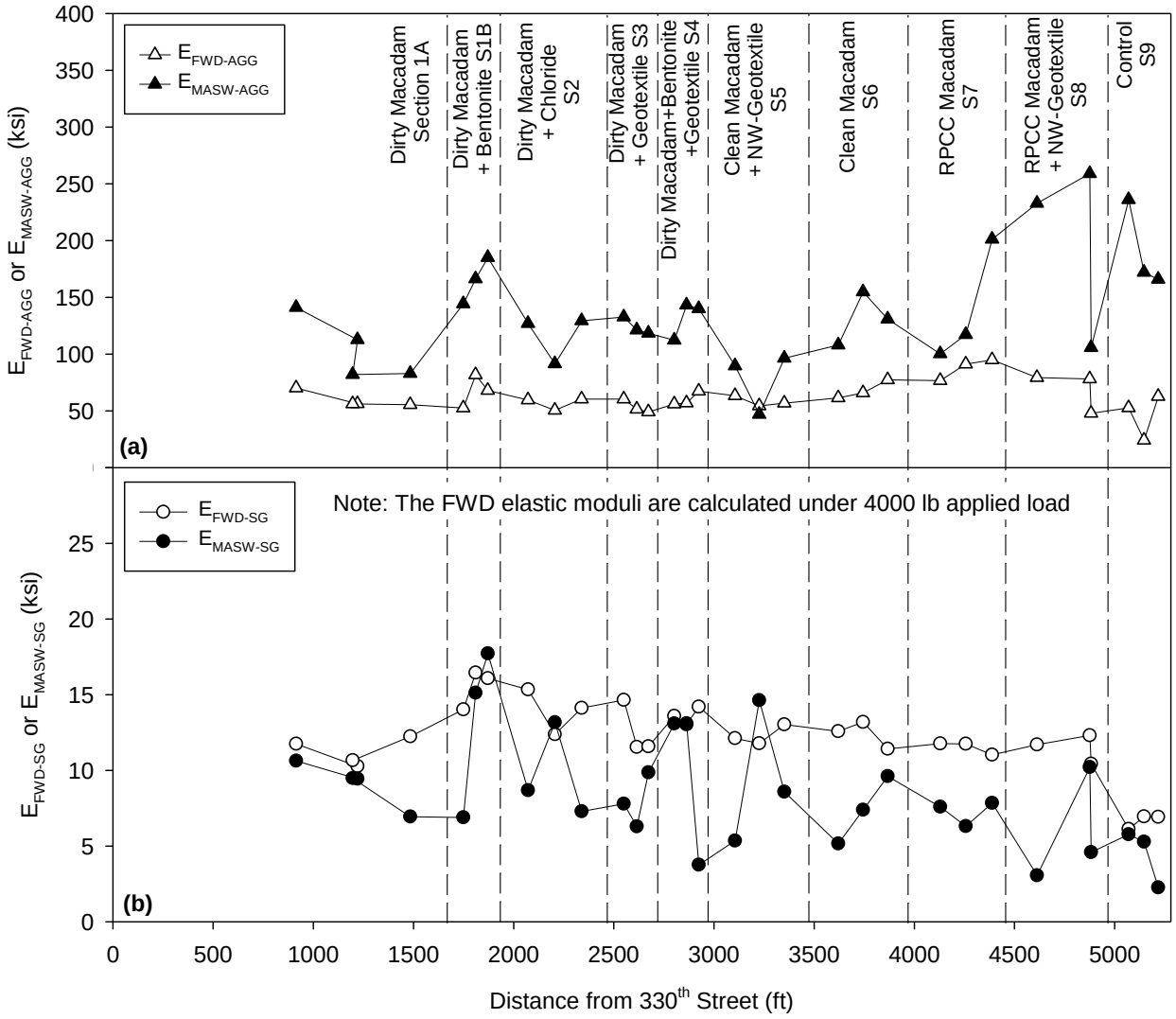

Figure 13. Comparison of 2017 post-thawing MASW and FWD test results for the first mile sections

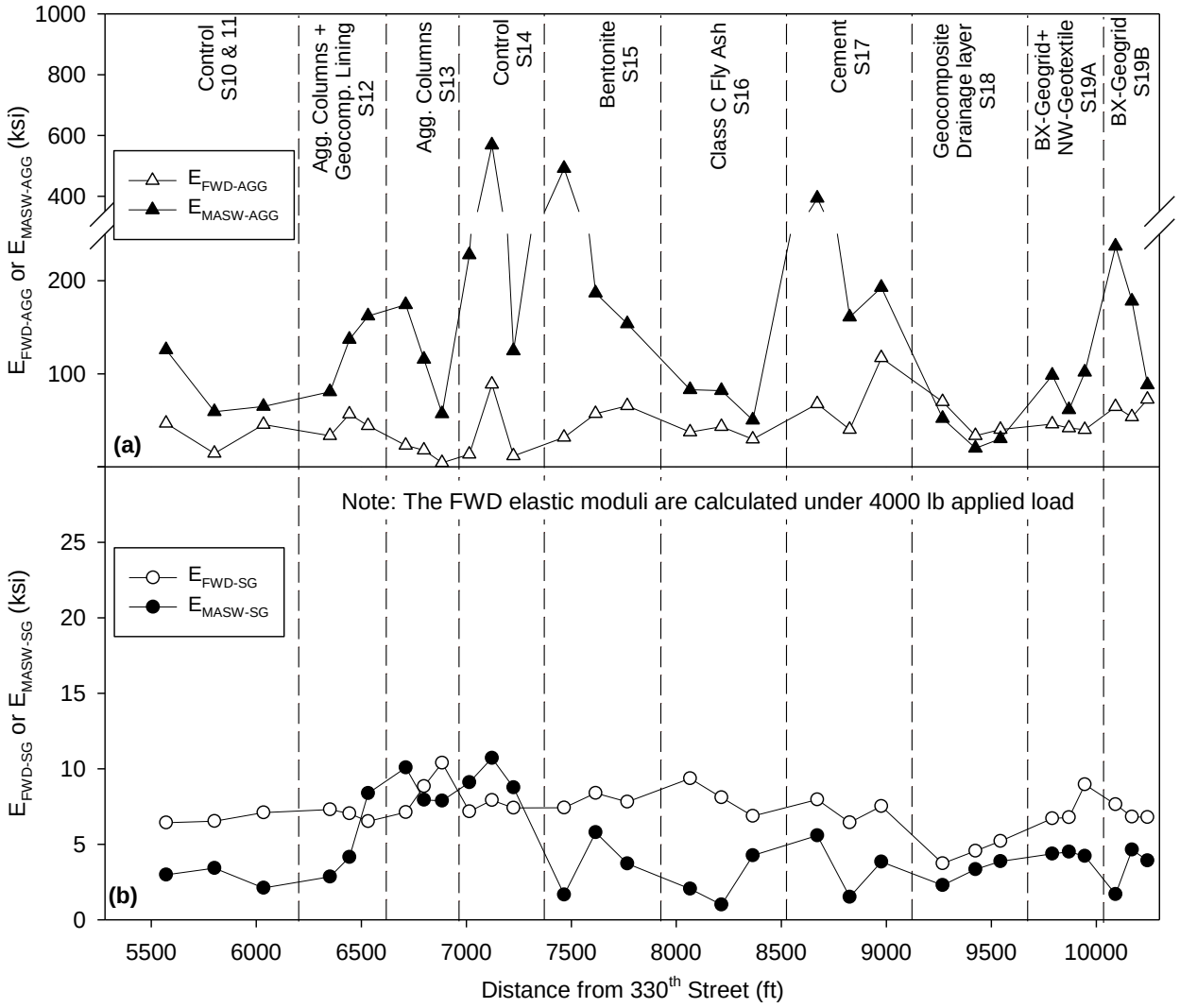

Figure 14. Comparison of 2017 post-thawing MASW and FWD test results for the second mile sections

As Figure 11 through Figure 14 show, in the TR-664 study the subgrade modulus values determined using the MASW test showed significantly greater variation than those of the FWD test. However, in the present study the two different testing methods show very similar trends for both the surface and subgrade materials.

For the surface aggregate layers, the MASW modulus values are much higher than those obtained from the FWD test, as is expected due to the lower strain levels induced in the MASW test. However, the MASW subgrade modulus values are of similar magnitude but overall slightly lower than those obtained from the FWD test, possibly due to the different measurement influence depths of the testing methods. Further study is being conducted to verify this hypothesis.

3.5 Survey Photos of the Test Sections

To monitor the surface conditions and performance of the test sections, survey photographs were taken during the 2015–2016 and 2016–2017 seasonal freeze-thaw periods. One group of survey photos taken on February 19, 2016 shows that the aggregate columns, fly ash- and cement-stabilized, and geosynthetic sections performed very well during the 2016 thawing period, while significant rutting and frost boils were observed for the control sections (Figure 15). All of the macadam stone-based sections on the first mile of test sections showed no surface damage, but survey photos were not taken at the time.

Figure 15. Survey photos of Sections 10 through 20 taken on February 19, 2016

For the 2016–2017 freeze-thaw period, a total of four groups of survey photos was taken. The pre-freezing surface conditions of the test sections are shown in Figure 16 and Figure 17. All sections performed well at the time, though a few potholes were observed in control Section 11.

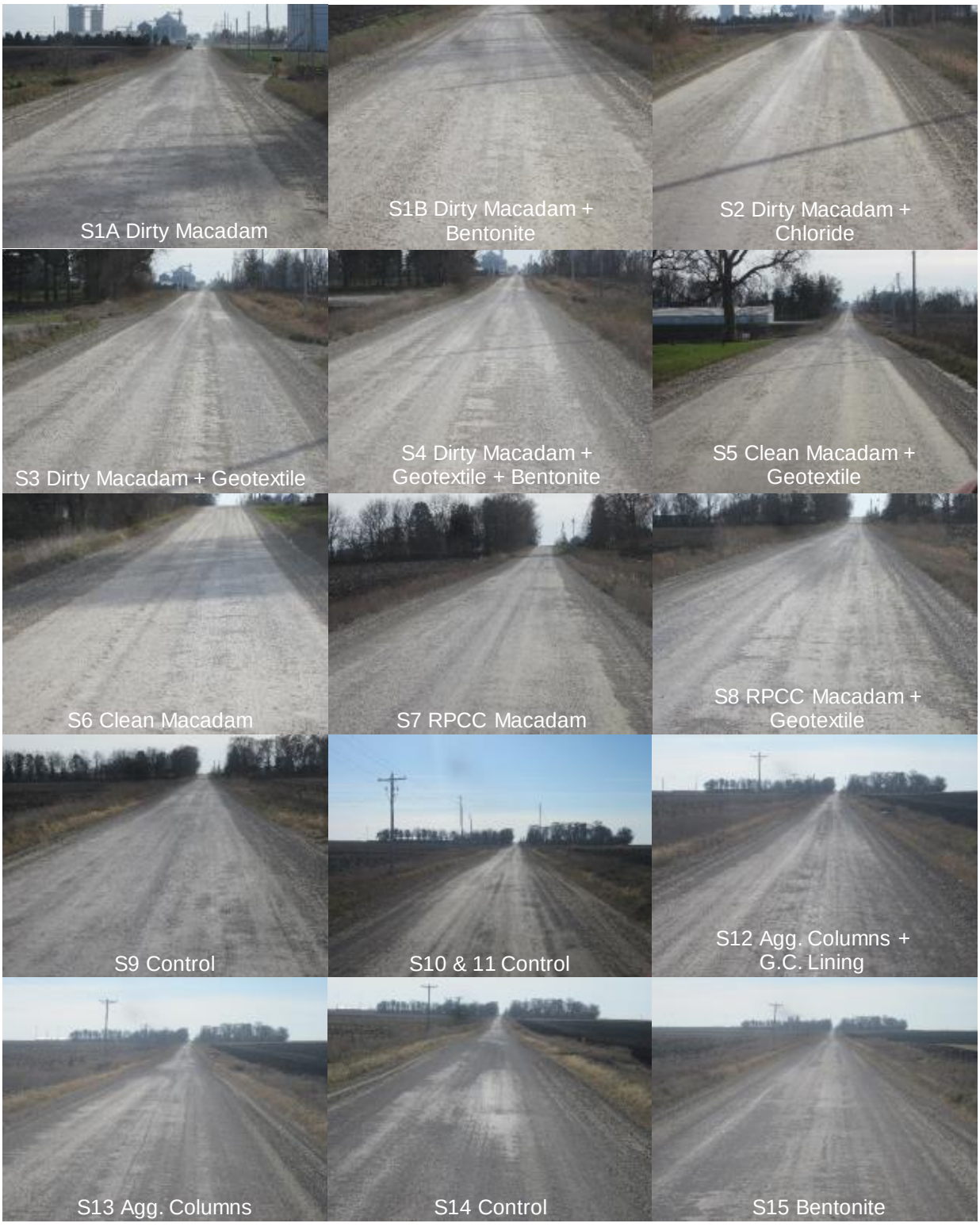

Figure 16. Survey photos of Sections 1A through 15 taken on November 21, 2016

Figure 17. Survey photos of Sections 16 through 19B taken on November 21, 2016

During the 2017 thawing period, the test sections performed very differently, as shown in Figure 18 and Figure 19.

Figure 18. Survey photos of test Sections 1A through 5 taken on February 1, 2017

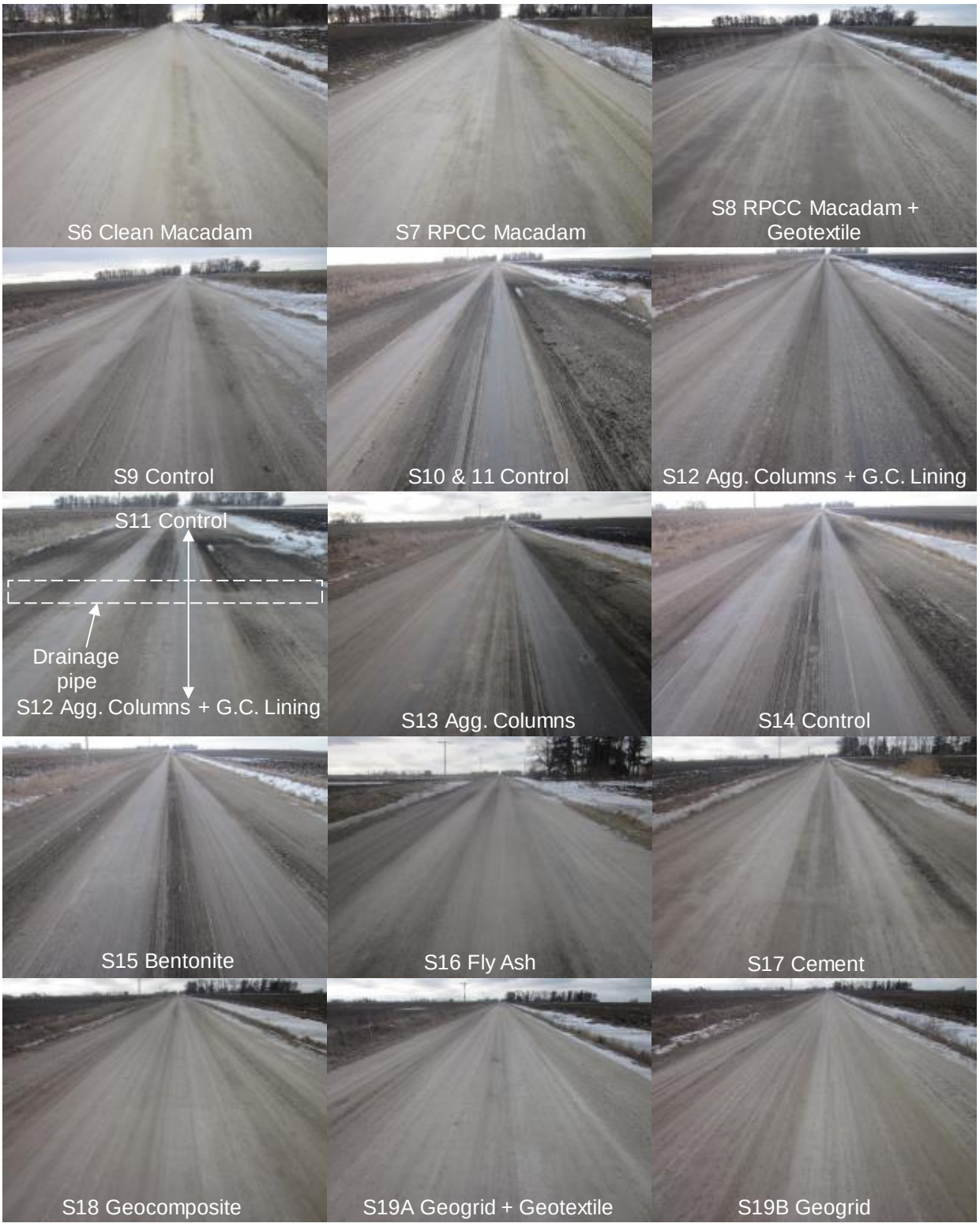

Figure 19. Survey photos of Sections 6 through 19B taken on February 1, 2017

The macadam stone-based sections (Sections 1A through 8) on the first mile showed almost no surface damage, but significant rutting and frost boils were observed in the control sections. The

cement and fly ash sections had minor rutting near the shoulders, and the bentonite section had a muddy surface and minor rutting. The first survey photo in the third row of Figure 19 also clearly demonstrates that aggregate columns with geocomposite liners are a very cost-effective solution for frost boils, evidenced by the state of the control section on the other side of the tile crossing.

Survey photos taken on March 19, 2017 show that all of the sections performed well except for the chloride-treated dirty macadam section (Section 2), which yielded more potholes than other sections, as shown in Figure 20 and Figure 21. Similar behaviors were observed during the 2014–2015 thawing period, as documented in the TR-664 project report.

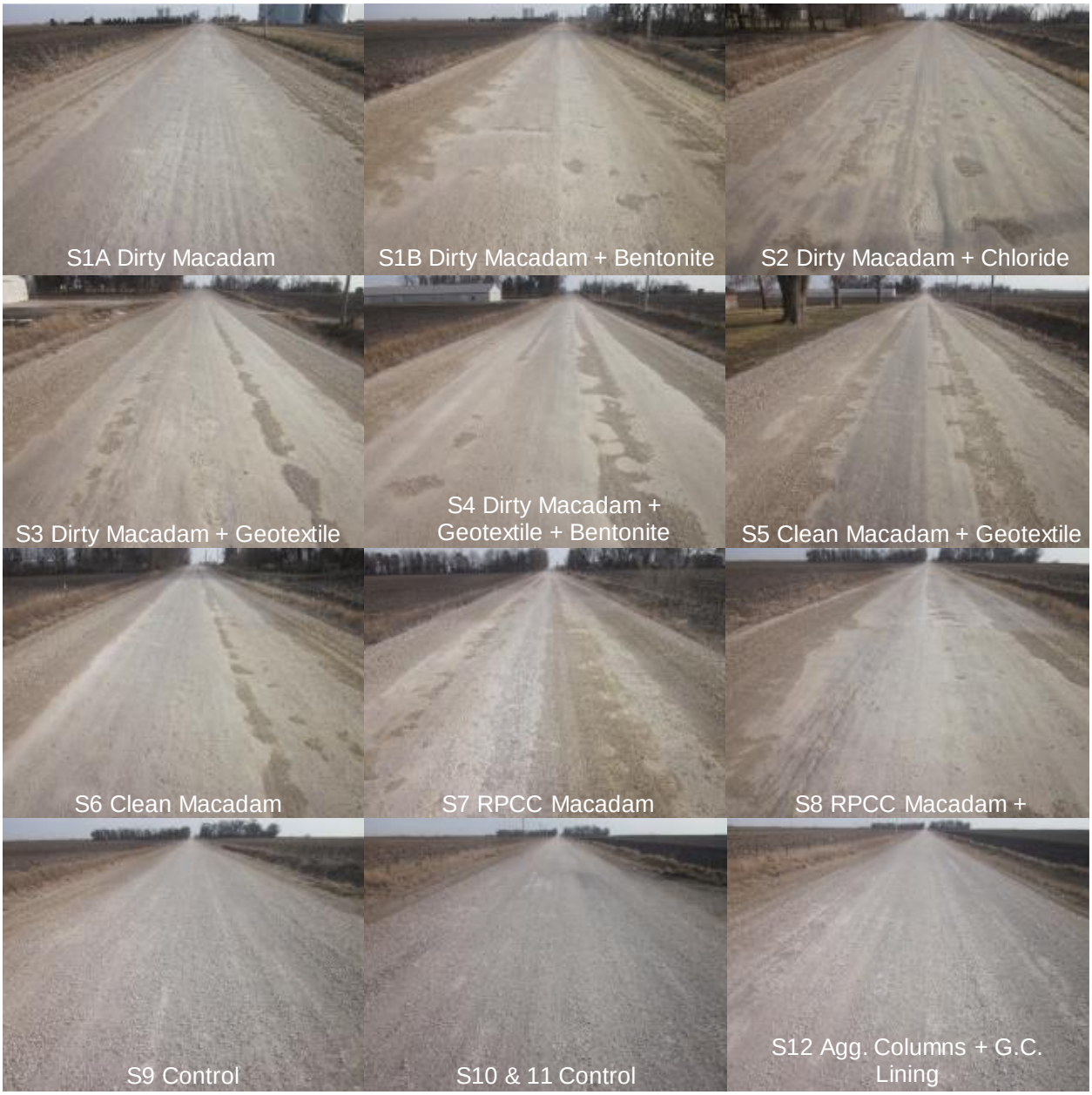

Figure 20. Survey photos of Sections 1A through 12 taken on March 19, 2017

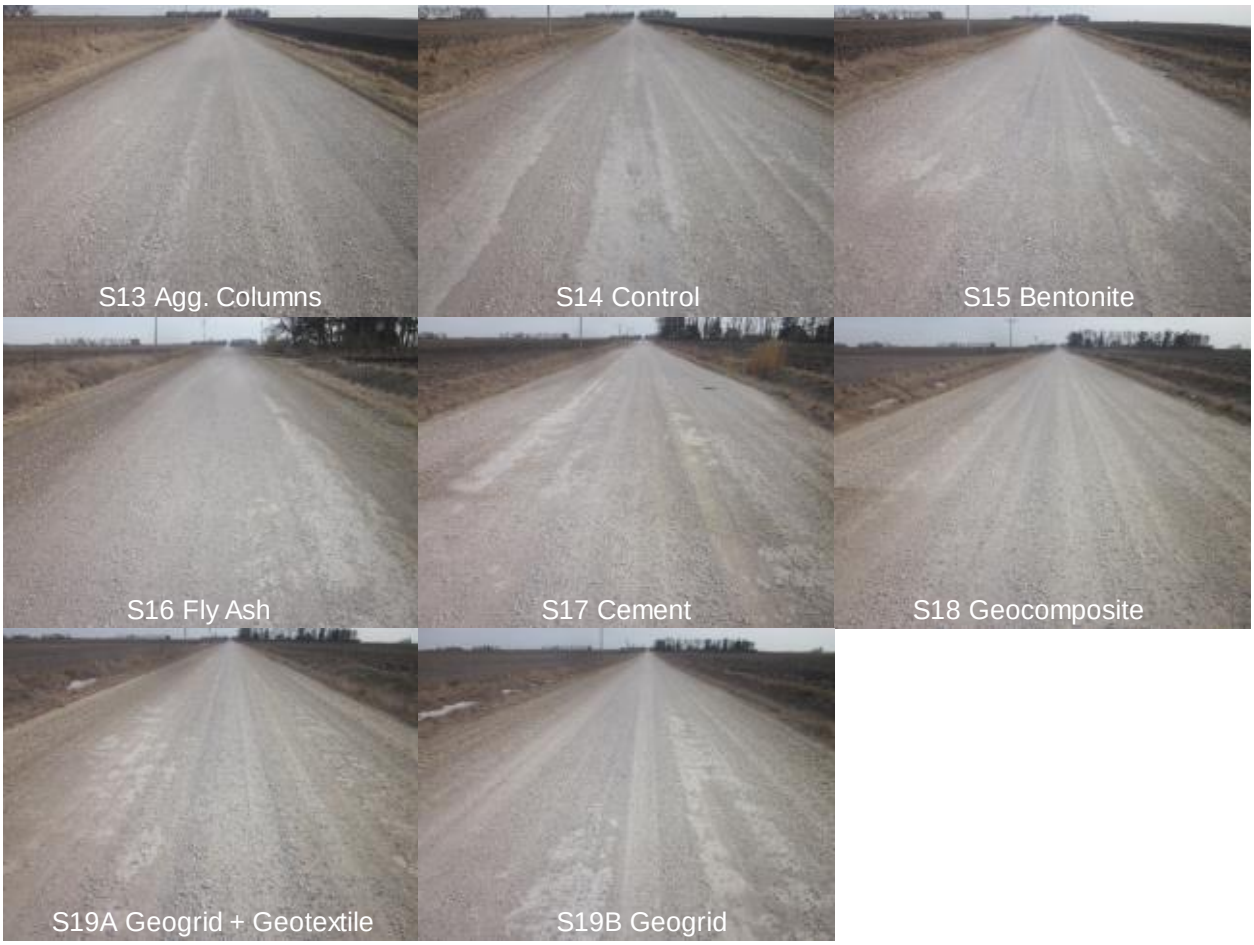

Figure 21. Survey photos of Sections 13 through 19B taken on March 19, 2017

Another group of survey photos was taken during the post-thawing field tests in April 2017 (Figure 22 and Figure 23).

Figure 22. Survey photos of Sections 1A through 12 taken on April 8, 2017

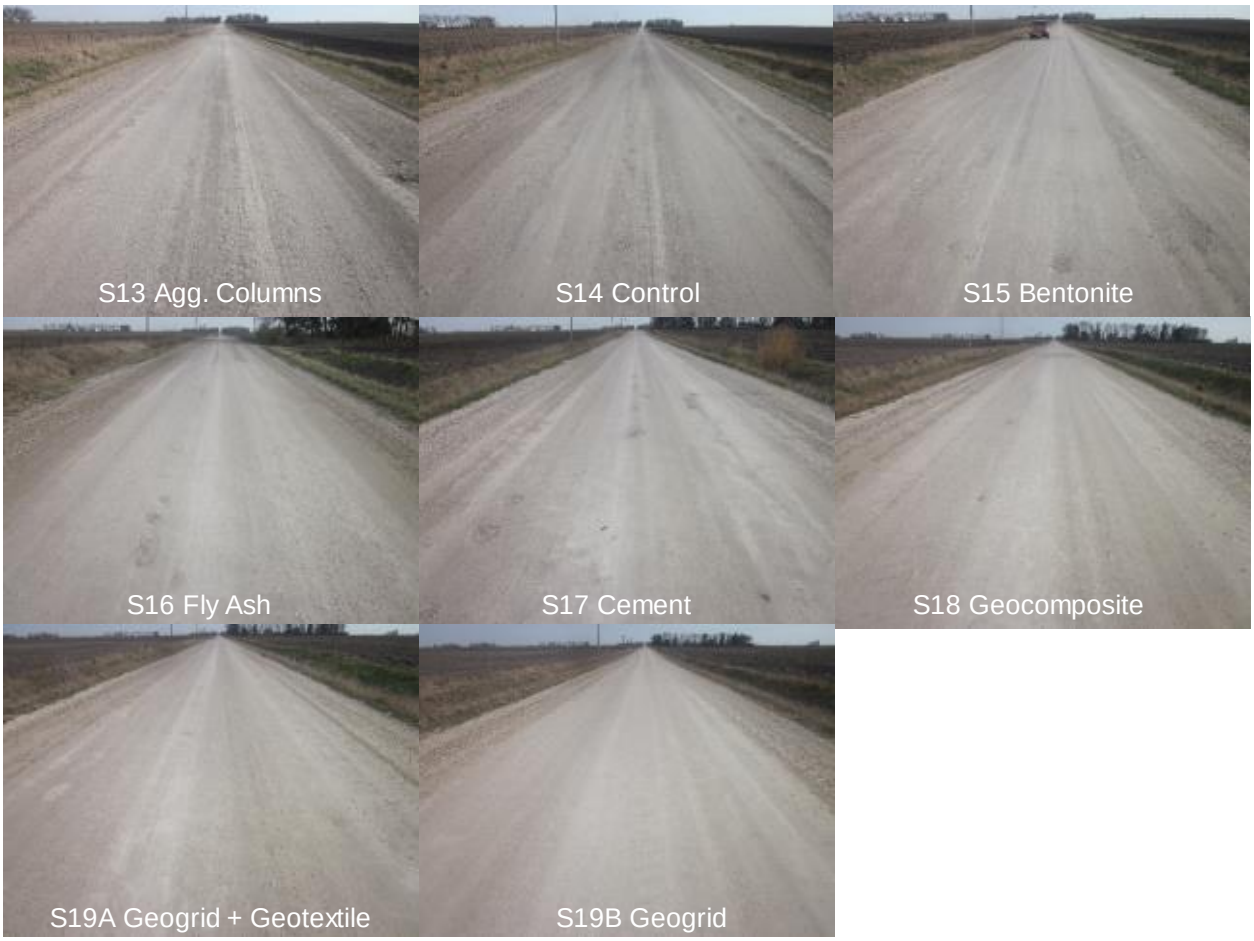

Figure 23. Survey photos of Sections 13 through 19B taken on April 8, 2017

Many potholes appeared in the macadam stone-based and chemically stabilized sections; these potholes were not observed in the 2014 and 2015 thawing periods. However, the shear strength and stiffness of the base materials of these sections were much higher than those of other sections. Therefore, the formation of potholes may be attributable to the gradation and quality of the new surfacing material and the non-uniform stiffness of the base materials. Further study is needed to better understand the mechanism of pothole formation in these sections.

CHAPTER 4. CONCLUSIONS AND RECOMMENDATIONS

In this project, the Vail Avenue rural surface alternatives demonstration sections were continuously monitored during the 2016–2017 seasonal freeze-thaw period. The weather and subgrade temperature profile were recorded and analyzed to determine the timing, duration, and depth of soil freezing. Compared to the 2013–2014 and 2014–2015 seasons, the winter of 2016–2017 was warmer and had shorter freezing and thawing periods (74 and 8 days, respectively), which resulted in a much shallower frost penetration depth of approximately 2.25 ft.

Performance-based field tests were conducted on the test sections before and after the seasonal freeze-thaw period. The thicknesses of the surface layers based on DCP tests were 2 to 3 in. thicker than the nominal as-constructed cross-section profiles. The difference might be due to adding the fresh resurfacing aggregate and the DCP test itself, because the stiff top layer of the subgrade usually has a shear strength that is similar to that of the aggregate material. The DCP test results showed that the surface layer thicknesses remained unchanged between the 2016 pre-freezing and 2017 post-thawing tests. The DCP-CBR values of the stabilized surface layers were above 60% before freezing, but the average CBR_{AGG} of the fly ash-stabilized section significantly decreased after two years of service. After thawing, the CBR values of most sections did not decrease significantly because of the relatively warmer and shorter winter. The subgrade CBR values of the macadam sections were about twice those of the other sections for both pre-freezing and post-thawing tests.

The FWD tests were conducted to determine the stiffness changes of the test sections and compare the FWD values to those obtained from previous test results. In this study, a different FWD device was used, and the applied impact load was 2,000 lbs less than that of the previous lowest impact load of the Kuab FWD device. The data showed that the 2016 pre-freezing FWD modulus values were higher than those obtained from the 2014 tests, except for the fly ash- and cement-treated sections, which exhibited significant reductions in stiffness after two years of service. For the 2016 pre-freezing tests, the stiffnesses of the macadam sections were still approximately twice those of the other sections. The dirty macadam with bentonite surface treatment and RPCC macadam sections yielded some of the highest average surface modulus values, likely due to the improved surface stability and continuous hydration of the recycled concrete material, respectively. The 2016–2017 pre-freezing and post-thawing FWD test results showed that the stiffness of most sections decreased after thawing, except for the clean macadam sections (Sections 5 and 6), whose stiffnesses remained almost constant. Compared to the 2013–2014 and 2014–2015 test results, the stiffness reductions were smaller due to the relatively short freezing-thawing periods, shallower frost penetration depth, and lower levels of precipitation during the 2017 thawing period.

The MASW test results showed trends that were very similar to those of the FWD test results. The MASW surface modulus values were much higher than those obtained from the FWD tests due to the much lower strain level imposed by the MASW test. For the subgrade, the MASW tests produced similar but somewhat lower modulus values than the FWD tests. This discrepancy can be caused by several factors and needs further study.

Maintenance activities and costs were recorded by the Hamilton County Secondary Roads Department. Except for a total of 640 tons of rock that was dumped to resurface the entire two-mile stretch of test sections, very few routine motor grader bladings were performed on the sections. Based on the additional maintenance cost data, the break-even periods of the various stabilization methods were recalculated and were found to be approximately the same as those calculated in the TR-664 project.

Survey photos taken during the 2016–2017 seasonal freeze-thaw periods showed that all of the stabilized sections had much less rutting than the control sections during the thawing period. However, many potholes that were not observed in the 2014 and 2015 thawing periods appeared on the macadam stone-based and chemically stabilized sections. In addition, the shear strength and stiffness of the base materials of these sections were much higher than those of other sections. Therefore, the formation of potholes may be attributable to the gradation and quality of the new surfacing material and the non-uniform stiffness of the base materials. Further study is needed to better understand the mechanism of pothole formation in these sections.

REFERENCES

AASHTO. 1993. *Guide for Design of Pavement Structures*. American Association of State Highway and Transportation Officials, Washington, DC.

Li, C., J. C. Ashlock, S. Lin, and P. K. R. Vennapusa. 2017a. Layered Elastic Moduli of Stabilized Unpaved Roads by Multichannel Analysis of Surface Waves and Falling Weight Deflectometer Tests. 96th Annual Meeting of the Transportation Research Board, Washington, DC, January 8–12.

Li, C., J. C. Ashlock, D. J. White, and P. K. R. Vennapusa. 2017b. Mechanistic-based comparisons of stabilised base and granular surface layers of low-volume roads. *International Journal of Pavement Engineering*, pp. 1–13.

Li, C., J. C. Ashlock, D. J. White, and P. Vennapusa. 2015. *Low-Cost Rural Surface Alternatives: Demonstration Project*. Institute for Transportation, Ames, IA.

Lin, S. 2014. Advancements in active surface wave methods: modeling, testing, and inversion. PhD dissertation. Iowa State University, Ames, IA.

Lin, S. and J. C. Ashlock. 2011. A Study on Issues Relating to Testing of Soils and Pavements by Surface Wave Methods. 38th Annual Review of Progress in Quantitative Nondestructive Evaluation, Burlington, VT, July 17–22.

Vennapusa, P. K. R. and D. J. White. 2009. Comparison of Light Weight Deflectometer Measurements for Pavement Foundation Materials. *Geotechnical Testing Journal*, Vol. 32, No. 3, pp. 239–251.

White, D. and P. Vennapusa. 2013. *Low-Cost Rural Surface Alternatives: Literature Review and Recommendations*. Institute for Transportation, Ames, IA.

APPENDIX A. 2016 PRE-FREEZING DCP TEST RESULTS

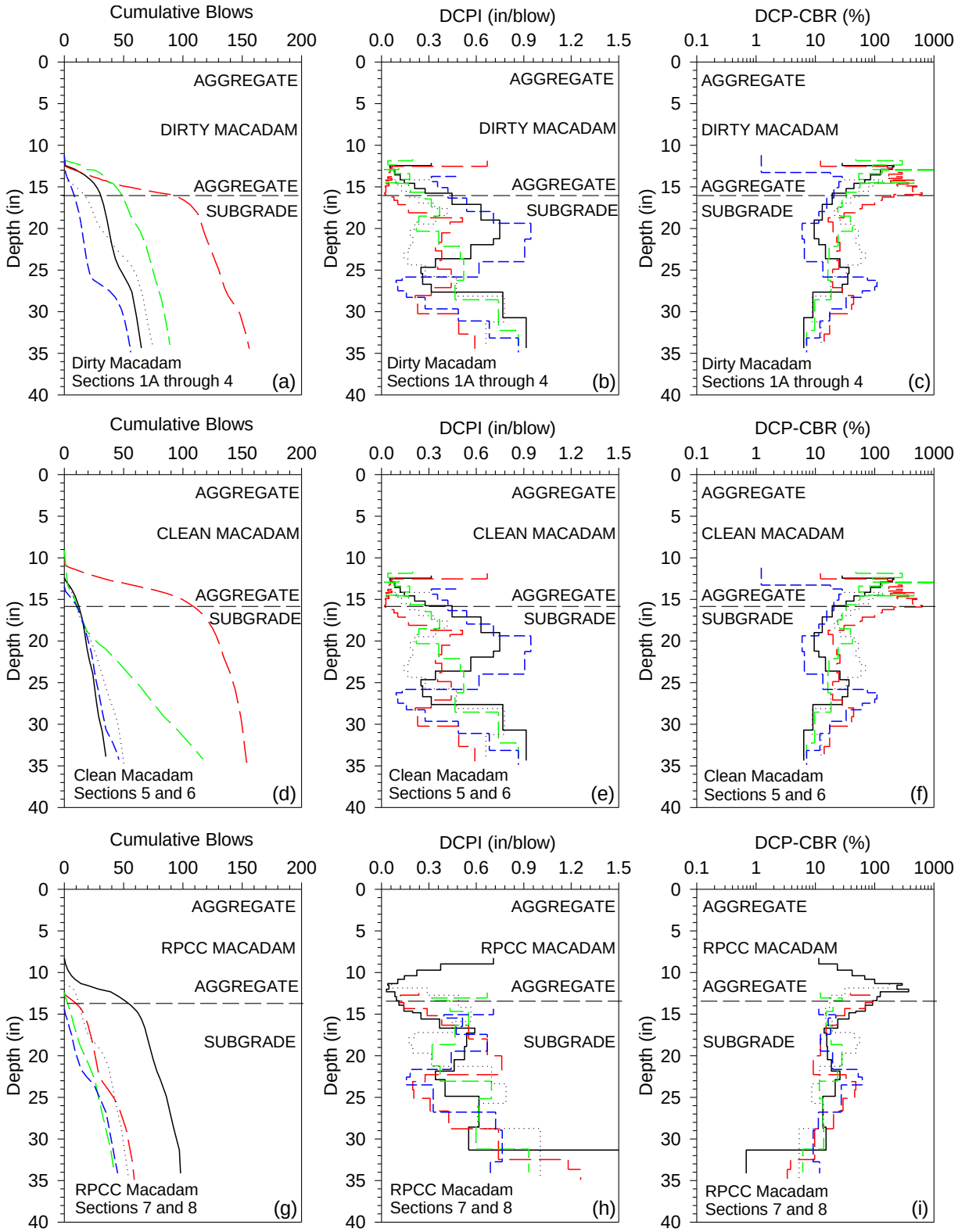

Figure 24. 2016 pre-freezing DCP test results for Sections 1A through 8

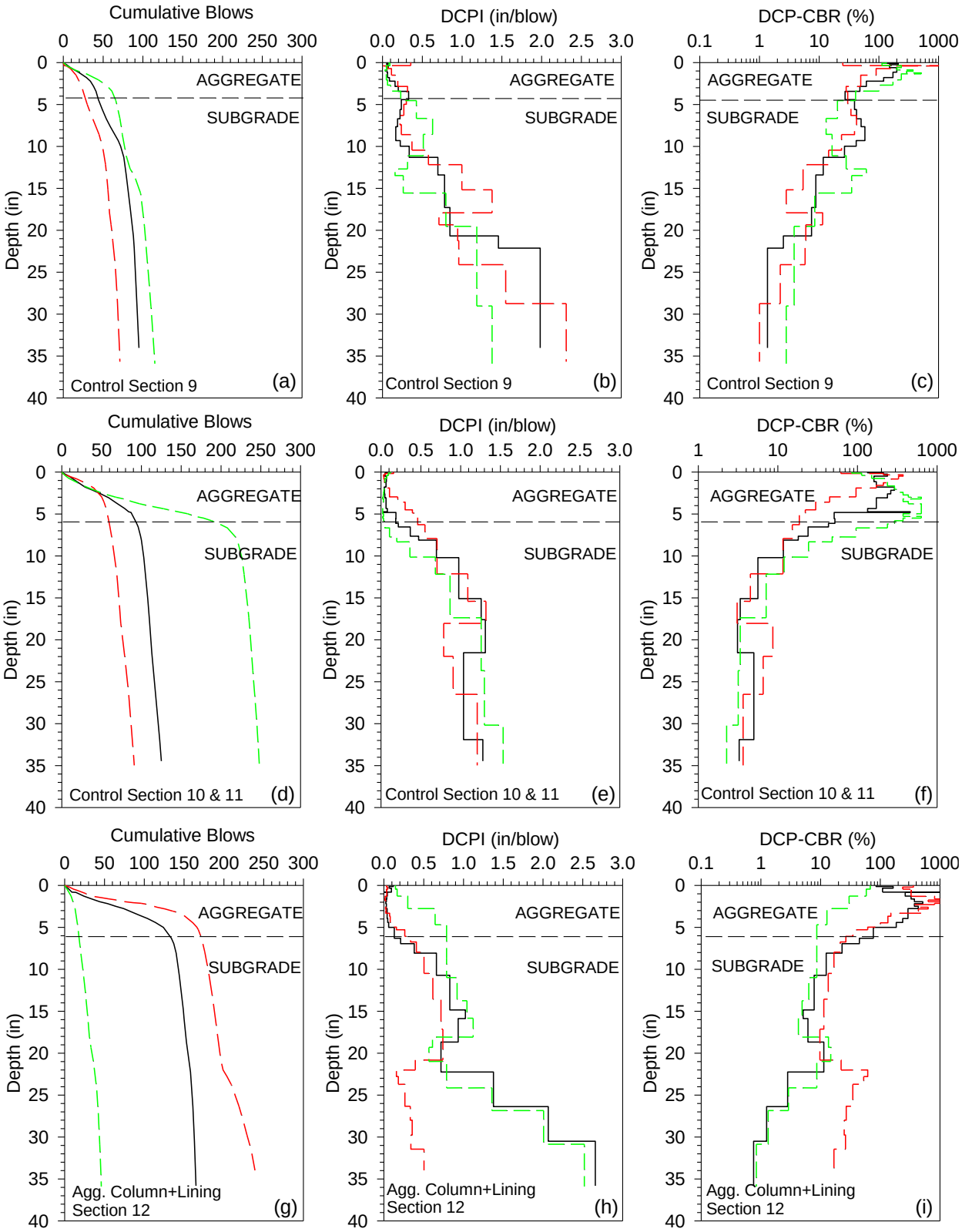

Figure 25. 2016 pre-freezing DCP test results for Sections 9 through 12

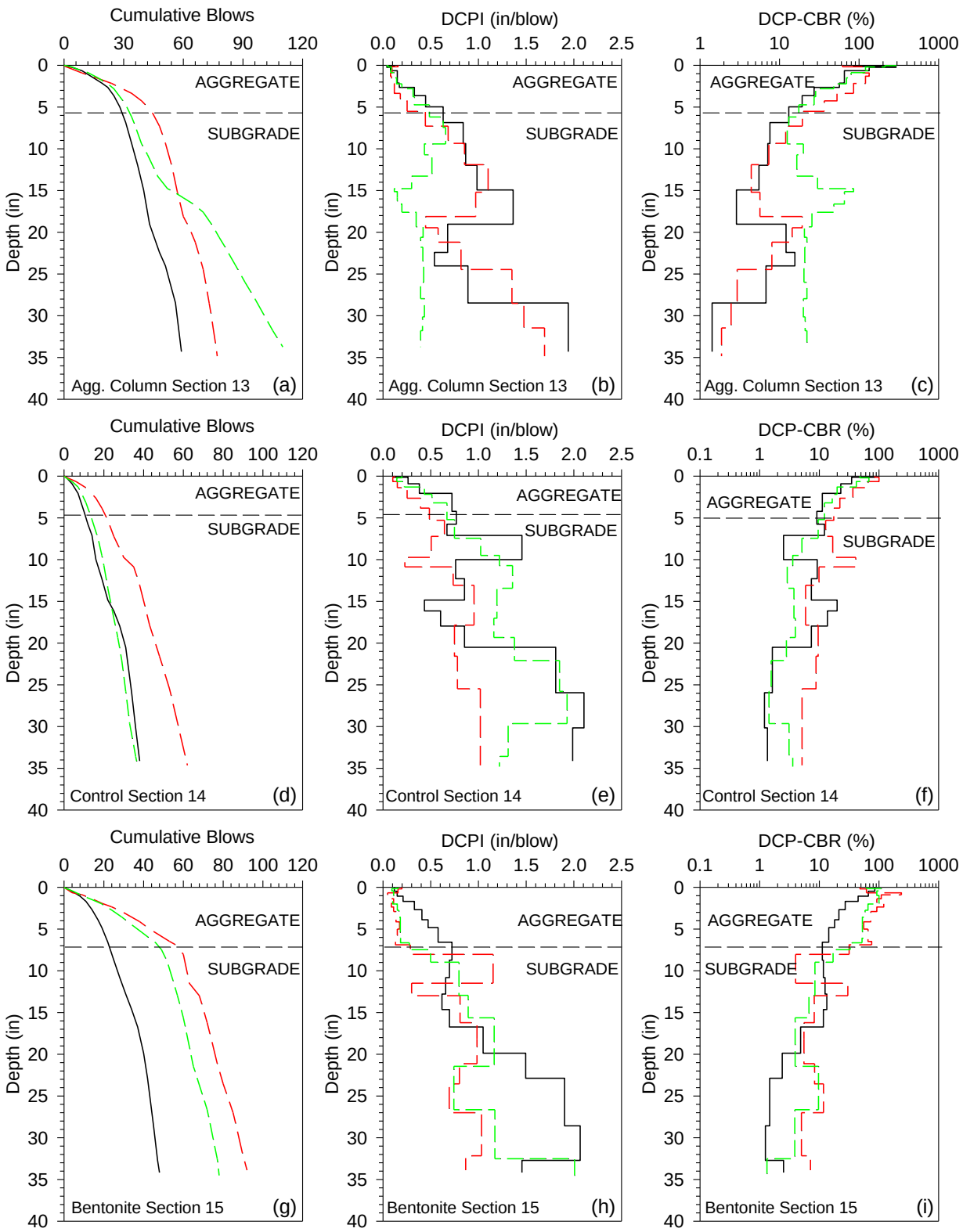

Figure 26. 2016 pre-freezing DCP test results for Sections 13 through 15

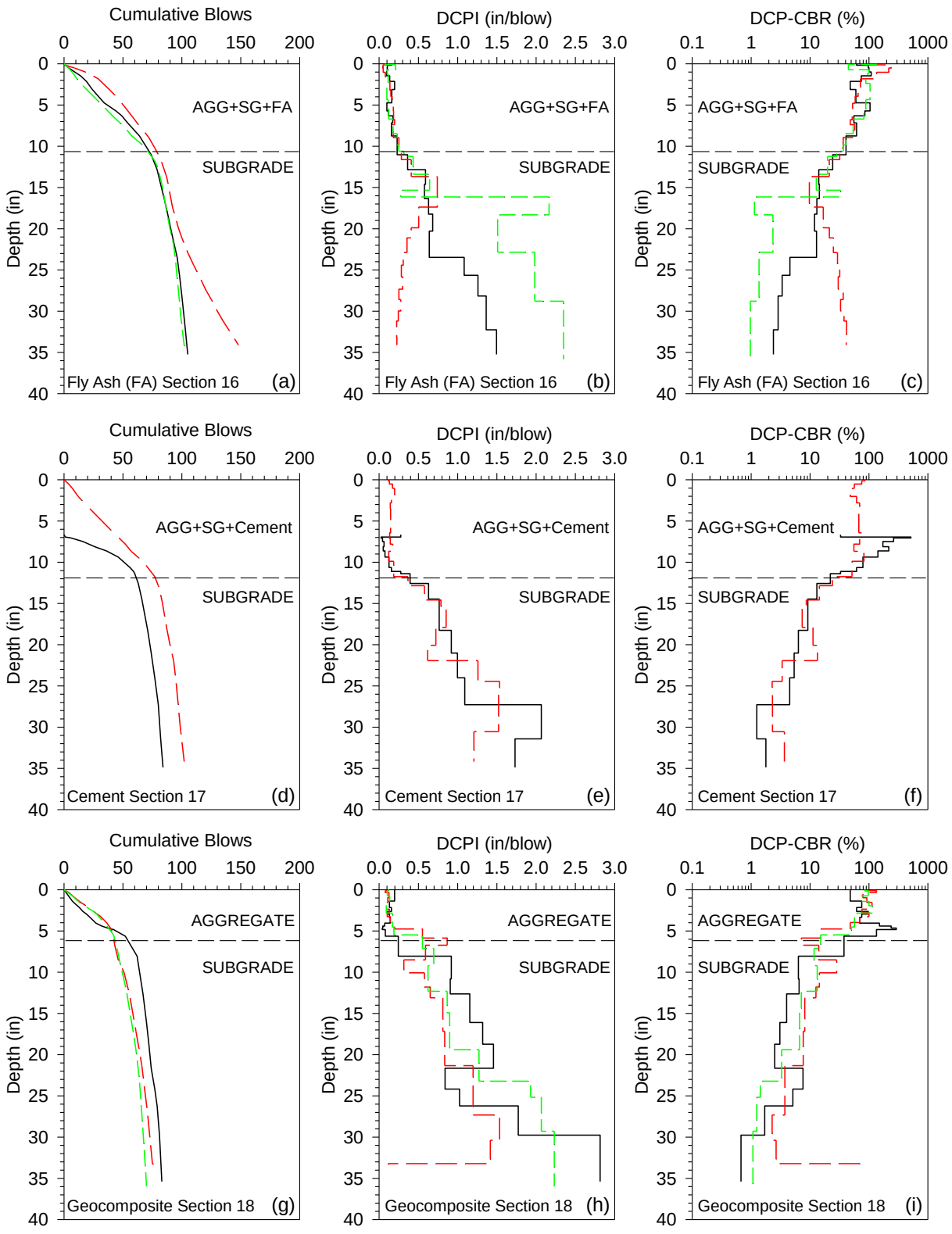

Figure 27. 2016 pre-freezing DCP test results for Sections 16 through 18

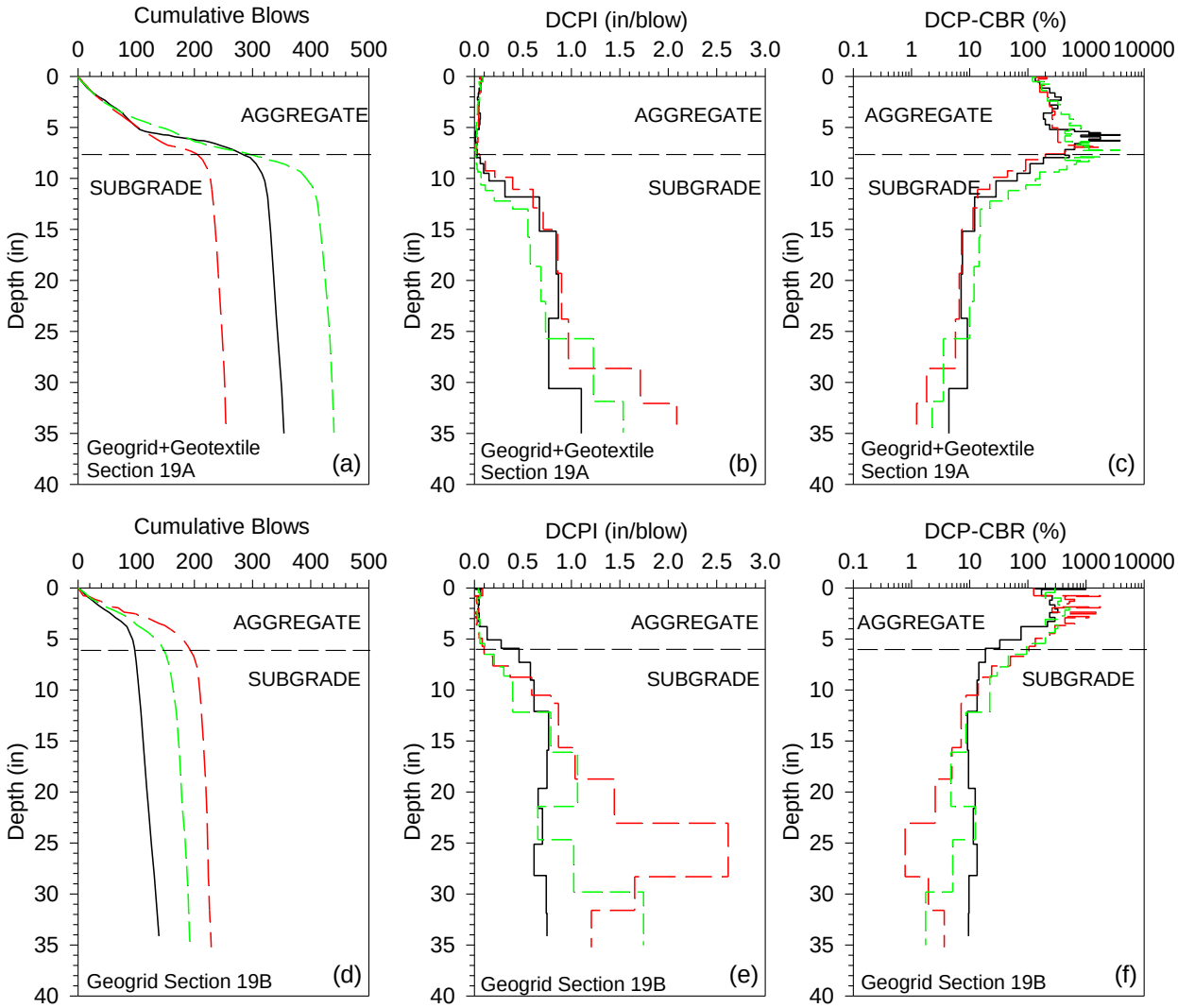

Figure 28. 2016 pre-freezing DCP test results for Sections 19A and 19B

APPENDIX B. 2017 POST-THAWING DCP TEST RESULTS

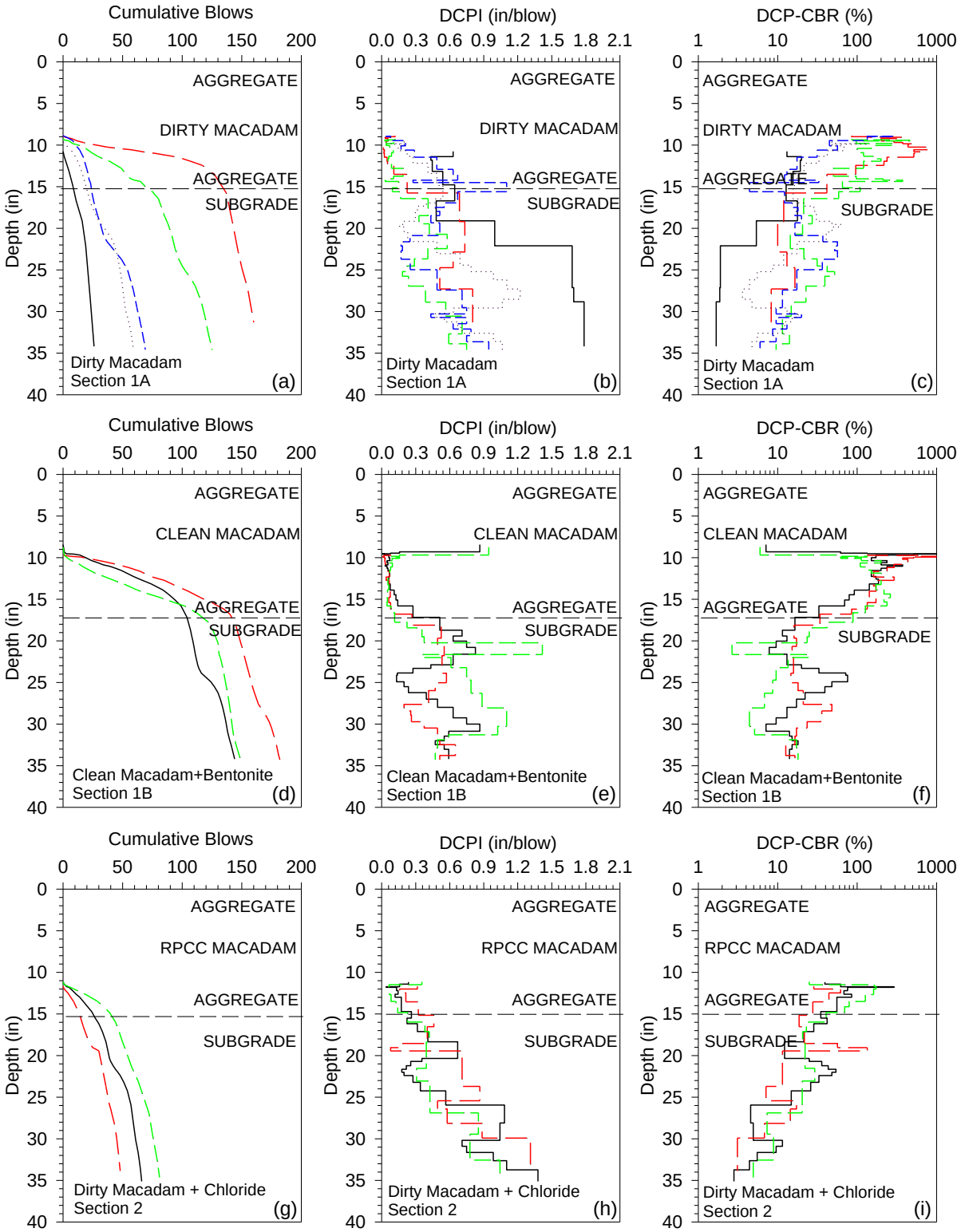

Figure 29. 2017 post-thawing DCP test results for Sections 1A through 2

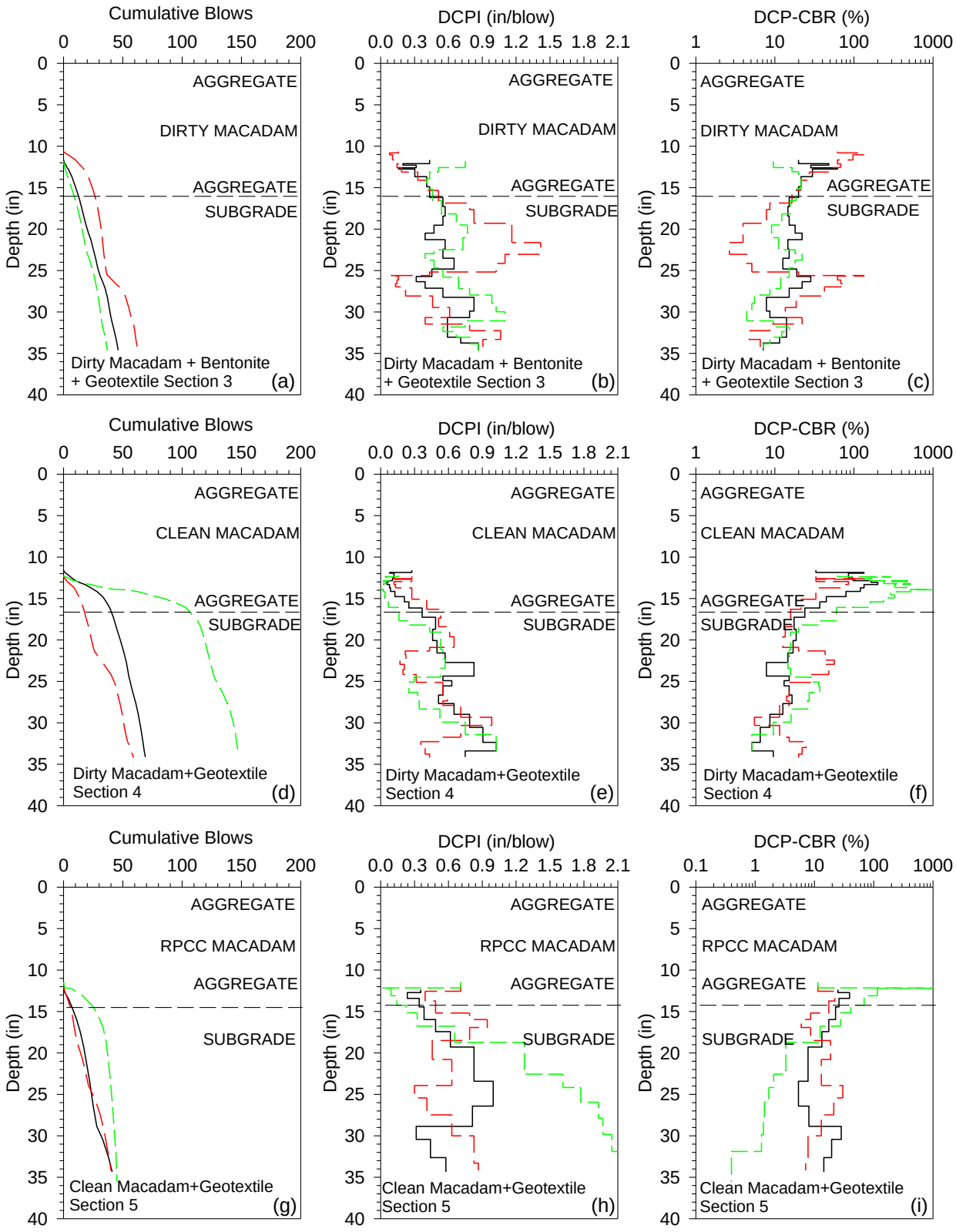

Figure 30. 2017 post-thawing DCP test results for Sections 3 through 5

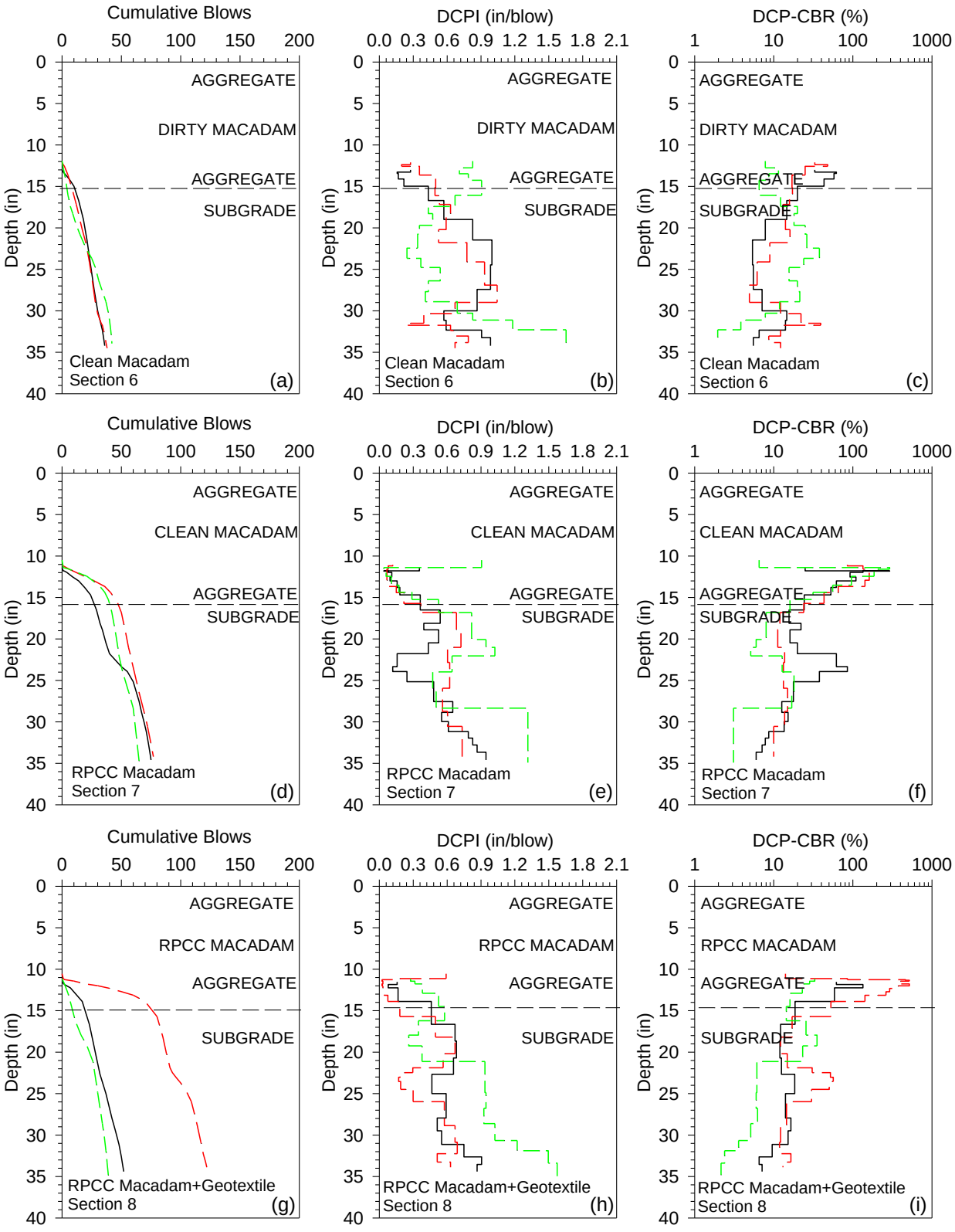

Figure 31. 2017 post-thawing DCP test results for Sections 6 through 8

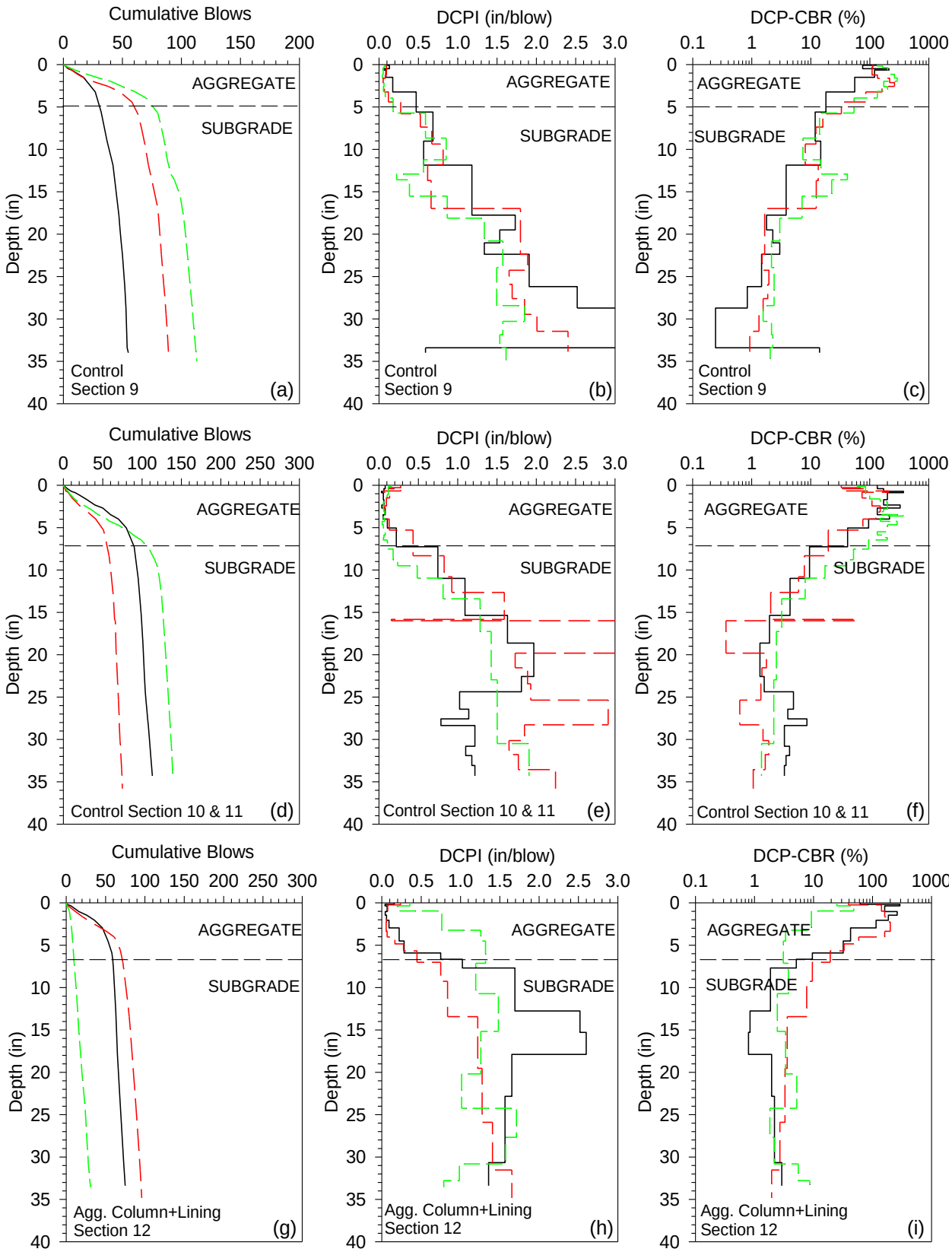

Figure 32. 2017 post-thawing DCP test results for Sections 9 through 12

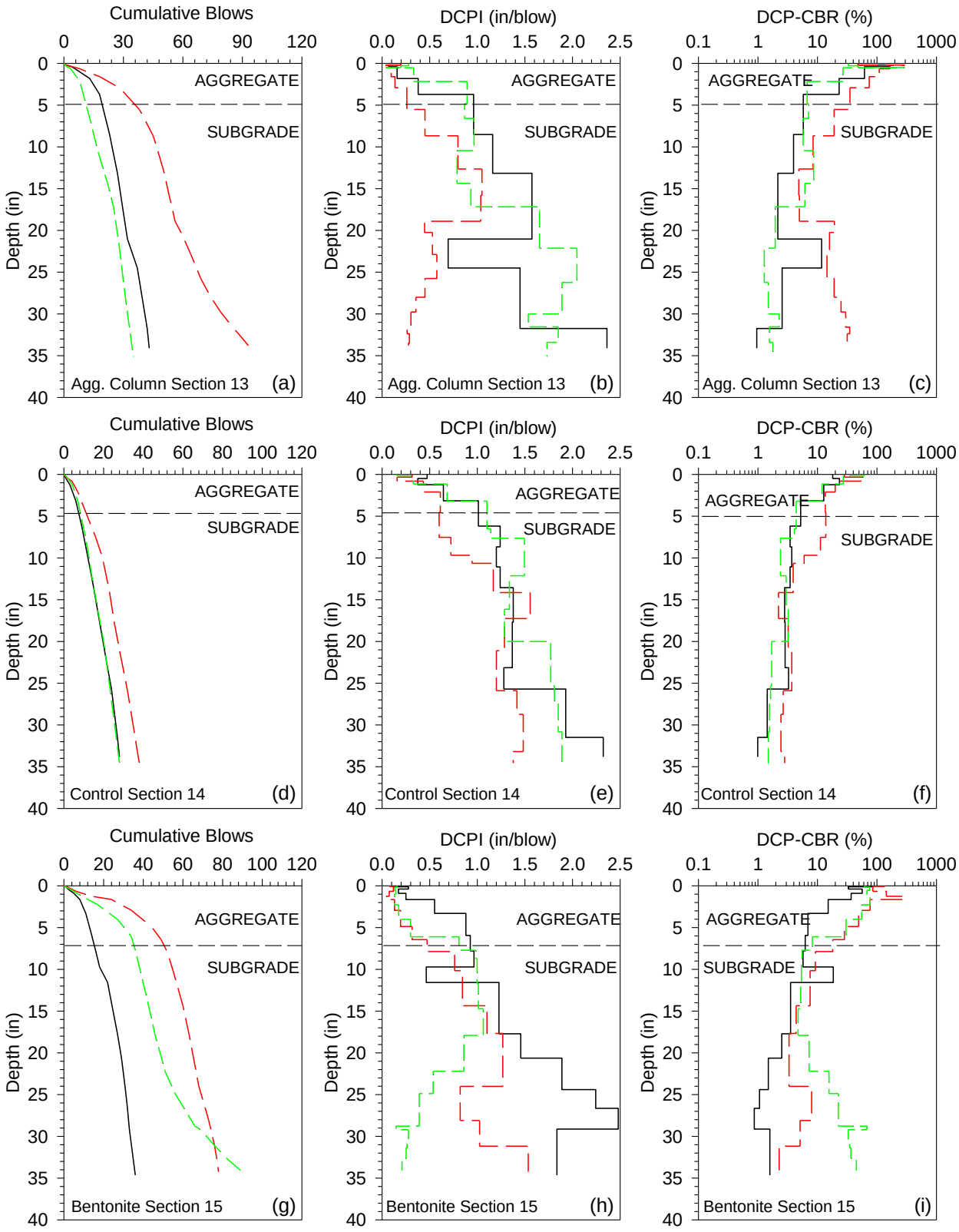

Figure 33. 2017 post-thawing DCP test results for Sections 13 through 15

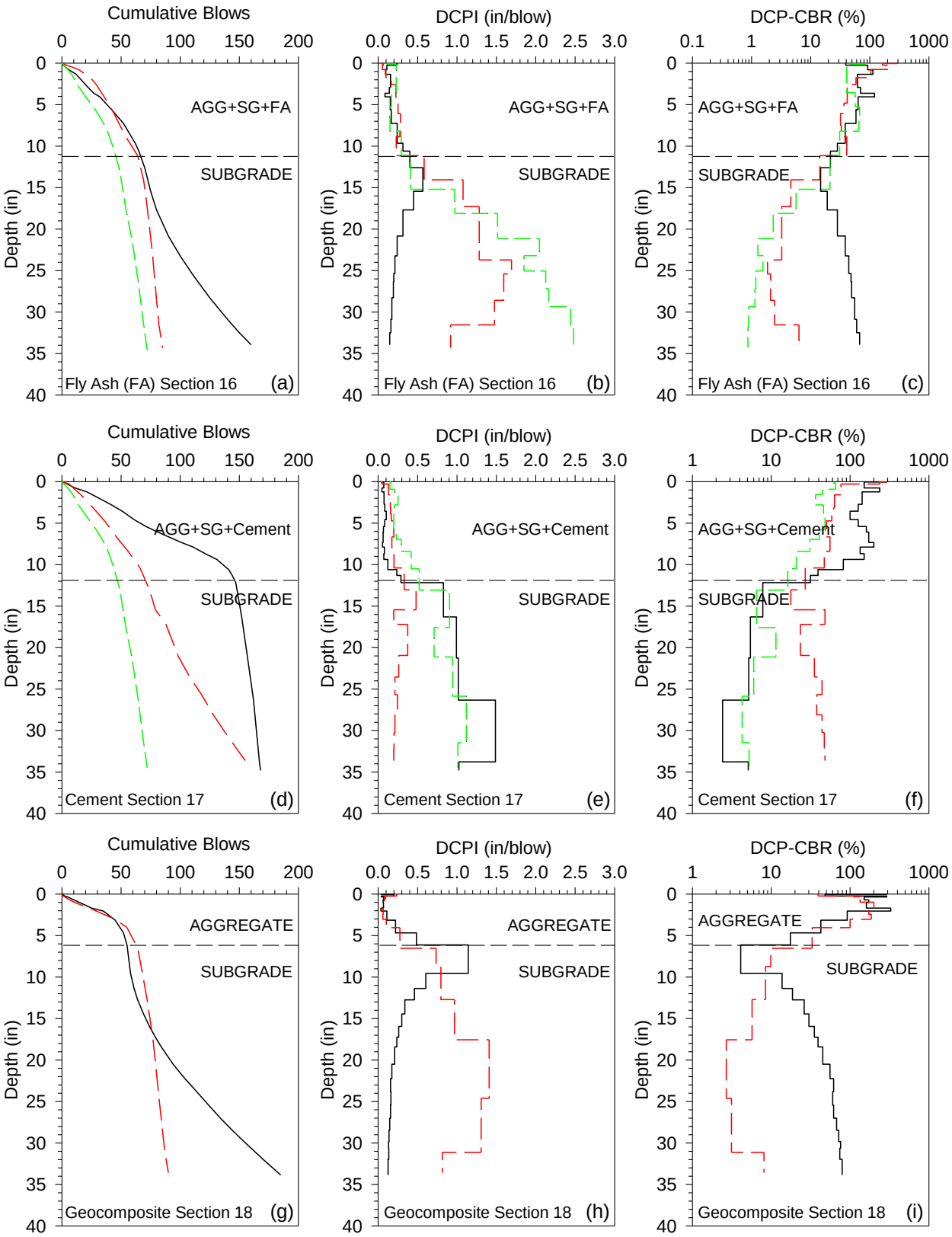

Figure 34. 2017 post-thawing DCP test results for Sections 16 through 18

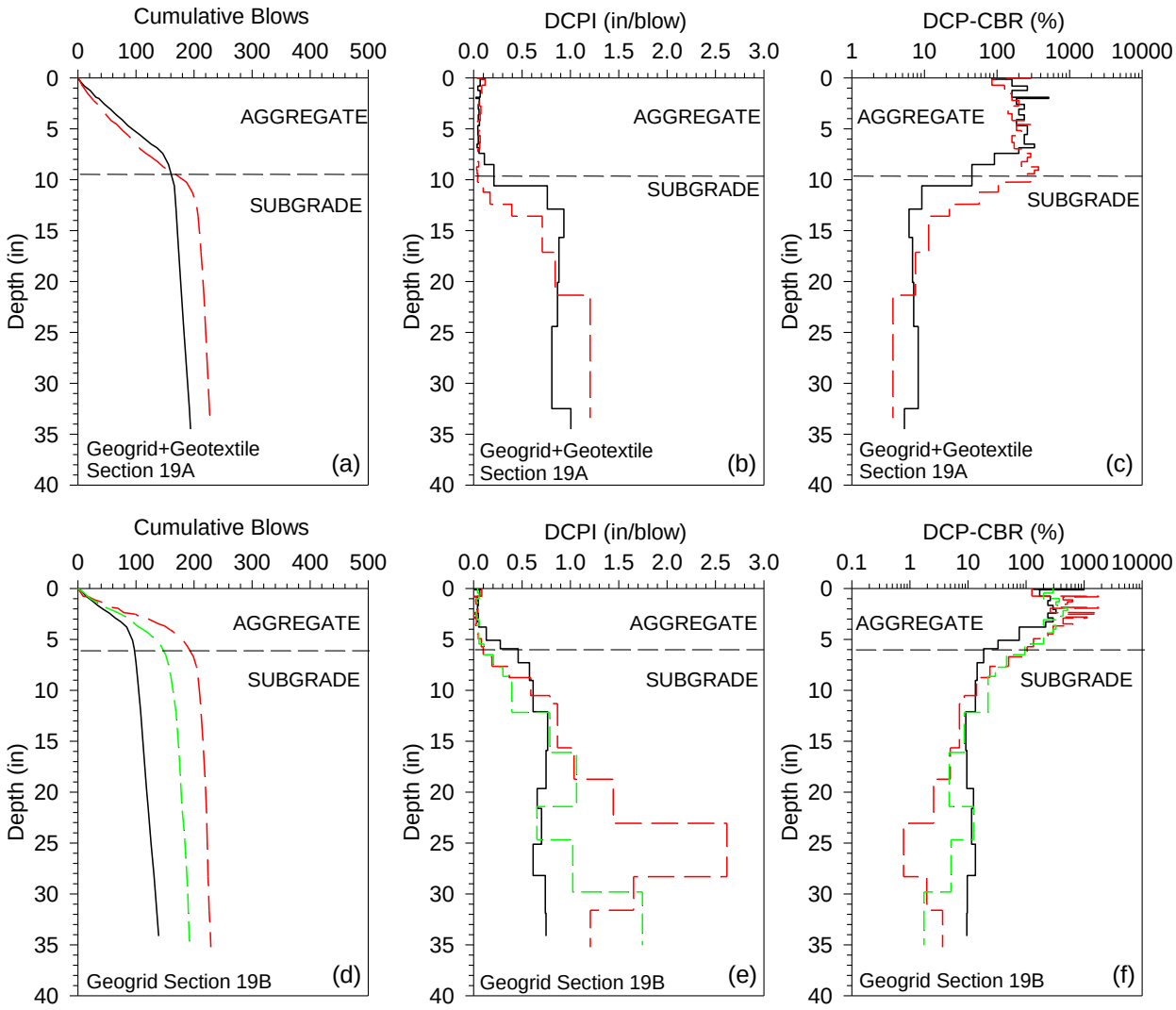

Figure 35. 2017 post-thawing DCP test results for Sections 19A and 19B

APPENDIX C. 2016–2017 FWD TEST RESULTS

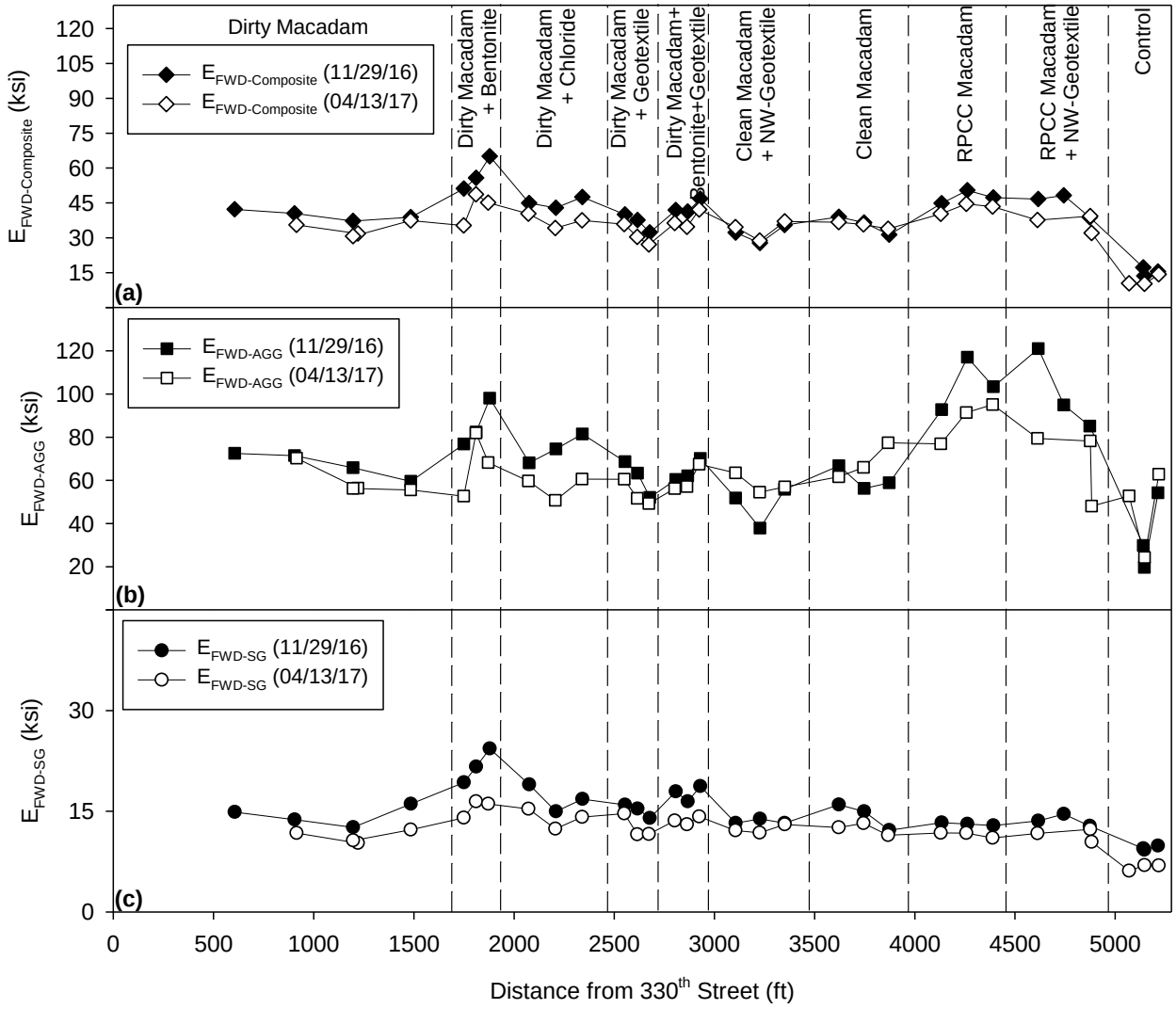

Figure 36. 2016–2017 pre-freezing and post-thawing FWD test results for first-mile sections

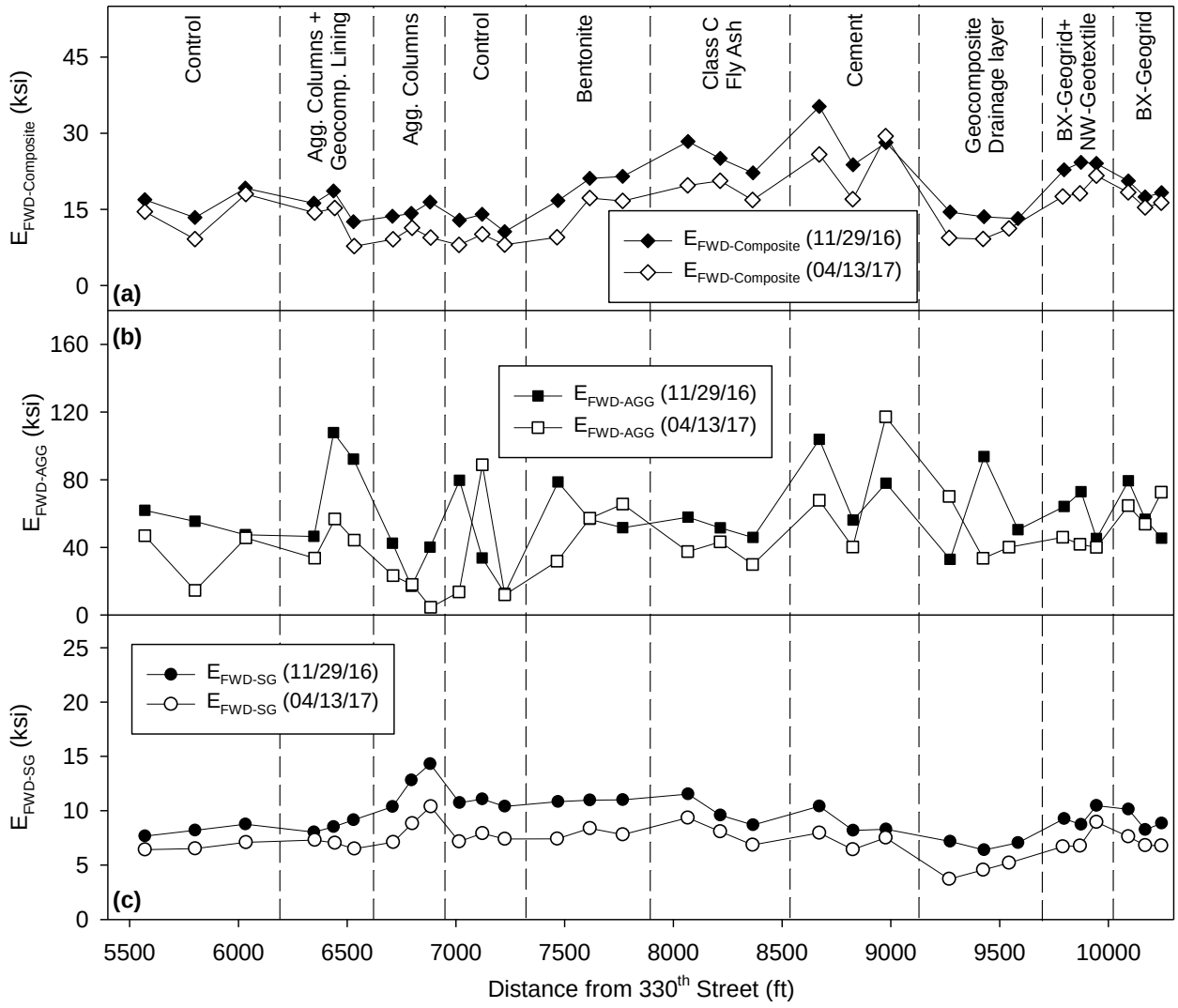

Figure 37. 2016–2017 pre-freezing and post-thawing FWD test results for second-mile sections

APPENDIX D. 2016 PRE-FREEZING MASW DISPERSION IMAGES

Section 1A Dirty Macadam

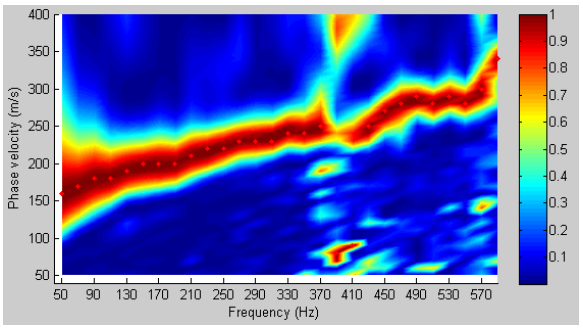

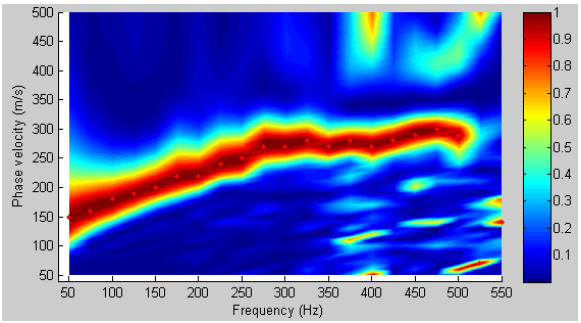

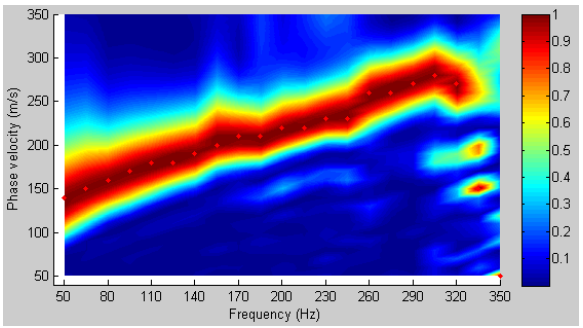

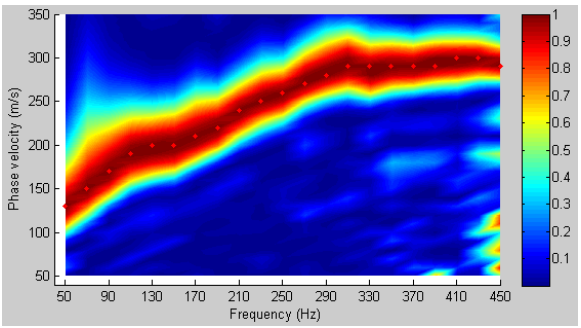

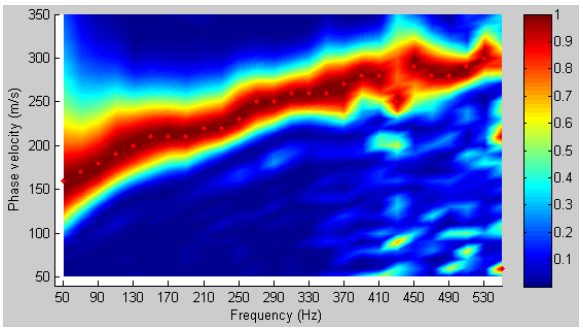

Section 1B Dirty Macadam + Bentonite

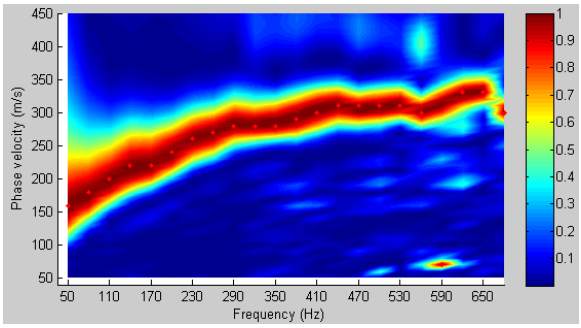

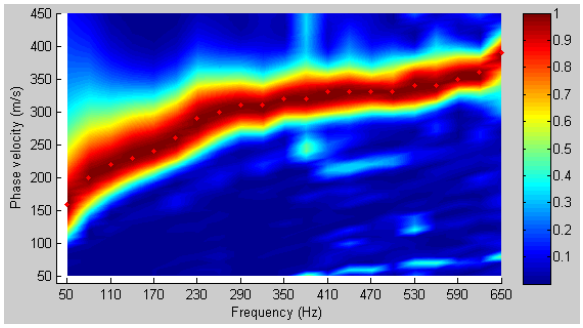

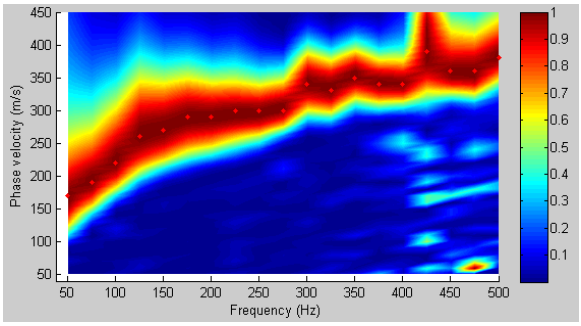

Section 2 Dirty Macadam + Calcium Chloride

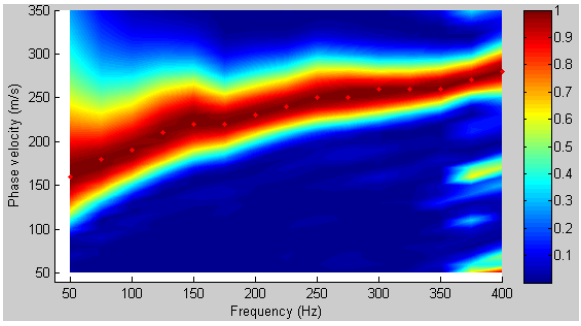

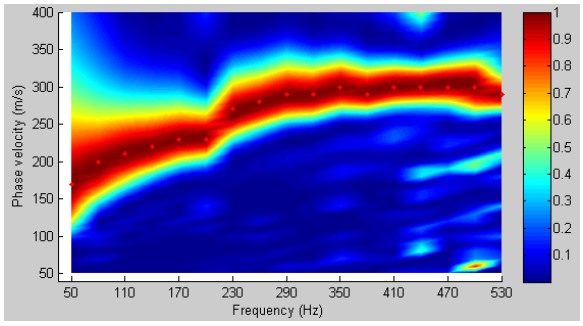

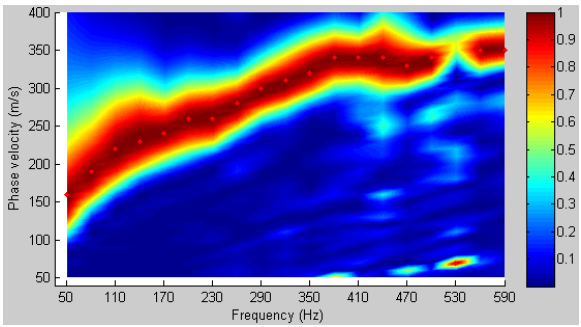

Section 3 Dirty Macadam + Bentonite + NW geotextile

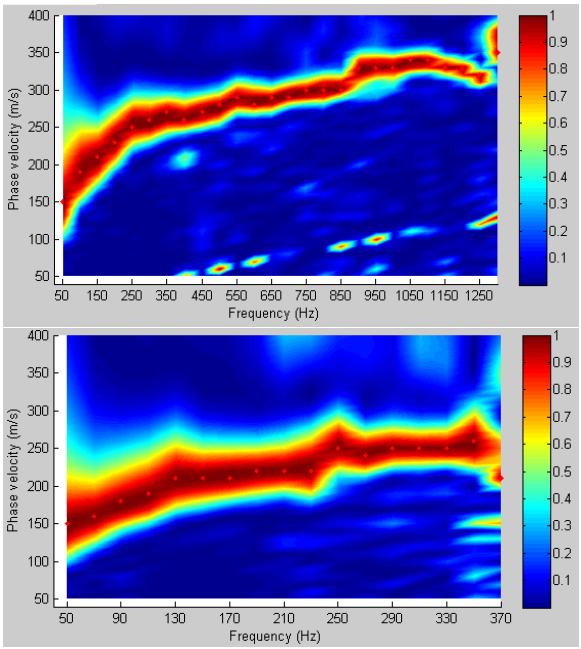

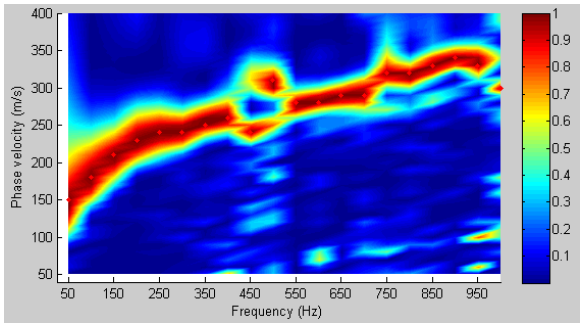

Section 4 Dirty Macadam + NW geotextile

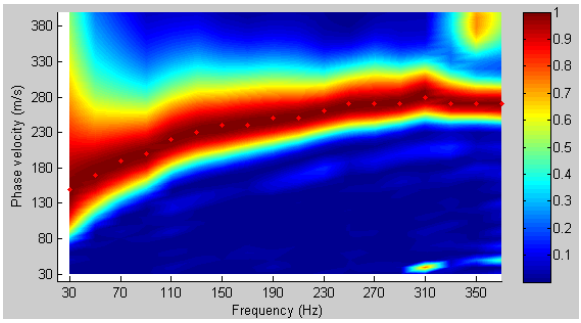

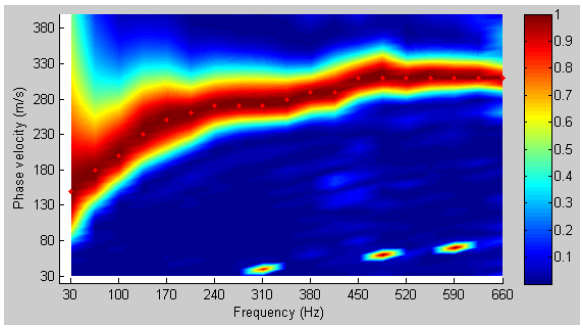

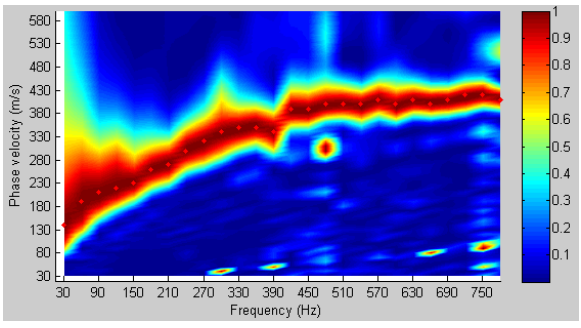

Section 5 Clean Macadam + NW geotextile

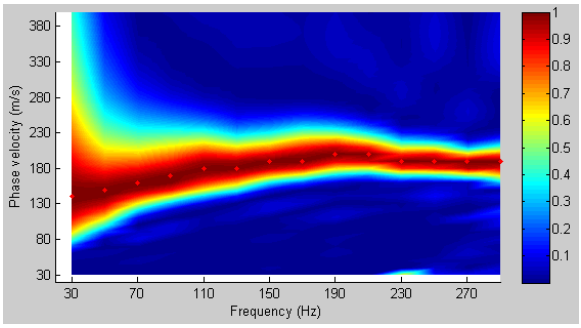

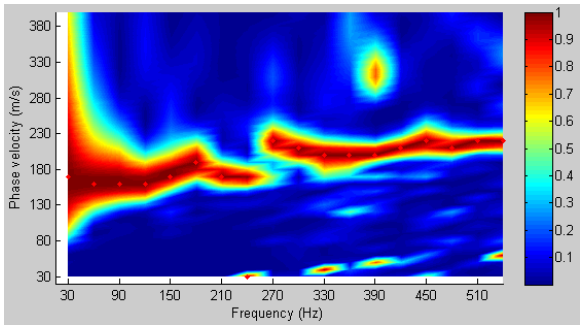

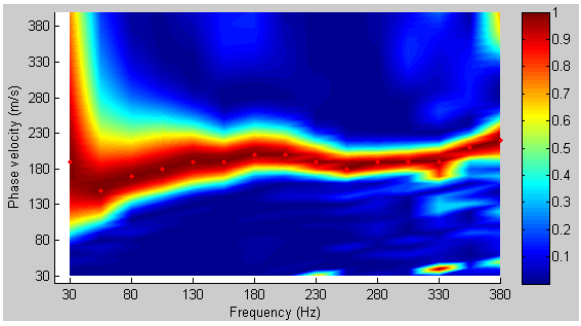

Section 6 Clean Macadam

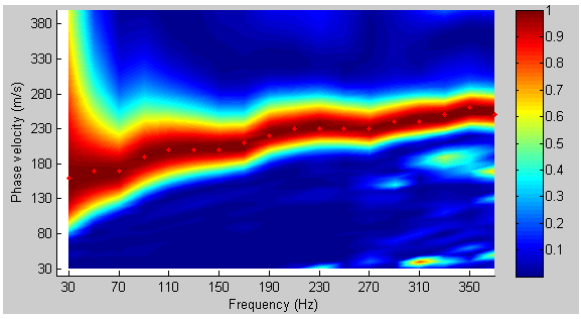

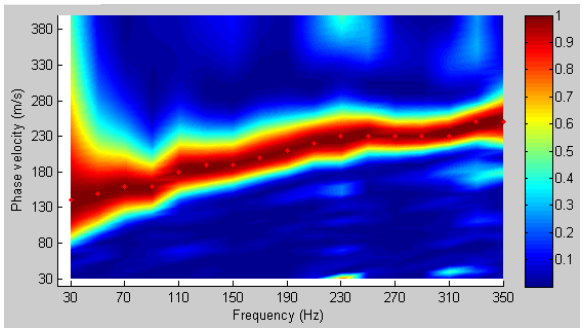

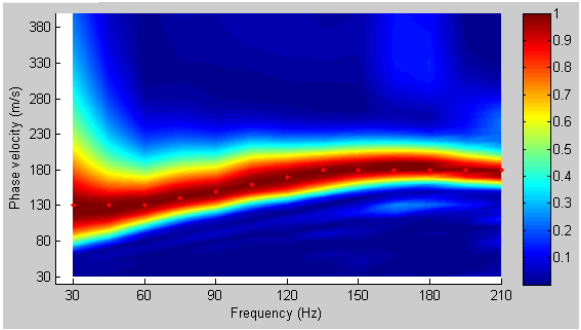

Section 7 RPCC Macadam

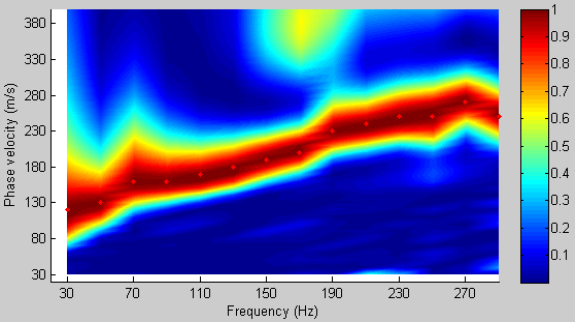

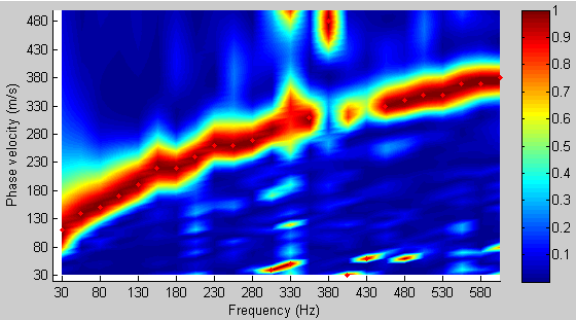

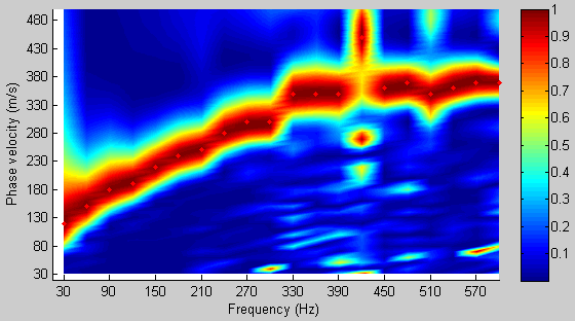

Section 8 RPCC Macadam + NW geotextile

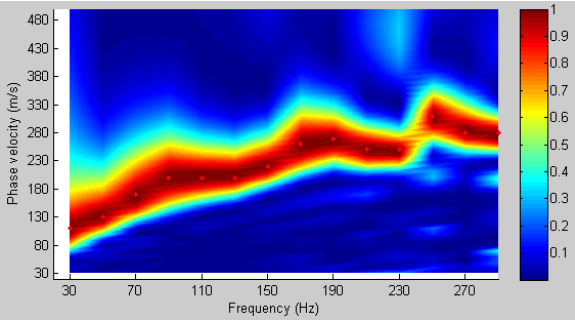

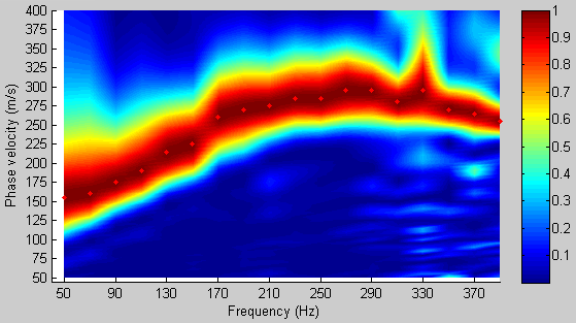

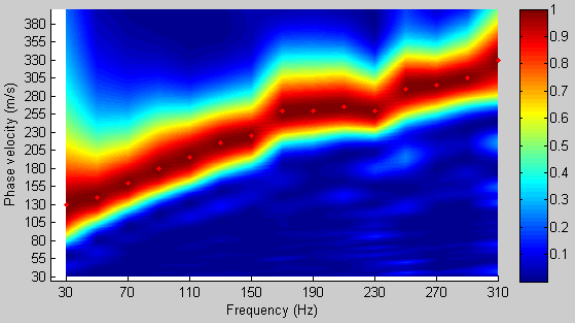

Section 9 Control

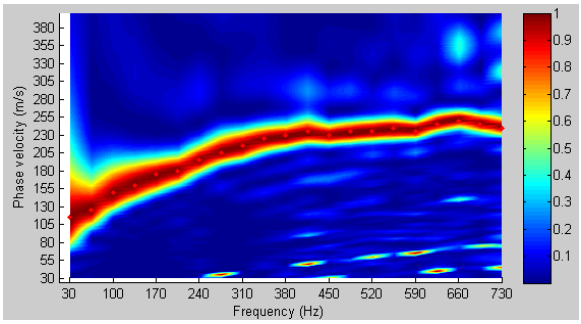

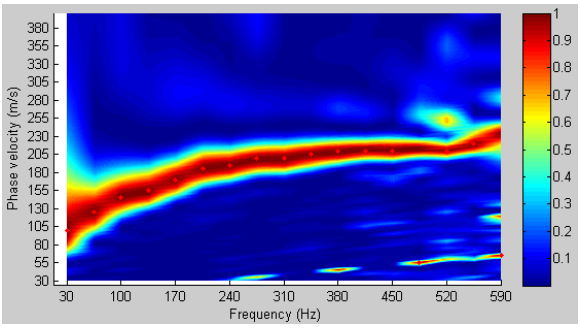

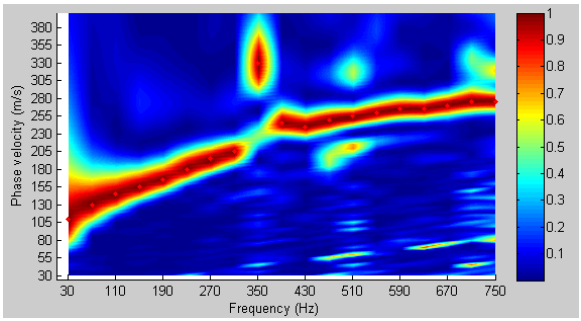

Section 10 & 11 Control

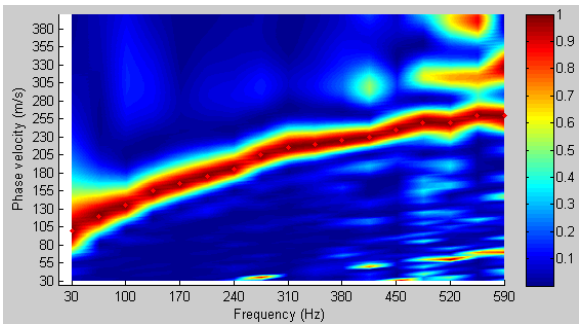

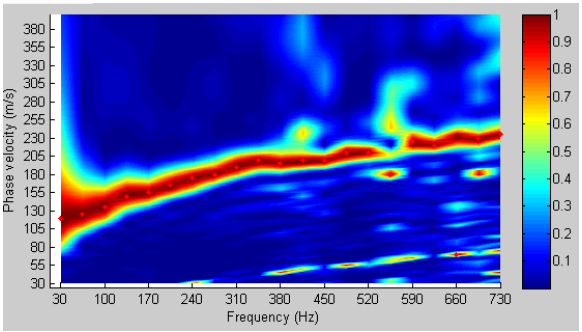

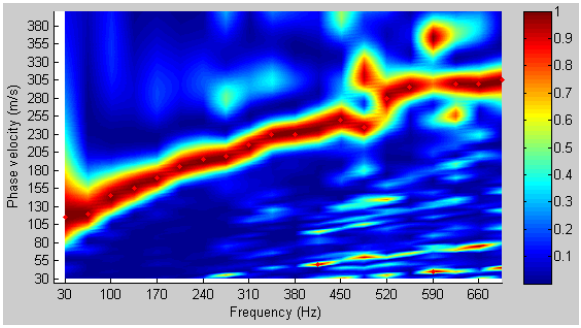

Section 12 Aggregate Columns + Geocomposite Linings

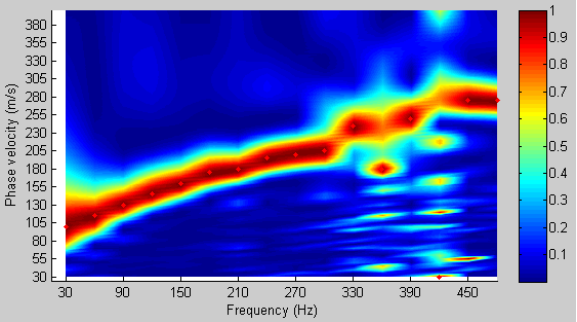

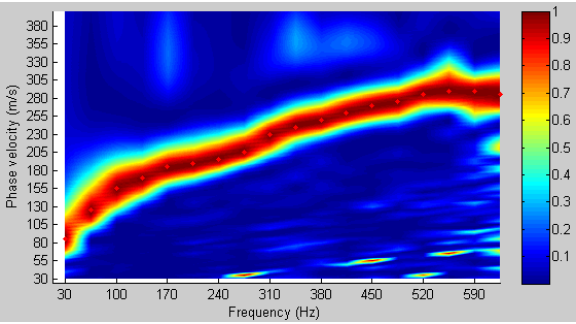

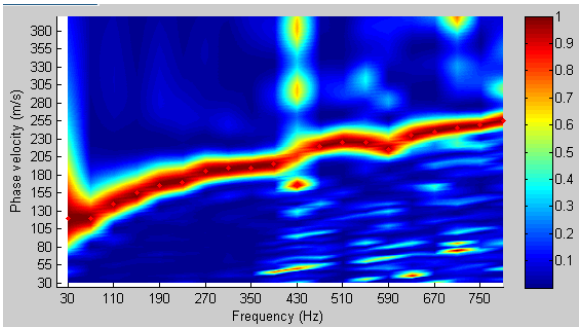

Section 13 Aggregate Columns

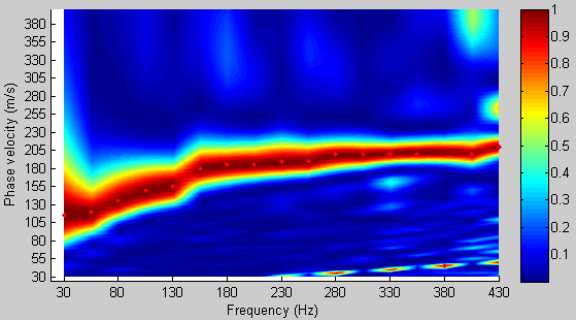

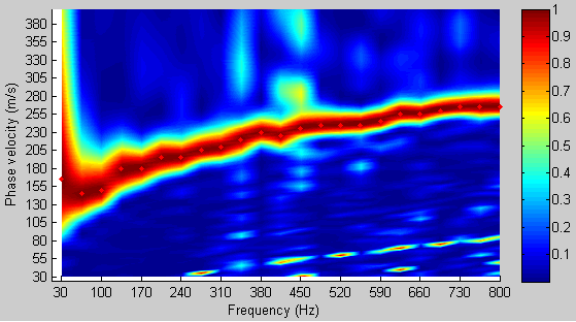

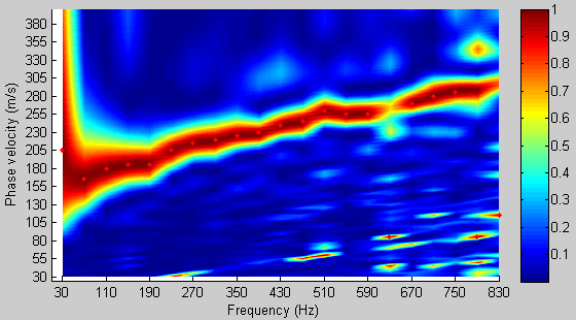

Section 15 Bentonite

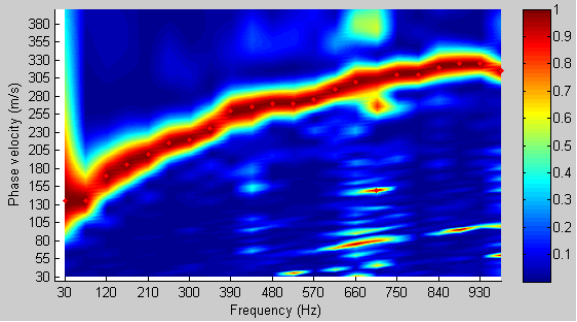

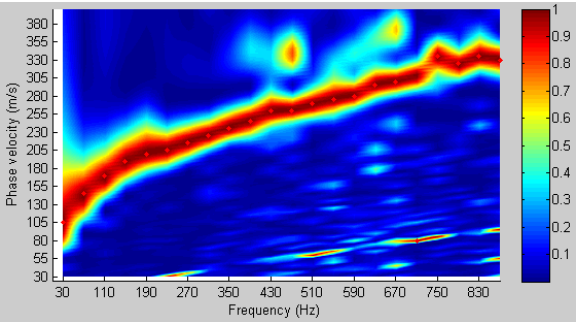

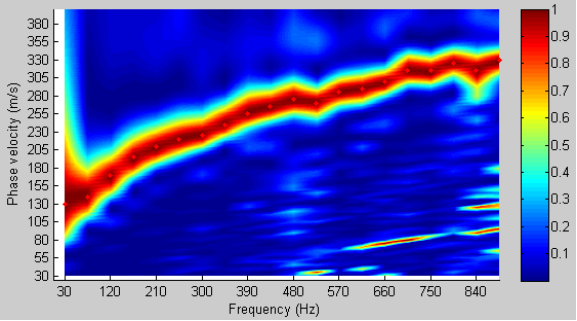

Section 16 Fly Ash

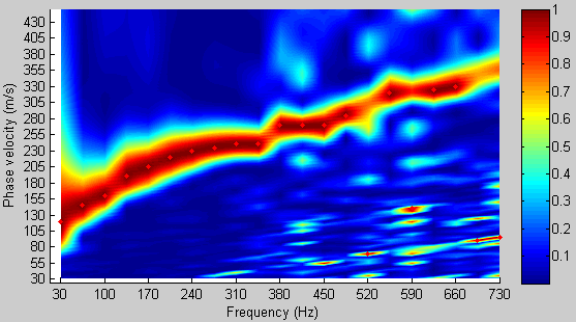

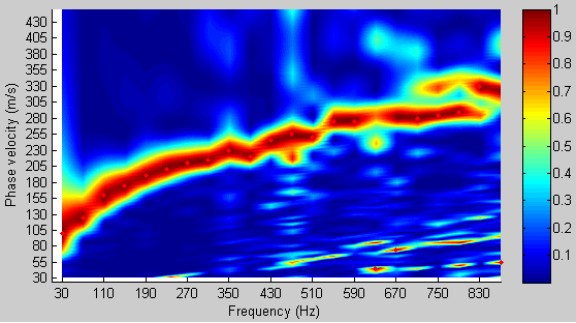

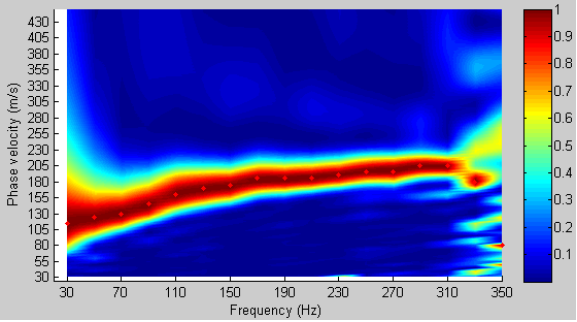

Section 17 Cement

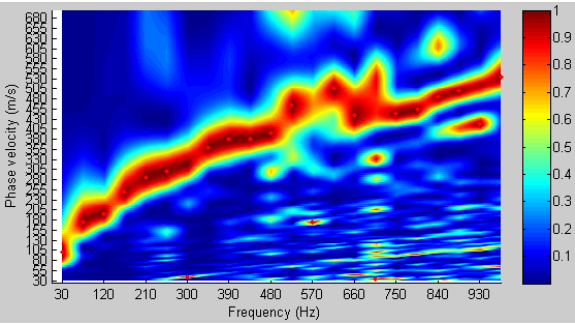

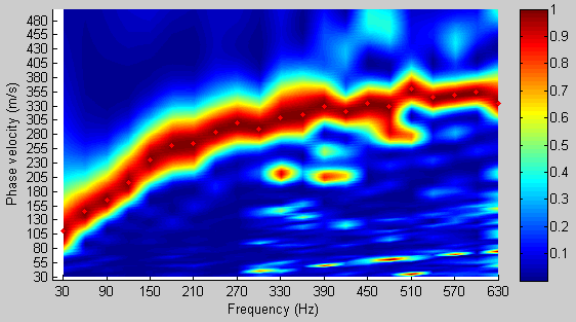

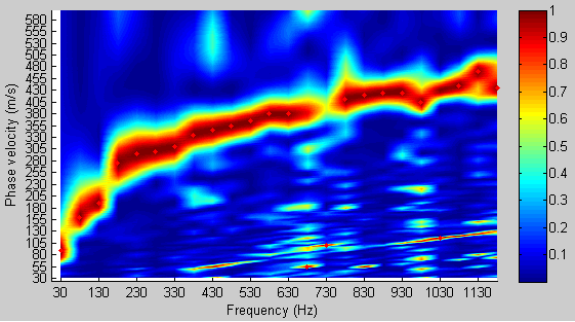

Section 18 Geocomposite Drainage Layer

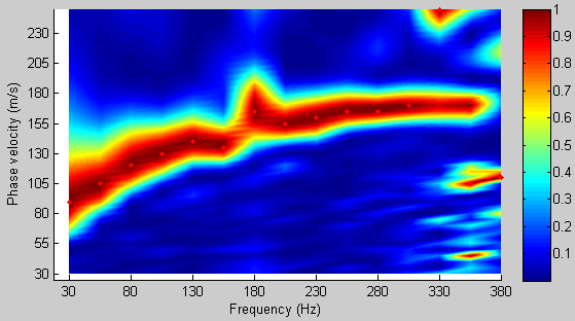

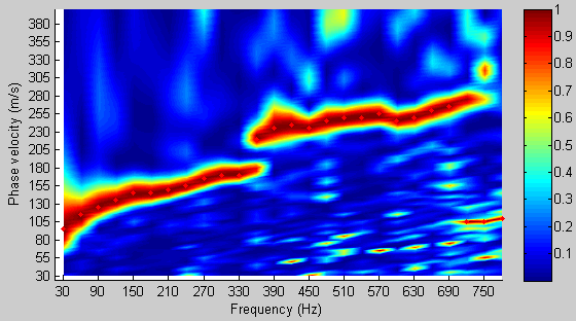

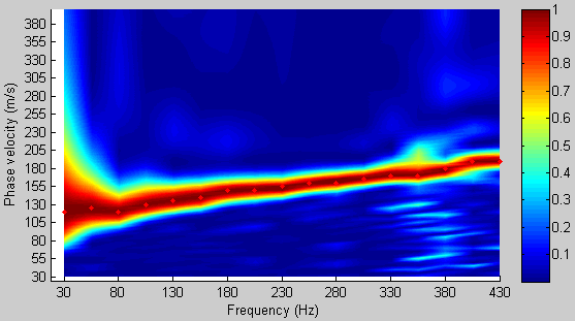

Section 19A BX-Geogrid + NW-Geotextile

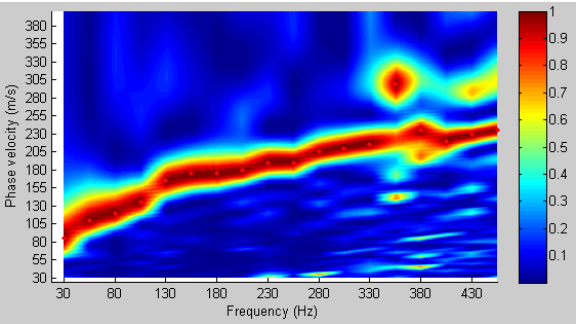

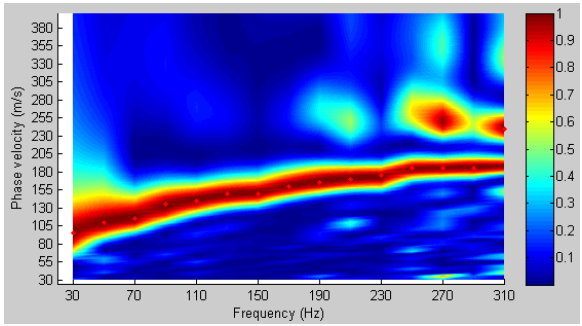

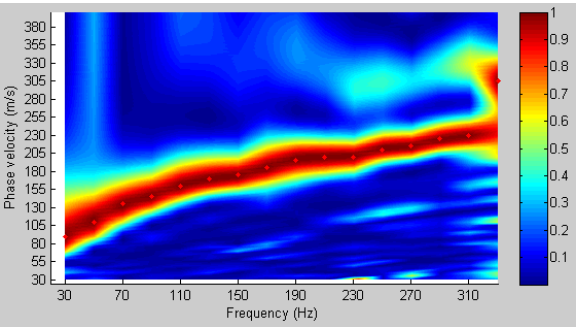

Section 19B BX-Geogrid

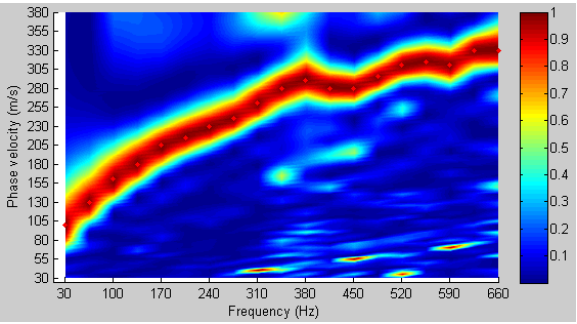

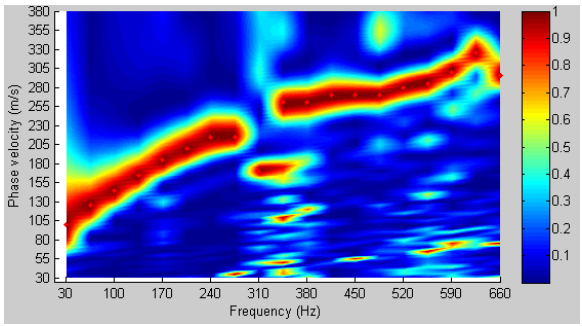

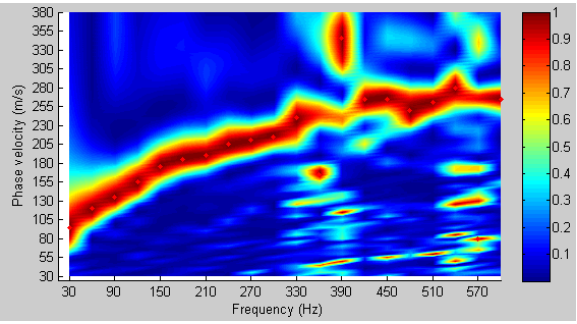

APPENDIX E. 2017 POST-THAWING MASW DISPERSION IMAGES

Section 1A Dirty Macadam

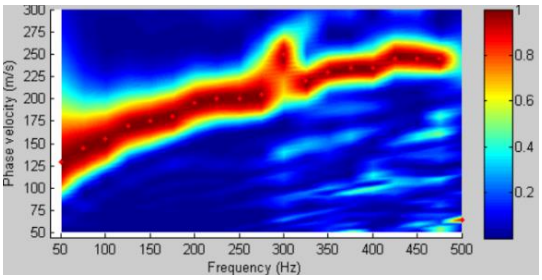

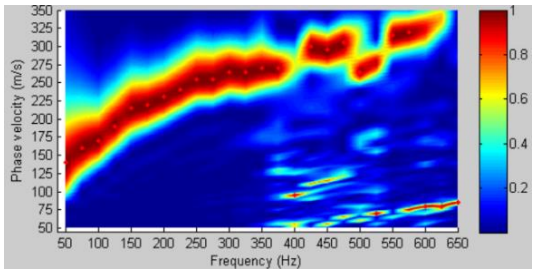

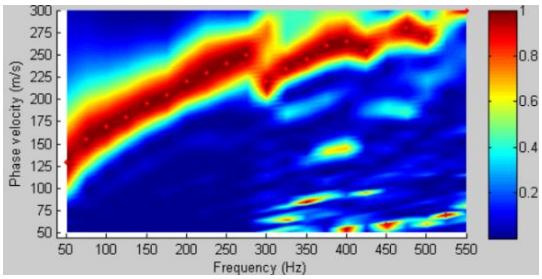

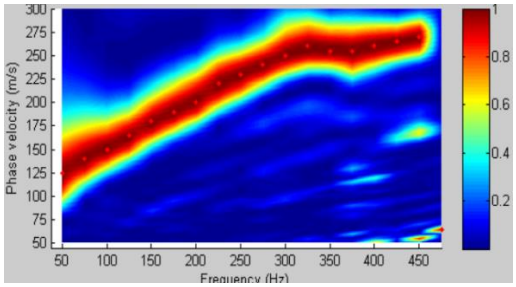

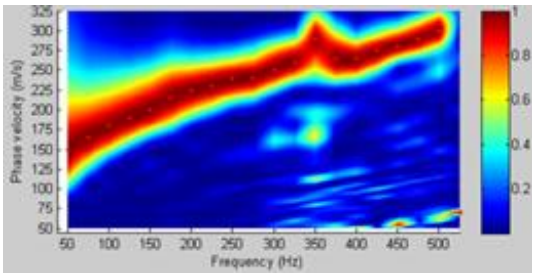

Section 1B Dirty Macadam + Bentonite

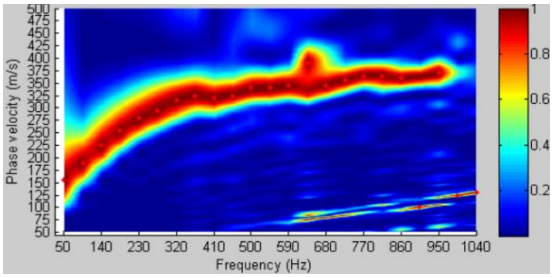

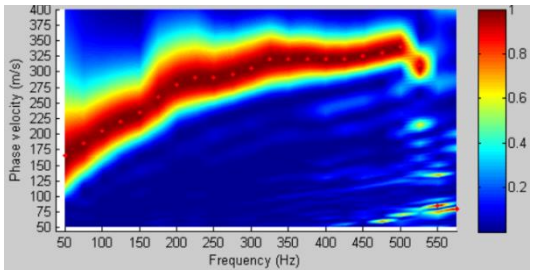

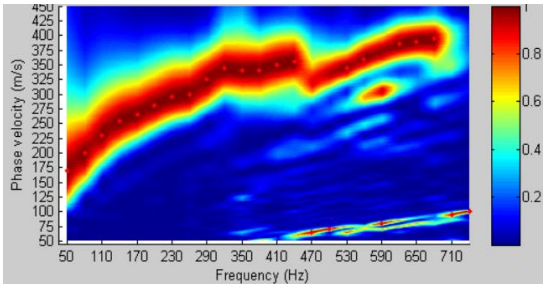

Section 2 Dirty Macadam + Calcium Chloride

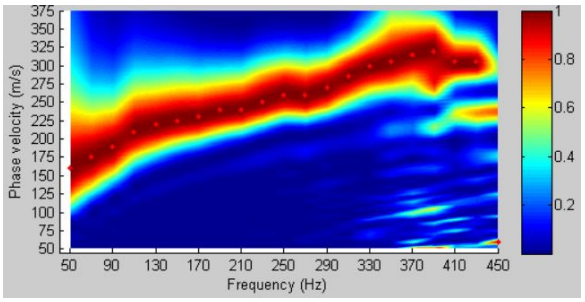

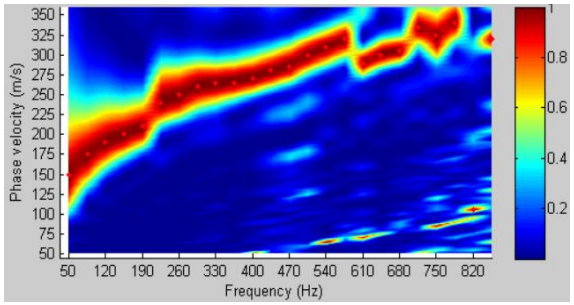

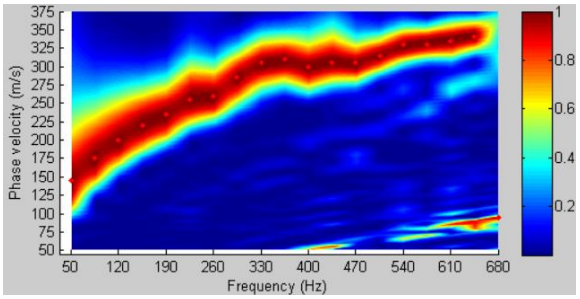

Section 3 Dirty Macadam + Bentonite + NW geotextile

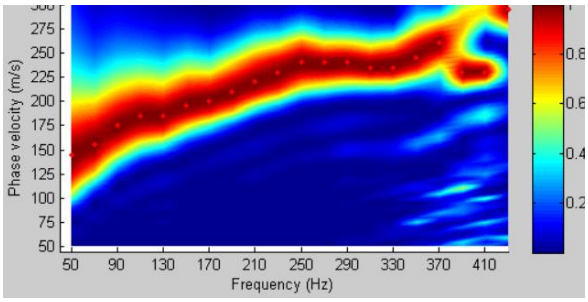

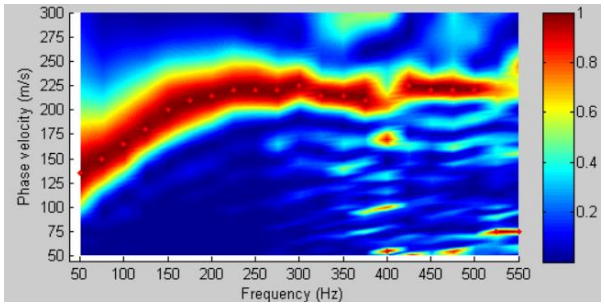

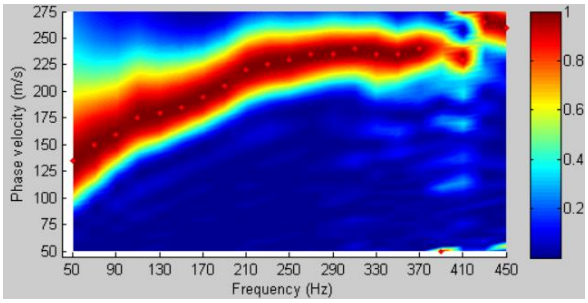

Section 4 Dirty Macadam + NW geotextile

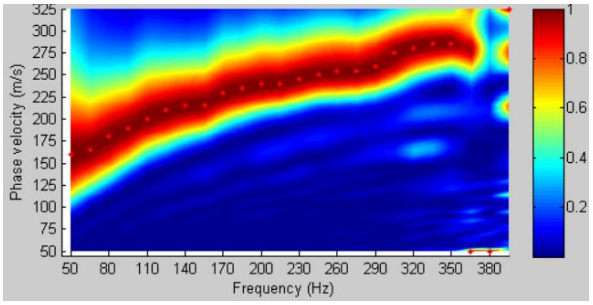

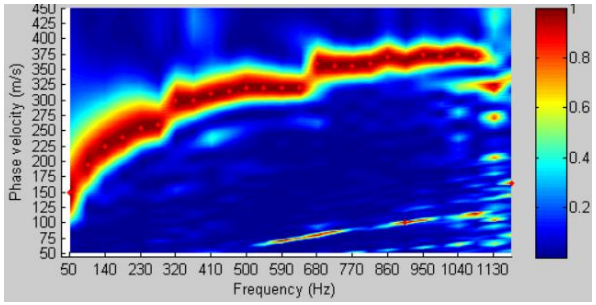

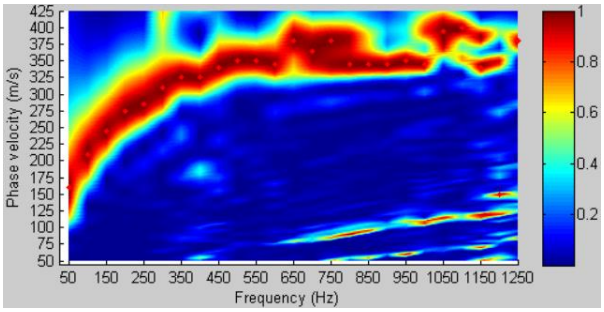

Section 5 Clean Macadam + NW geotextile

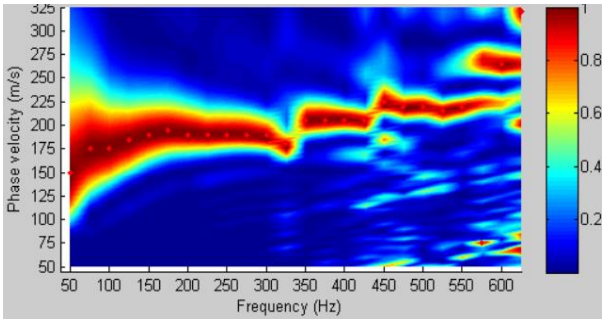

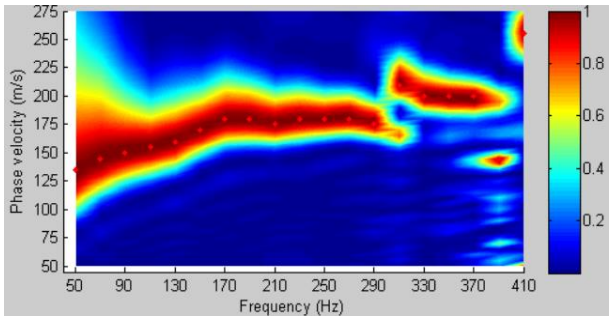

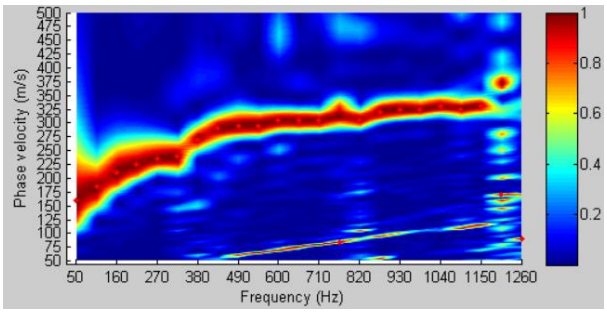

Section 6 Clean Macadam

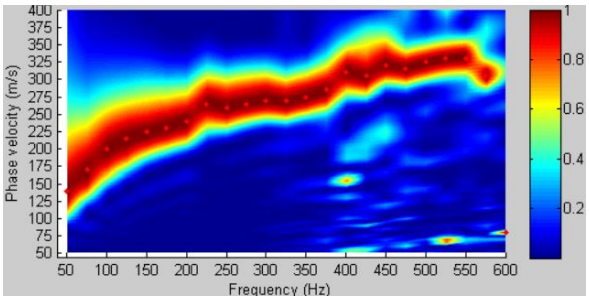

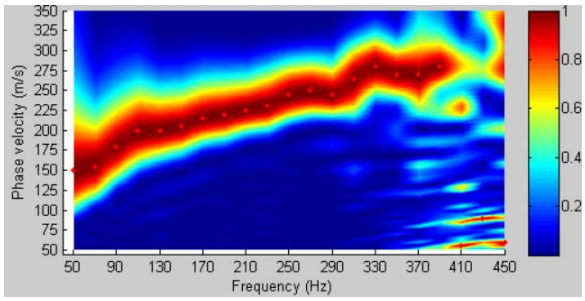

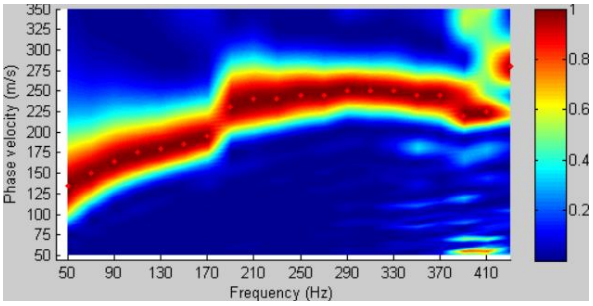

Section 7 RPCC Macadam

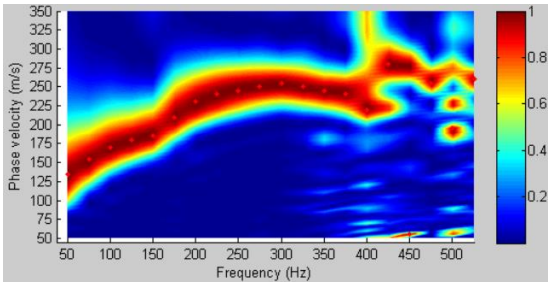

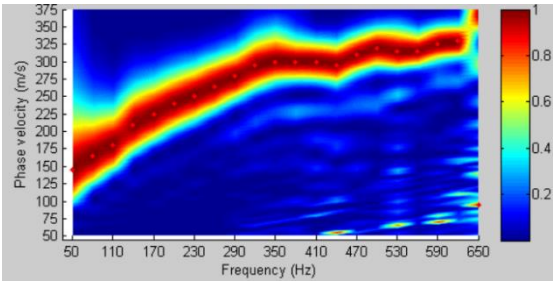

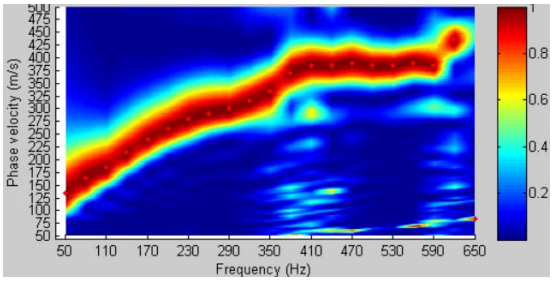

Section 8 RPCC Macadam + NW geotextile

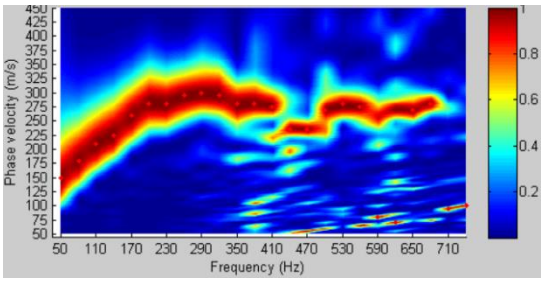

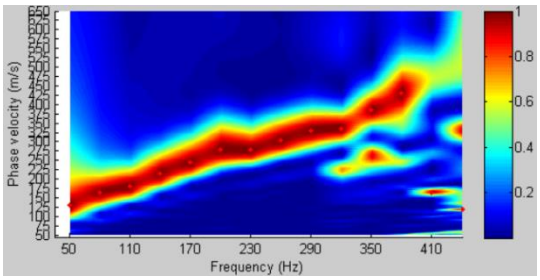

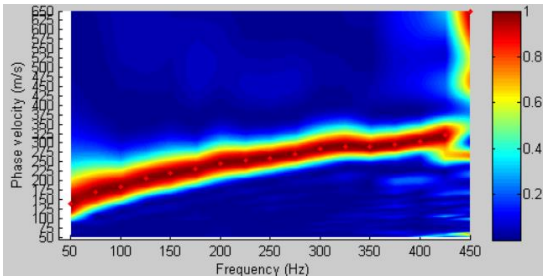

Section 9 Control

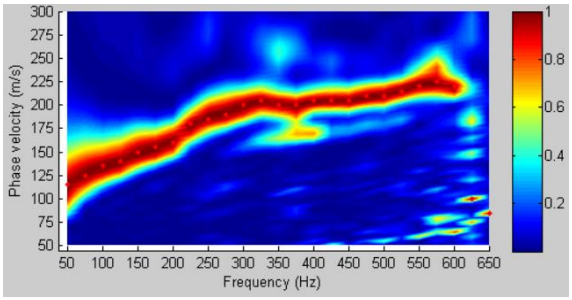

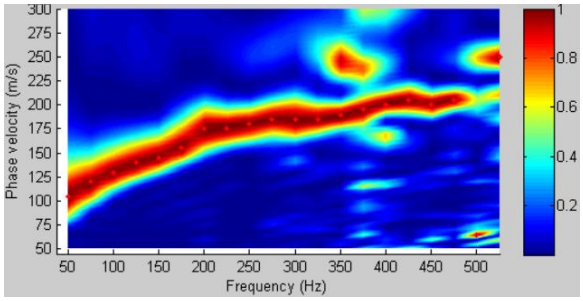

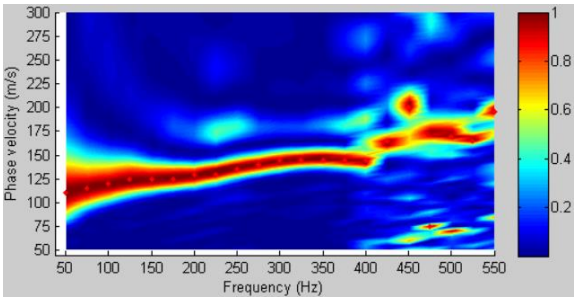

Section 10 & 11 Control

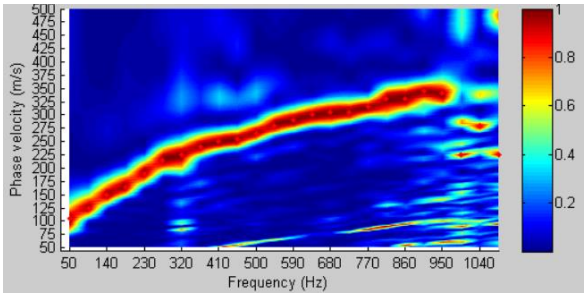

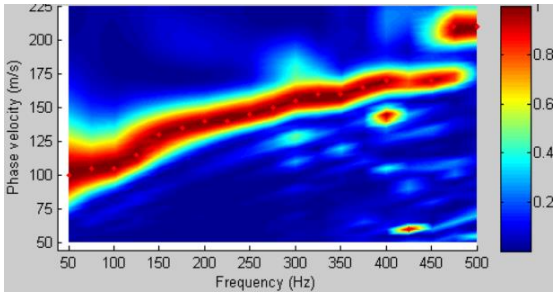

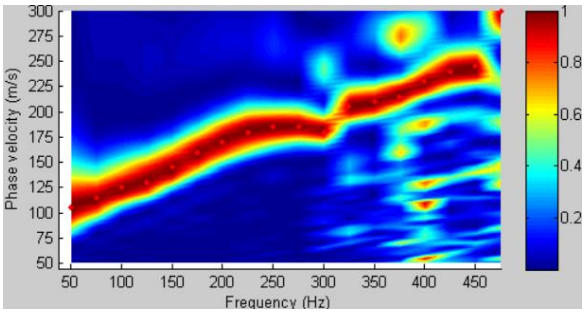

Section 12 Aggregate Columns + Geocomposite Linings

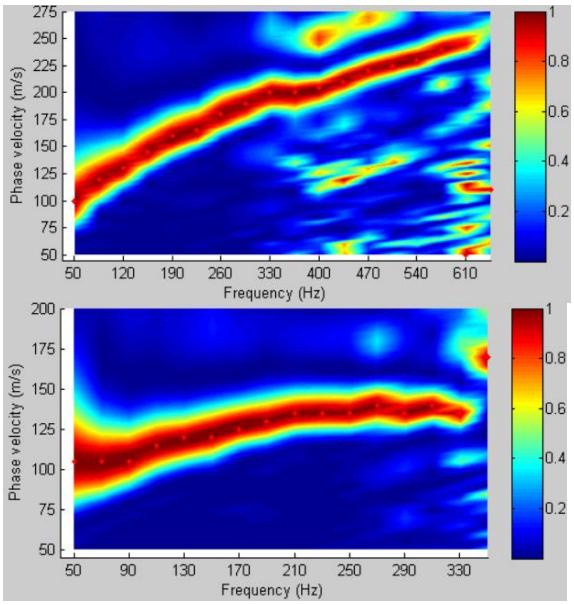

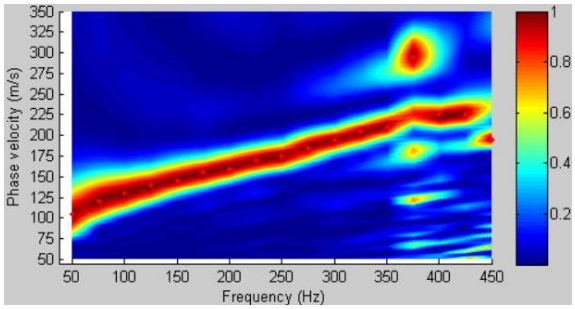

Section 13 Aggregate Columns

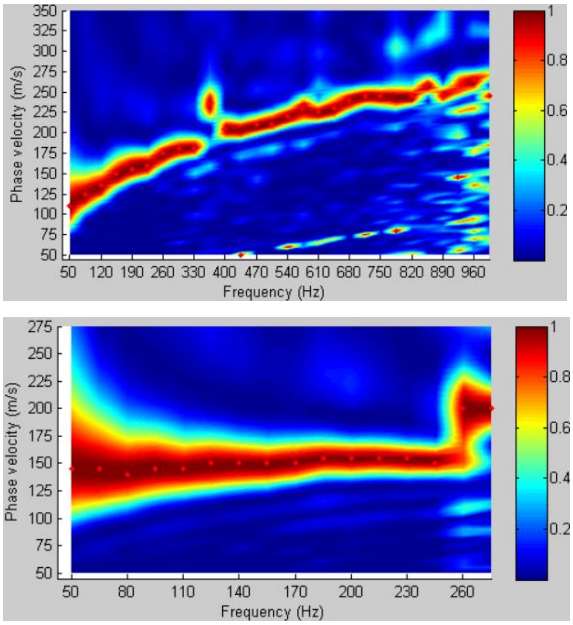

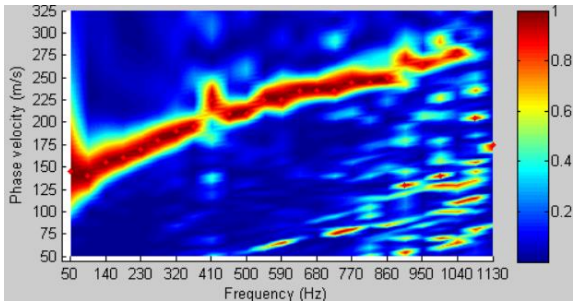

Section 14 Control

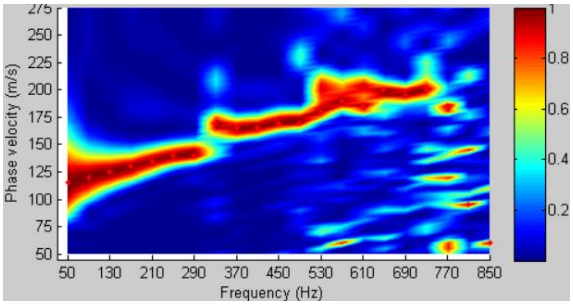

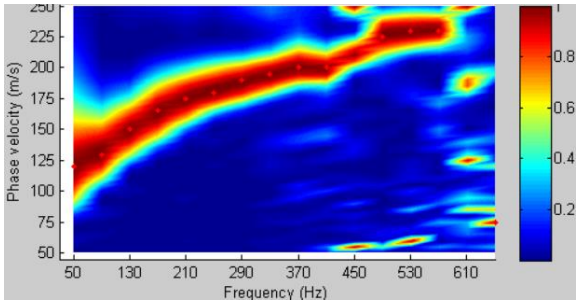

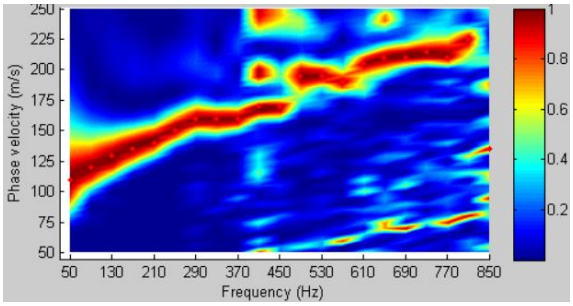

Section 15 Bentonite

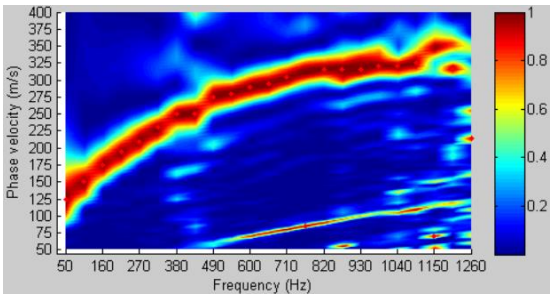

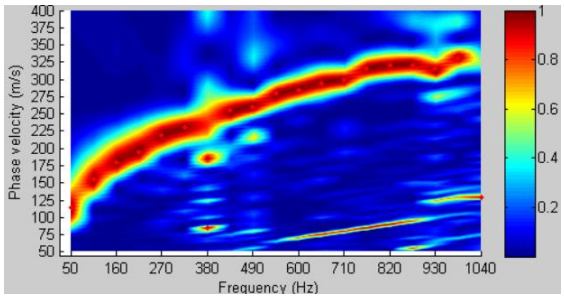

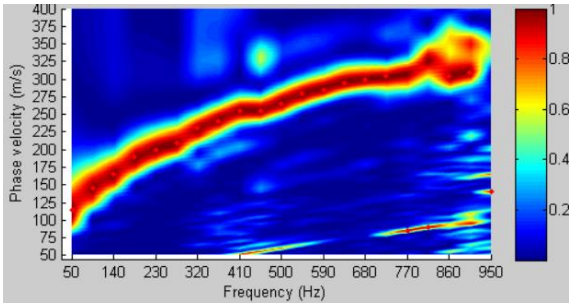

Section 16 Fly Ash

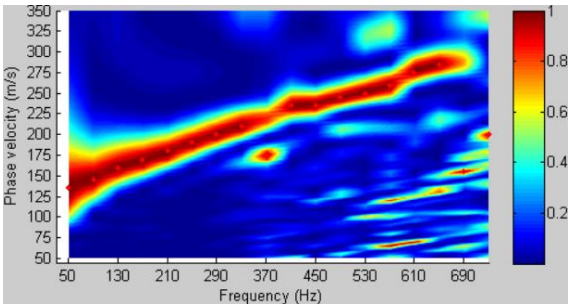

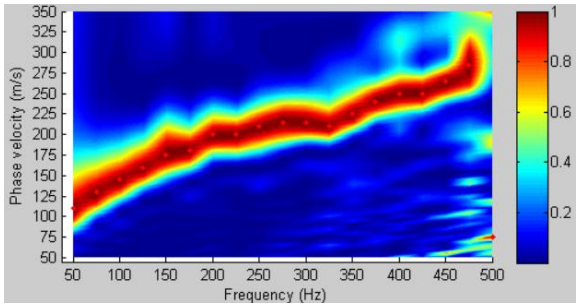

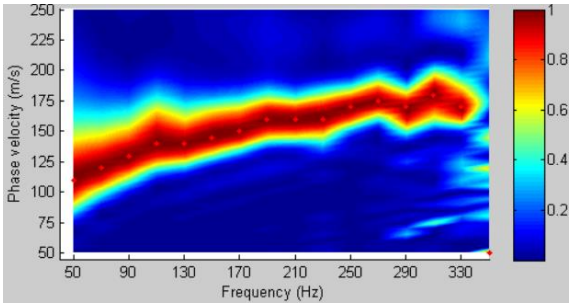

Section 17 Cement

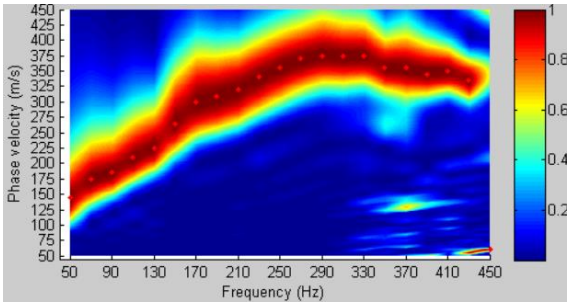

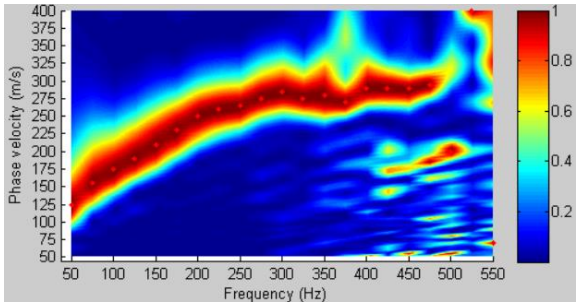

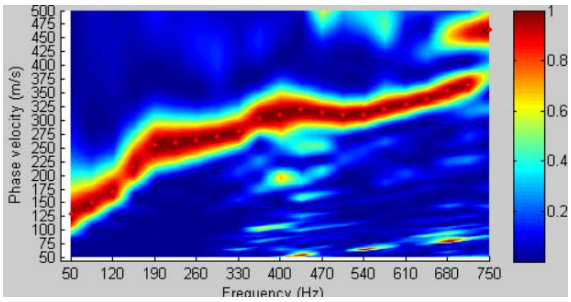

Section 18 Geocomposite Drainage Layer

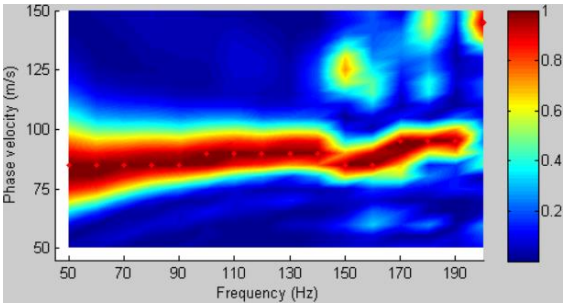

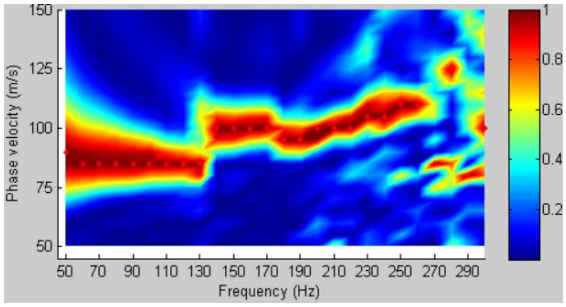

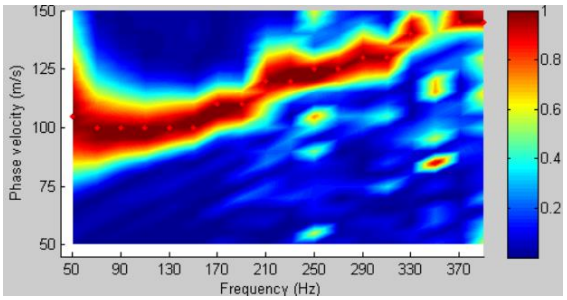

Section 19A BX-Geogrid + NW-Geotextile

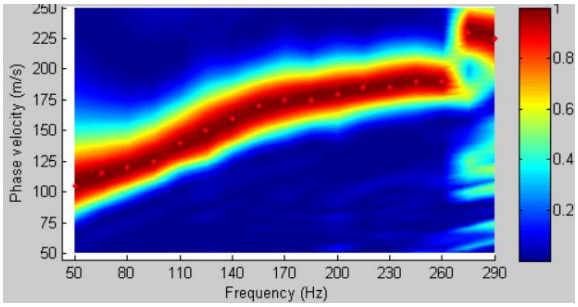

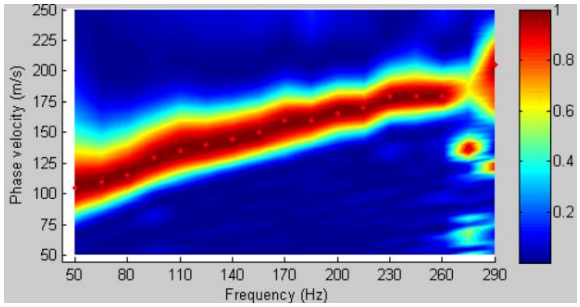

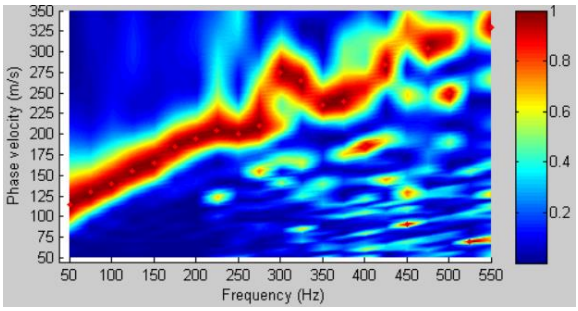

Section 19B BX-Geogrid